UNIVERSITAT POLITÈCNICA DE CATALUNYA
BARCELONATECH
Escola d'Enginyeria de Telecomunicació
i Aeroespacial de Castelldefels

NANOSAT LAB

BACHELOR'S THESIS

TFG TITLE: Analysis and design of the 3Cat-8 Pointing control system for high-volume data downlink

DEGREE: Bachelor's degree in Aerospace Systems Engineering
Bachelor's degree in Telecommunications Systems Engineering

AUTHOR: Alberto Cruz Martínez

ADVISOR: Hyuk Park

SUPERVISOR: Luis Juan Contreras Benito

DATE: June 20, 2023

Título: Análisis y diseño del sistema de control de apuntado de la misión 3Cat-8 para un radioenlace de bajada de datos de alto volumen
Autor: Alberto Cruz Martínez

Director: Hyuk Park

Supervisor: Luis Juan Contreras Benito

Fecha: 20 de junio de 2023

Resumen

El objetivo de esta bachelor's thesis es realizar un analisis exhaustivo de los subsistemas de comunicaciones de las bandas UHF, S y X de la misión 3Cat-8. Esta misión tiene como objetivo desarrollar un satélite bajo el estándar CubeSat que permita estudiar diferentes fenómenos físicos como los efectos de la emisión de las auroras en la propagación de ondas a través de la ionosfera. Además, en este proyecto también se desarrolla el diseño de una antena parche de banda S con el objetivo tanto de comprender el diseño de una antena de aplicación espacial, como implementarla en el mismo satélite y compararla con otras opciones comerciales.

Además, la órbita de tipo polar que describirá el satélite tiene como consecuencia que el satélite no siempre tenga la oportunidad de realizar descargas de datos, por lo que será necesario diseñar y dimensionar los actuadores magnéticos con fin de posibilitar al satélite apuntar a la estación terrestre. En este documento se aborda el estudio, diseño y manufactura de estos elementos con el fin de capacitar al satélite el apuntado de sus antenas a la estación terrestre.

En conjunto, este trabajo representa una contribución significativa a la misión 3Cat-8. A lo largo de este proyecto se han realizado diversas actividades que engloban ámbitos de la ingeniería aeroespacial y de telecomunicaciones.

Title : Analysis and design of the 3Cat-8 Pointing control system for high-volume data downlink

Author: Alberto Cruz Martínez

Advisor: Hyuk Park

Supervisor: Luis Juan Contreras Benito

Date: June 20, 2023

Overview

The objective of this bachelor's thesis is to conduct a comprehensive analysis of the communication subsystems in the UHF, S, and X bands of the 3Cat-8 mission. This mission aims to develop a satellite under the CubeSat standard that allows the study of different physical phenomena, such as the effects of auroral emissions on wave propagation through the ionosphere. Furthermore, this project also includes the design of an S-band patch antenna, both to understand the design of a space application antenna and to implement it on the same satellite and compare it with other commercial options.

In addition, the polar orbit described by the satellite results in limited opportunities for data downlink, making it necessary to design and dimension magnetic actuators to enable the satellite to point towards the ground station. This document addresses the study, design, and manufacturing of these elements in order to enable the satellite to aim its antennas at the ground station.

Overall, this work represents a significant contribution to the 3Cat-8 mission. Throughout this project, various activities encompassing the fields of aerospace engineering and telecommunications have been carried out.

"The only man who does not make a mistake is the man who does nothing"
- *Johann Wolfgang von Goethe.*

"As long as men are free to ask what they must, free to say what they think, free to think what they will, freedom will never be lost and science will never retreat."
- *J. Robert Oppenheimer.*

CONTENTS

LIST OF FIGURES

LIST OF TABLES

ACRONYMS

AC Alternating current. 79

ADCS Attitude Determination and Control System. 7–9, 61, 70, 82, 87

AGW American Wire Gauge. 70

AOCS Attitude and Orbit Control System. 70

AR Axial Ratio. x, 52, 57–59

BER Bit Error Rate. 31, 32, 41–44

CAD Computer-aided Design. ix, x, 5, 61

COTS Commertial Off-The-Shelf. 13

CuPID CubeSat PocketQube Integrated Deployer. 7

DC Duty Cycle. 83

DC Direct Current. x, 79, 81

DSP Digital Signal Processor. 6

EETAC Escola d'Enginyeria de Telecomunicació i Aeroespacial de Castelldefels. 79

EM Engineering Model. x, 2, 3, 59, 70, 76–78

EPS Electric Power Subsystem. 70

ESA European Space Agency. ix, 14

FM Flight Model. 3, 70, 76, 77

FZP Fresnel Zone Plate. 6

GEO Geosynchronous Earth Orbit. 25

GS Ground Station. xii, 23, 42, 43, 45, 47, 48, 59, 61, 62, 82, 87

HEO High Earth Orbit. 25

HPBW Half Power Beam Width. 31, 43, 48, 58

IEEC Instituto de estudios espaciales de Cataluña. 5, 6

ISI Grup d'Instrumentació, Sensors i Interfícies. 79

ISS International Space Station. 23

LEO Low Earth Orbit. 25–27

LHCP Left Handed Circular Polarization. 52, 58

MEO Medium Earth Orbit. 25

MTQ Magnetorquer. x, xii, 65, 68–70, 72–87

NASA National Aeronautics and Space Administration. 91

OAdM Observatorio Astronómico del Montsec. ix, 4, 19, 29, 36, 47, 62, 88

OBC On-Board Computer. 6, 8, 9, 61, 62, 64, 66, 82, 84

PCB Printed Circuit Board. 66

PLF Polarization Loss Factor. 37

PMAC Passive Magnetic Attitude Control. ix, 19, 20

PWM Pulse Width Modulation. x, 64, 65, 79, 81, 82

RF Radio Frequency. 49, 53, 54

RHCP Right Handed Circular Polarization. 3, 52, 53, 57, 58

RL Return Losses. 58

SDR Software Defined Radio. 6

SNR Signal to Noise Ratio. 1–3, 29, 31, 32, 39, 40, 59, 87

TBD To Be Determined. 42–44

TLE Two-Line Element. 24, 26

TT&C Telemetry, Tracking and Command. 9, 15, 23, 41, 45

UHF Ultra High Frequency. 8, 9, 15

UPC Universidad poltécnica de Cataluña. 4–6

VHF Very Hight Frequency. 9

ACKNOWLEDGEMENTS

I would like to express my deep gratitude to my parents, who have been my unconditional support throughout this exciting academic journey. Your dedication, love and sacrifice have been instrumental in my education and achievements. You were always there to provide me with words of encouragement, motivation and guidance in every step I took. Your confidence in me has propelled me to overcome obstacles and persevere through difficult times. Without your constant presence, understanding and support, this achievement would not have been possible. Thank you for being my pillars and for believing in my dreams.

To Paula. I want to express my sincere thanks. You have been my rock during these years of study, my source of inspiration and my constant motivation. Your words have given me the strength to keep going even in the moments of greatest pressure. Thank you for being by my side, for believing in me and for sharing this path with me.

And finally to Luis, Adriano and Hyuk, I would like to express my deepest gratitude for your dedication, expertise and knowledge imparted throughout this final thesis. Your guidance and mentorship have been invaluable to my intellectual and professional growth. Your influence has been crucial in my education and I will be eternally grateful for the impact you have had on my life.

CHAPTER 1. INTRODUCTION

Human curiosity is the main ingredient that has allowed human beings to develop their knowledge in order to understand and predict the world around them. Thanks to this capacity, it has been possible to develop tools and technologies that are used to analyze the environment by gathering data from it. One of the most productive ways to obtain data about the our planet is through satellites.

Orbiting around the Earth, satellites are capable of gathering information about its surface. The reception of electromagnetic waves emitted from the surface has multiple applications, such as measuring water salinity, detecting crop pests, as well as providing telecommunications services like satellite television.

In recent decades, the space sector has thrived due to the miniaturization and cost reduction of the technology required to build satellites of any kind. Whether for scientific purposes (exploration or experimentation, remote sensing, etc.) or commercial applications (5G services, IoT, etc.), this revolution has enabled the private sector to access space with much smaller budgets. As a result, there has been a significant increase in the number of missions launched in recent years.

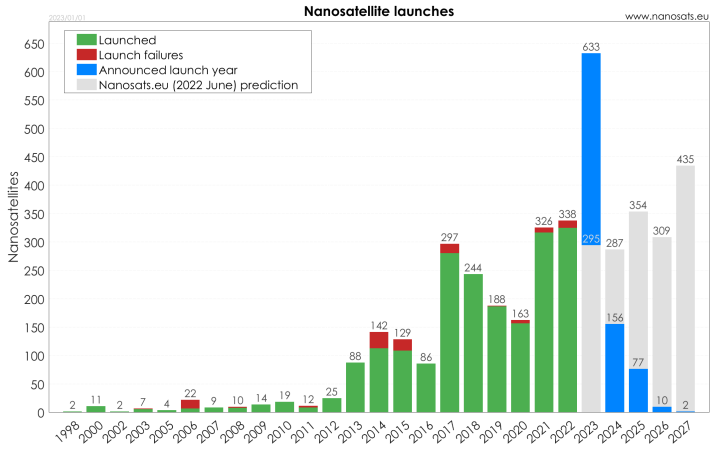

Figure 1.1: Number of nanosatellites per year. [1]

This work has been performed in collaboration with the NanoSatellites and Payloads Laboratory (UPC NanoSat Lab), located in Campus Nord of the Technical University of Catalonia. Throughout this chapter, a detailed introduction is provided regarding the topics addressed and the context of this work, aiming to offer the clearest possible understanding of the research conducted.

1.1. Objectives

This Bachelor's thesis primarily aims to analyze the X, S, and UHF subsystems of the 3Cat-8 mission, a 6U CubeSat mission (detailed in section 2.2.). The main focus is determining the power budget of the mission through the analysis of the Signal to Noise Ratio (SNR) at different elevation angles among other factors. The objective of this analysis is to verify the

feasibility of these communication systems and address uncertainties such as the required transmitted power from the satellite to ensure data downlink and the bandwidth of the transmissions. Additionally, it is necessary to select the type of X-band antenna that will be implemented in the satellite.

Additionally, it was necessary to develop magnetic actuators, referred to as magnetorquers (MTQ), to provide the satellite with the capability to point towards the ground station when required.

In this thesis, a patch antenna for the S-band is also designed with the objectives of learning the development and simulation of a space application antenna, comparing it with similar commercial antennas, and, if possible, implementing it in the satellite in the future.

1.2. Scope

This bachelor's thesis covers areas of engineering related to the two degrees it aims to culminate. This work encompasses fields of science and engineering such as electromagnetic wave propagation, satellite application antenna design, electromagnetic phenomena, and satellite attitude control mechanisms.

The objective of this Bachelor's thesis is to simulate the performance of the communication links of 3Cat-8 by simulating its orbit and obtaining an estimation of the radio link quality.

The S-band communication antenna will be simulated to verify the possibility of implementing it on the satellite and compare it with other commercial options.

Additionally, the design of magnetic actuators is developed, an Engineering Model (EM) of these actuators is manufactured, and a test is conducted to verify that the results align with the design and meet the required performance specifications for the feasibility of the communication link.

1.3. Requirements

In this section, the preliminary requirements for each subsystem and the requirements for their respective devices are described.

1.3.1. Communication system requirements

- Conduct a preliminary study of the SNR at different elevation angles for each of the three subsystems.
- Perform a comparison among the different combinations of values that characterize the radio link.
- The analysis of the radio link must take into account all the possible effects that the transmitted signal might suffer.
- The values used to simulate the link must be as realistic as possible. This means using the values of the actual transmitter and receivers of the ground station.

1.3.2. Antenna requirements

- Simulate the S-Band antenna and check that its characteristics meet the requirements of the radio link.
- The dimensions of the patch antenna must be smaller than the size of one face of a 1U CubeSat (10x10 cm).
- The antennas must have Right Handed Circular Polarization (RHCP).
- They must be made with materials that are suitable for use in space.
- The antenna must have a gain that meets and fulfils the requirements of the satellite link analysis.

1.3.3. Attitude Determination and Control System (ADCS) requirements

- Conduct a detailed preliminary study that allows for the determination of the construction parameters of the magnetorquers (MTQ) while respecting the dimensional and power constraints.
- Perform an Engineering Model (EM) simulation of the simulated magnetorquer.
- Conduct tests to verify the accuracy of the simulations compared to real-world scenarios.
- The size of the devices must fit in the space available (detailed in the section 4.4.0.1.).
- The actuators must meet the actuating requirements in order to make feasible the communication links (section 4.4.0.2.).
- The power consumed by the magnetorquers must be less than the maximum power available for this subsystem detailed in the power budget (section 4.4.0.3.).
- The materials that will be used in the Flight Model (FM) must be suitable for use in space (section 4.4.0.4.).

1.4. Methodology

Initially, a *MATLAB* code will be developed to simulate power budgeting and calculate the Signal to Noise Ratio (SNR) for different elevation angles. It will be necessary to evaluate various important values in data transmission that greatly affect the SNR, such as transmitted power, bandwidth, and the types of antennas used both in the satellite and the ground station. Following this analysis, a decision will be made regarding the type of antenna to be used for the X-band system.

Furthermore, using the electromagnetic simulation tool *CST Studio Suite*, the design of the S-band antenna will be developed according to the previously stated requirements.

Finally, the design and fabrication of the satellite's magnetorquers is carried out. Firstly, simulations are performed using a *MATLAB* code. Then, an Electromagnetic (EM) simulation of one of the magnetorquers is conducted, followed by 3D printing of its structure and winding the coil with an AWG-standard cable of the selected diameter based on the previous study. Lastly, impedance tests are conducted to analyze their influence on the system and verify the fidelity of the generated magnetic field compared to the previous simulations. These tests also assess whether the magnetorquers can effectively enable the satellite to perform detumbling and ground station pointing maneuvers.

1.5. The UPC NanoSat Lab

The Nano-Satellite and Payload Laboratory is an initiative of the Telecommunications Engineering School of Barcelona to develop and launch nano-satellites for educational and scientific purposes. This Bachelor's Thesis describes the development of various subsystems of one of the missions. Specifically, the 3Cat-8 mission, which is detailed in the following section. Some of the scientific payloads that are integrated into the CubeCat missions are developed by other research teams of the UPC such as the Remote Sensing Lab.

The NanoSat Lab is located at the UPC Campus Nord. Almost all of its facilities are located there, among which are included an ISO 8 Cleanroom, a vibration table and a Helmholtz coil. In addition, they are capable of transmitting commands and receiving data to orbiting satellites through two ground stations, a primary one located at the Observatorio Astronómico del Montsec (OAdM) and a backup station at UPC's Campus Nord.

During its journey, the NanoSat Lab has developed and placed several satellites in orbit, such as *3Cat-1*, the first satellite developed in Catalonia, the *FSSCat*, which was the first CubeSat to provide data to the ESA Copernicus system (an European initiative for Earth observation), and the *3Cat-4* which is pending to receive launch date.

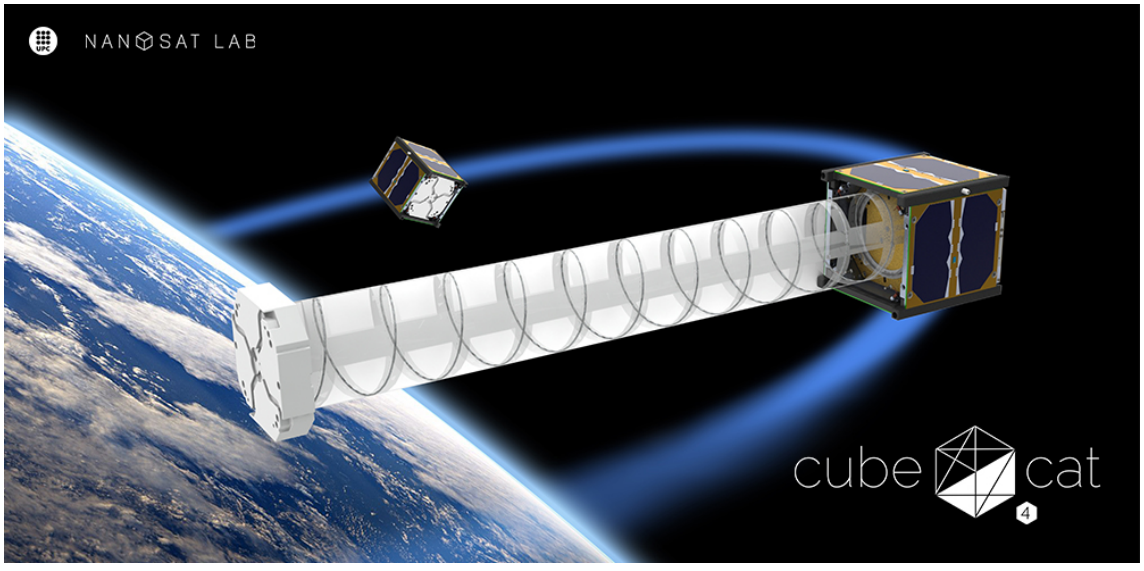

Figure 1.2: 3Cat-4 presentation picture. [2]

1.6. The 3Cat-8 mission

As this Bachelor's thesis is part of the development of the 3Cat-8 mission, a detailed description of the satellite will be offered in the following sections.

The 3Cat-8 mission is one of the youngest satellites of the UPC NanoSat Lab. It is a 6-unit (6U) educational mission which comprises several different payloads and technology demonstrators, some of which have been provided by several organizations and companies, such as IENAI Space, Alén Space or the IEEC. To carry out the onboard scientific experiments, the satellite must be able to correctly perform different tasks such as controlling its attitude or transmitting the gathered data to the ground station.

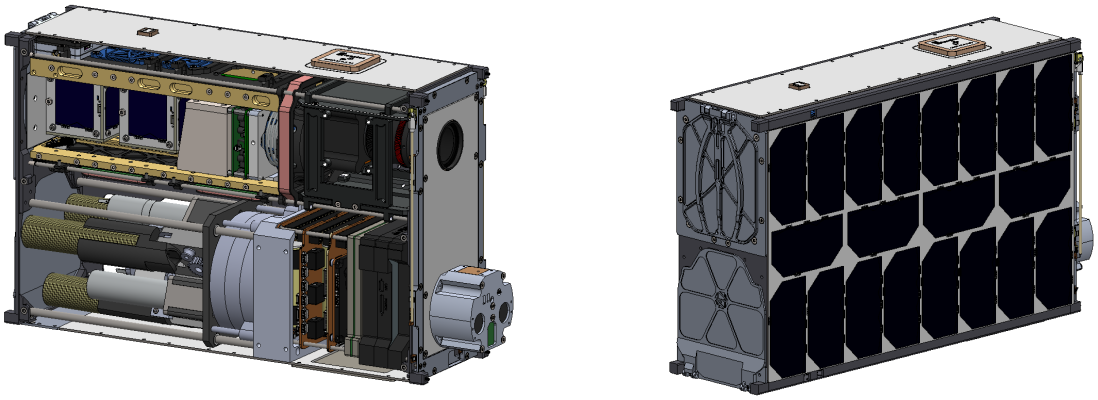

(a) Stowed configuration, inner view of the 3Cat-8.

(b) Stowed configuration, outer view of the 3Cat-8.

Figure 1.3: 3Cat-8 CAD images.

1.6.1. Mission Payloads

The mission Payloads or Scientific experiments are the main characteristics that give meaning to the mission, otherwise, it would not have an objective.

Payloads can be categorized by their purpose. They may have a scientific purpose, a technological purpose or an educational purpose. The first has a clear purpose, gather information to support a scientific study and draw a conclusion from it. The second ones are basically technology demonstrators, their main idea is to demonstrate that this technology can be feasible in CubeSat-type satellites. And the third parties have the purpose of offering a didactic experience for the members of the NanoSat Lab (UPC students).

1.6.1.1. SUSIE camera (3Cat-Gea)

3Cat-Gea is a multi-Spectral (8 spectral bands) camera that will take images of the "aurora borealis and australis" phenomena. The main goal is to study the effects of the auroral emissions in the transmission of radio and navigation signals through the ionosphere. This camera will capture the visible emission of the particles that emit radiation at specific wavelengths.

1.6.1.2. C3SatP

The C3SatP Payload will be the main controller for the data handling of the 3Cat-Gea payload. It is a CubeSat standardised module developed by the IEEC. It will perform as a secondary On-Board Computer (OBC), a data handling system and also as an SDR DSP that will generate the S-Band signals. These signals will then be sent to the ground station. See reference [3].

1.6.1.3. Fresnel zone plate antenna

The Fresnel zone plate antenna is a deployable antenna developed by the UPC NanoSat Lab. It will consist of a Fresnel Zone Plate (FZP) crown and a net. Its main goal is to receive navigation signals that travel across the atmosphere. These signals experience a distortion that will allow us to study and obtain the physical properties of the atmosphere.

The antenna is designed to fit in a 2U volume. The deployment will be carried out by means of three motorized arms. The antenna can be seen in the stowed configuration in the bottom left part of the satellite in the figure 1.3(a), and the deployed configuration is shown below (1.4):

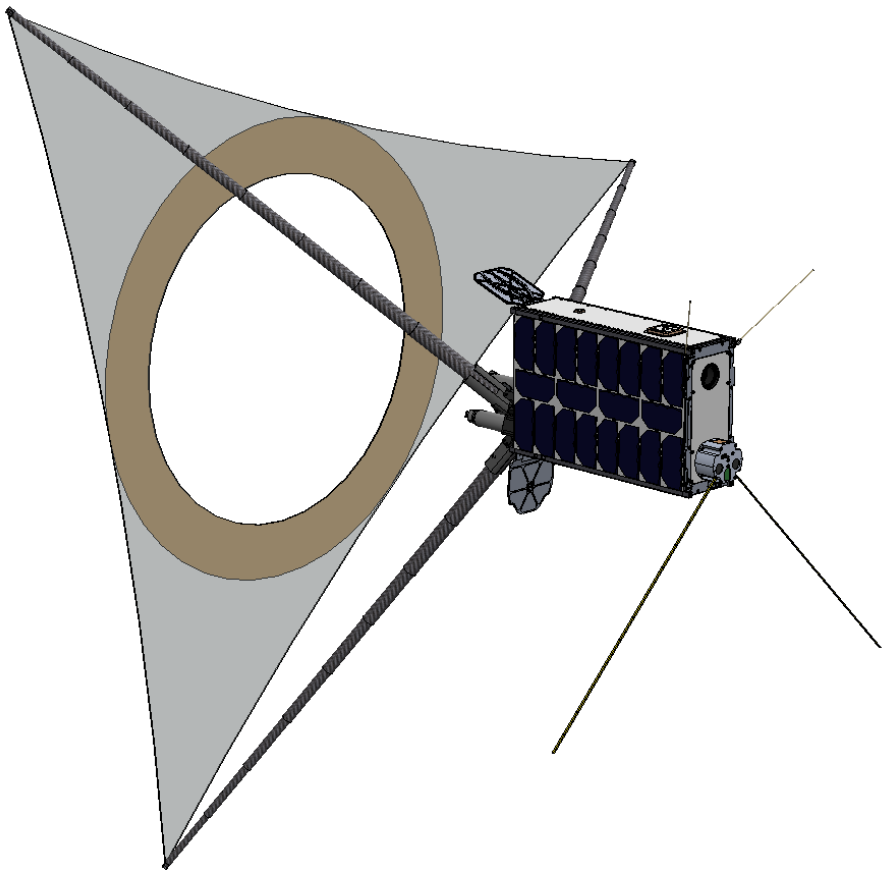

Figure 1.4: Deployed Fresnel zone plate antenna picture.

1.6.1.4. PocketQubes

The 3-Cat8 Satellite will carry two PocketQubes that will be deployed after the detumbling phase. These small pico-satellites will be ejected by the CuPID which also contains Ienai's Athena thruster. The PocketQubes will form a federated satellite system with 3Cat-8, through LoRa inter-satellite link (ISL).

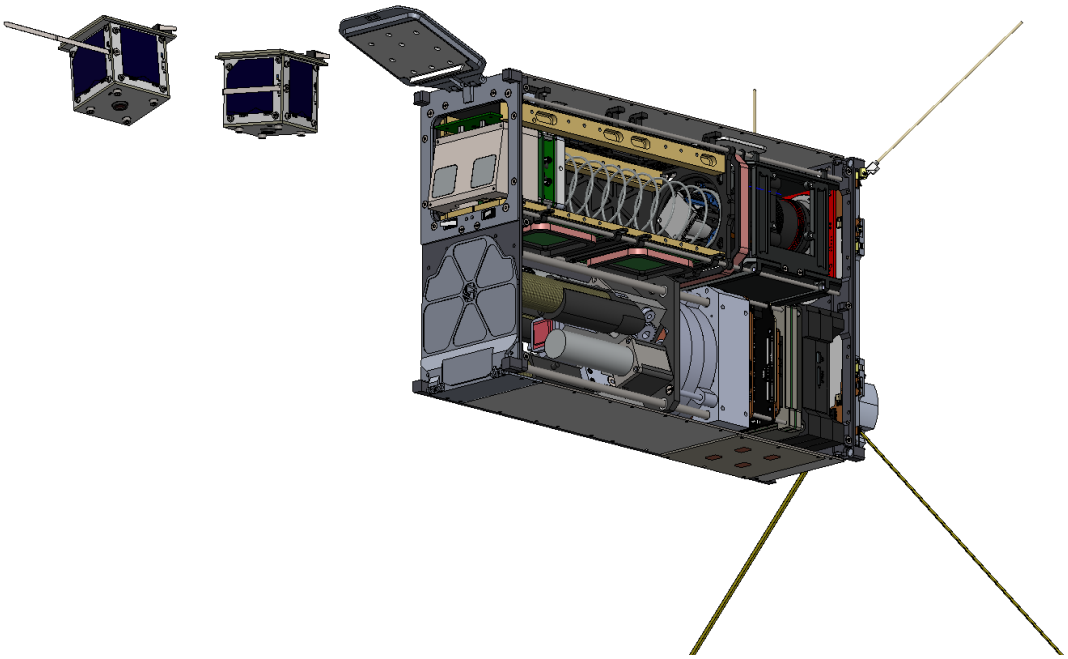

Figure 1.5: Deployed PocketQubes.

1.6.1.5. Athena thruster

The Athena thruster is an ionic thruster developed by IENAI SPACE. It is a technology demonstrator with the aim of studying the viability of electrospray micro-propulsion for small satellites. See reference [4].

1.6.2. Mission's main subsystems

In this section, the objectives and functionalities of the main subsystems of the satellite are described. Below is an image depicting the internal architecture of the relevant subsystems for this Bachelor's Thesis, the Attitude Determination and Control System (ADCS) and the Communications subsystem.

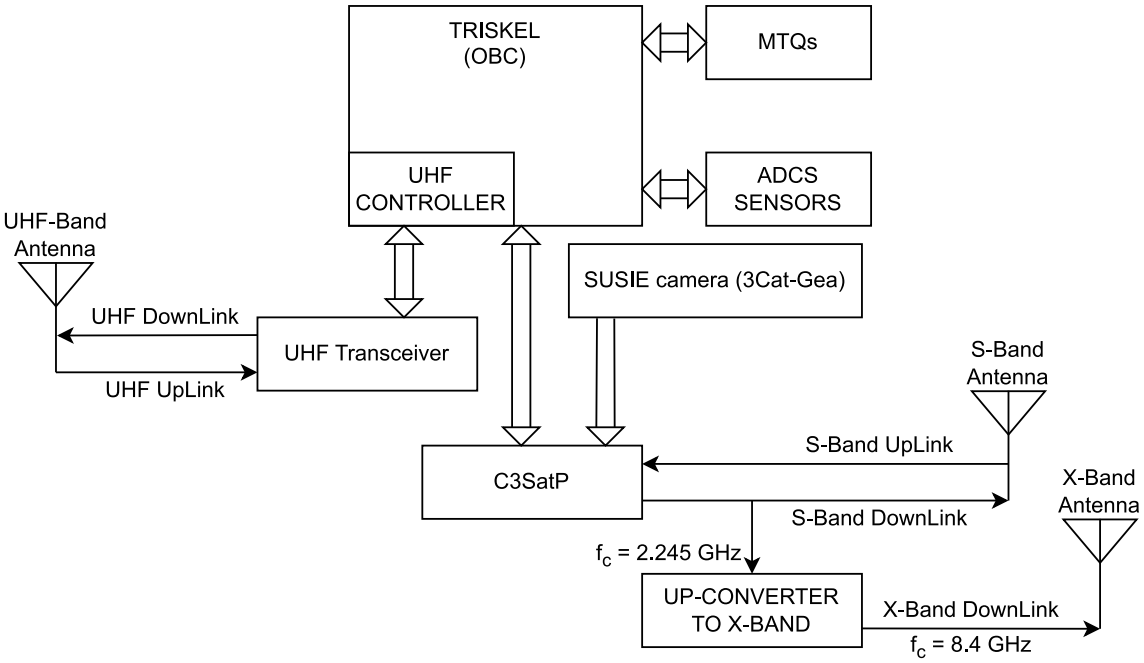

Figure 1.6: 3Cat8 subsystem architecture.

1.6.2.1. Electric Power Subsystem (EPS)

The EPS is in charge to gather, store and distribute electrical power to the satellite. It consists of a battery that is recharged through solar panels installed on the outer surface of the satellite, as well as all the power distribution elements for the other subsystems, such as the On-Board Computer (OBC).

1.6.2.2. Attitude Determination and Control System (ADCS)

The ADCS subsystem will enable the system to perform its missions properly such as mitigating oscillations after deployment (detumbling maneuver), pointing to the ground station allowing the communications system to work correctly or pointing to the sun (Sun Pointing) to obtain energy through the photovoltaic cells installed on the outer surface of the entire satellite.

The actuator devices that this system will consist of will be 6 magnetorquers (2 per axis to increase the control authority while keeping the power consumption between margins).

1.6.2.3. Communications subsystem (COMMS)

Regarding the Communications systems, there will be principally five subsystems:

- **UHF** is a very limited link so it will only be able to send simple messages. It will be used to upload telecommands or download telemetry and tracking information.
- **S-Band** will have two main tasks: The downlink will be responsible for downloading data from scientific experiments and the uplink for sending updates to the software of the satellite (new configurations or small programs).

- **LoRa** subsystem will be the main gate to communicate with the two PocketQubes. This subsystem will not take importance in this Bachelor's thesis.
- **X-Band** subsystem will mainly be used to download the scientific data.
- **Iridium** will be used to transmit telemetry data such as the satellite's GPS position.

1.6.2.4. On-Board Computer (OBC)

The On-Board Computer will be Alen Space's Triskel. The company's OBC also includes a Telemetry, Tracking and Command (TT&C) module. This computer also provides ADCS interfaces, this fact will become important in the chapter 4

1.6.2.5. Ground segment (GS)

The Ground segment is a crucial component of the mission. It is where the data gathered by the satellite is received and the telecommands are sent.

The main facility of the NanoSat Lab Ground segment is the ground station located in the Montsec mountain. There, the operator has the capability of uploading telecommands and downloading data from previously launched missions. This ground station has three transceivers that allow it to operate in UHF, VHF and S-Band. However, there are still no X-Band capabilities, which will be necessary for the 3Cat-8 mission and it is currently in its early development phase.

CHAPTER 2. STATE OF THE ART

The objective of this chapter is to provide the current context of space technology and offer a summary of the current state of relevant technology for this Bachelor's thesis.

2.1. Historical introduction

The event that marked the beginning of the space age in 1957 was the publication of the rocket equation by the Russian scientist Konstantin Tsiolkovsky in 1903 (see Equation 2.1). This equation implied that a device could eject a portion of its mass in one direction to obtain acceleration in the opposite direction. It is the fundamental principle on which all rocket science is based today. This principle allowed for the appearance of satellites in the mid-20th century.

$$\Delta v = v_e \ln \frac{m_0}{m_1} \tag{2.1}$$

The space age began in a context of tension between the Western and Eastern blocks that emerged after World War II. The main characters in this conflict were the United States (US) and the Union of Soviet Socialist Republics (USSR). This confrontation started at the end of World War II and lasted until the fall of the USSR in 1991. In this context of political, economic, social, ideological, and military rivalry, both blocks devoted significant amounts of time and economic resources to the development of technologies with military intentions. In 1957, the Soviets achieved the launch and orbiting of the first satellite in history, Sputnik I. This event marked the beginning of what was called the space race. Over the following years, a technological revolution took place, propelling the emergence and development of new technologies intended for espionage and, if necessary, for warfare. However, many of these technologies not only proved to be useful for space systems but also laid the foundation for other important applications, such as Magnetic Resonance Imaging (MRI). Another example is the development of GPS technology. In 1961, the USSR initiated human space travel by sending Yuri Alekséyevich Gagarin into space. One of the greatest milestones of the space race occurred in 1969 when the United States successfully landed a man on the moon, and Neil Armstrong uttered the famous phrase, "That's one small step for man, one giant leap for mankind".

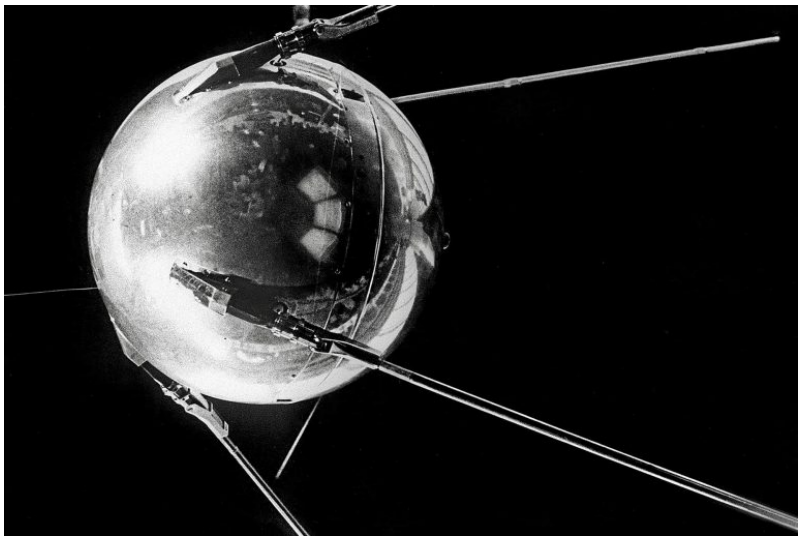

Figure 2.1: Sputnik I, the first satellite. [5]

In December 1958, the *Signal Communication by Orbiting Relay Equipment* was launched, considered the first communications satellite. However, it was a mission aimed at studying the feasibility of satellite communication links. It wasn't until 1962 that NASA launched *Telstar 1*, which performed the first transmission of television images, telephone calls, and telegraph images. It also achieved the first live transatlantic television broadcast.

Figure 2.2: Telstar 1. [7]

After the Apollo moon landing, subsequent missions focused primarily on the exploration of the solar system. The early missions aimed at exploring Venus, Mars, and the Moon. The *Venera 7* probe was the first to transmit data from the surface of another planet. Additionally, the *Pioneer* probes were sent to primarily explore the gas giant planets (Jupiter, Saturn, Uranus, and Neptune). Later, in 1977, the *Voyager* probes were launched ([8]).

Their main objective was to explore the outer reaches of the solar system. Both Voyager probes are still active today. In 2022, NASA reported that Voyager 1 was located approximately 23.733.708.715 km from Earth.

Figure 2.3: Voyager 2. [9]

During the first five decades of the space age, all launches were carried out by governmental organizations. This was mainly due to the enormous economic and human resources required to undertake such large-scale missions. However, the flourishing of the private space sector has greatly facilitated access for companies aiming to make their mark in this still relatively unexplored industry. This new phase, characterized by the commercialization of services through space systems, is known as *"NewSpace"*. One of the most important elements in this context is the *CubeSat Standard* ([10]).

2.2. The CubeSat Standard & Nano-satellites

The CubeSat standard was created by Stanford University and Cal Poly with the aim of enabling access to space for research institutions. The main idea is to standardize the size and weight to provide an affordable and reliable supply of Commertial Off-The-Shelf (COTS) components. By regularizing the size of the satellites, it becomes possible to replicate launches using platforms called P-PODs. This allows the opportunity to piggyback these small projects on the launches of larger missions and send them into space.

Nano-satellites are low-cost satellites that range in weight from 1 to 10 Kg. These kinds of satellites are usually developed following the 'CubeSat Standard'. A 1 Unit CubeSat is a 10x10x10 cm size cube. Multiple configurations of greater size and weight are also according to the mission's requirements. Some usual configurations are shown in 2.4.

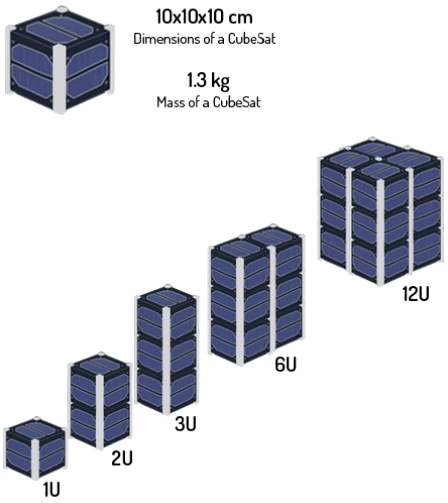

Figure 2.4: CubeSat Unit standards. [12]

The principal advantage of nano-satellites is the cheap and easy access to space, allowing the deployment of satellites for education. It is also an advantage for small companies or start-ups that want to develop space projects in order to offer commercial services.

In recent years, and thanks to the mentioned CubeSat Standard, the space sector has flourished increasing the number of satellites sent into space (figure 1.1). In addition, multiple organisations, both private and public, that promote space exploration have emerged such as the NanoSat Lab, Sateliot, Fossa Systems, etc. (2.5).

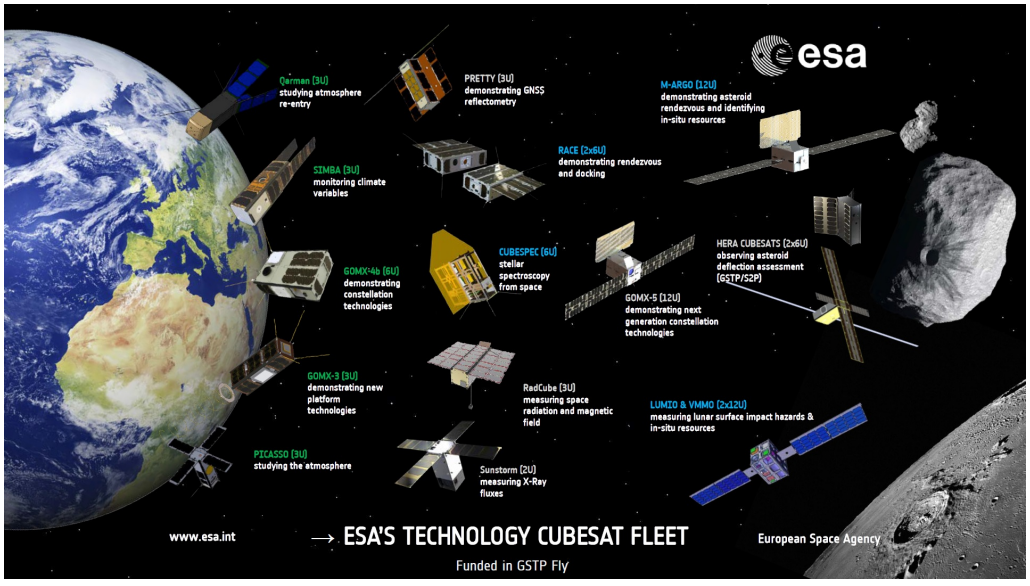

Figure 2.5: ESA's Technology CubeSats. [11]

2.3. CubeSat Antennas

Antennas are one of the most important elements in the design and manufacture of nanosatellites as they allow communication with the satellite.

Below are described the most commonly used antennas in CubeSats, as well as their characteristics, advantages, disadvantages, and commercial and homemade solutions for them.

2.3.1. Dipole and Monopole Antennas

One of the most commonly used types of antennas in general are dipole and monopole antennas, such as those used in television and radio. Specifically, monopole antennas are one of the most important types of antennas in CubeSat applications.

Monopole antennas are basically metal rods. They are very cheap and easy to manufacture. They have an omnidirectional radiation pattern, which allows for a much longer contact time between the satellite and the ground station than any other antenna, without the need for tracking. However, they are antennas that provide poor link characteristics, mainly due to their low transmission speed and small gains. For this reason, they are used in the UHF and VHF frequency range and are also only used in Telemetry, Tracking and Command transmissions, or to transmit small amounts of data transmissions.

Currently, there are multiple companies in the market that offer commercial solutions for this type of antenna, such as ISISPACE or NanoAvionics.

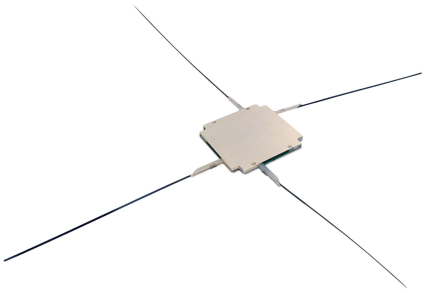

(a) ISISPACE Dipole antenna. [13]

(b) NanoAvionics Monopole antennas. [14]

Figure 2.6: CubeSat Antenna examples.

In educational environments such as the NanoSat Lab, where the production cost is an influential factor in the design of nanosatellites, these antennas have historically been manufactured using a tape measure. This is a low-cost and easy-to-manufacture solution.

Below are two examples of such implementations: NASA's "PhoneSat 2.5" satellite and NanoSat Lab's "3Cat1" (Figure 2.7).

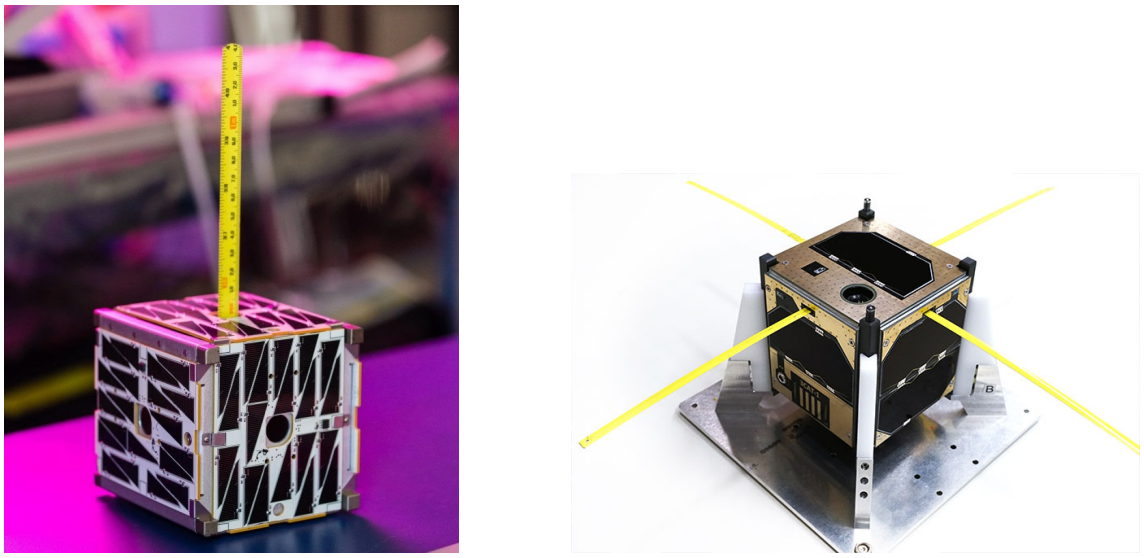

(a) NASA's PhoneSat 2.5 CubeSat. [13]

(b) 3Cat-1.

Figure 2.7: Examples of homemade measure tape antennas.

2.3.2. Patch Antennas

This type of antenna is the most commonly used in CubeSat satellites due to their physical characteristics. Firstly, they are flat antennas, which makes it very easy to install them on the surface of one side of the satellite. In addition, these antennas have radiation characteristics that facilitate the operation of the communication system. Their characteristic radiation pattern presents intermediate gains (between 5 and 7 dBi) and a considerably wide beam width (around 70 degrees). A typical radiation pattern of a patch antenna can be seen in the diagram below.

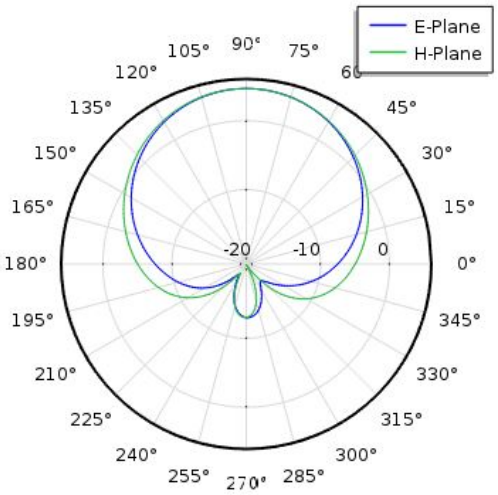

Figure 2.8: Patch antenna radiation pattern. [16]

These antennas are commonly called "microstrip antennas" because they are designed using this technology. They are formed by a ground plane, a dielectric substrate, and the

antenna patch plane. The typical architecture of a patch antenna can be seen in Figure 2.9.

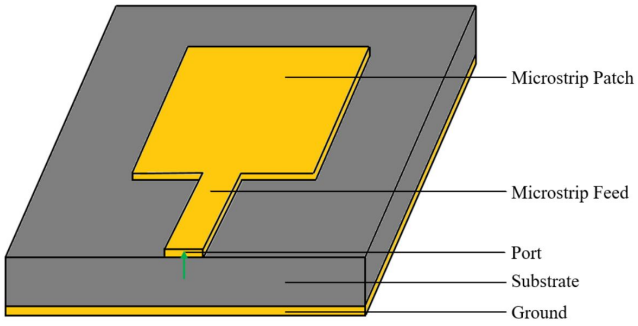

Figure 2.9: Patch antenna architecture. [17]

There are several companies that offer commercial, compact, and efficient patch antenna solutions, such as EnduroSat, ISISPACE, and many others. Below are some examples of these products.

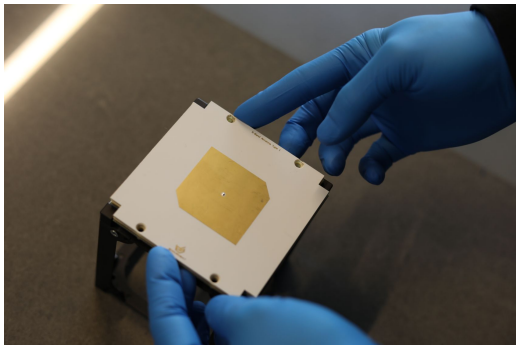

(a) EnduroSat S-band Patch antenna.

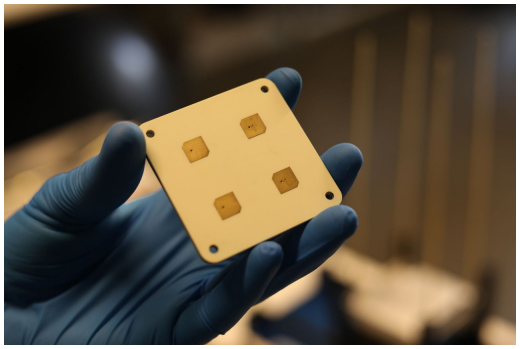

(b) EnduroSat X-Band antenna Array.

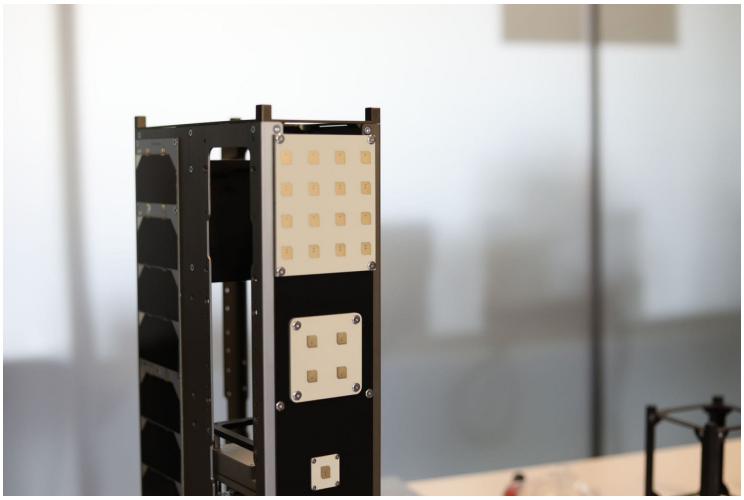

(c) EnduroSat X-Band Antenna family installed in a CubeSat structure.

Figure 2.10: Commercial Patch antennas. [18]

2.3.3. Other Antennas

Due to the limitations of the CubeSat standard, it is difficult to install high-gain antennas in these types of missions. The development of high-gain antennas for CubeSat systems could be a significant advancement in improving Earth-space radio links and increasing achievable data rates. This section briefly describes some experiments carried out or in progress with respect to this type of antenna.

The first example is deployable helical antennas. These types of antennas are constructed with one or more spiral-shaped rods. These antennas are stowed inside the satellite and are deployed when it is in orbit after the detumbling maneuver. These antennas are characterized by offering very high gains and circular polarizations. An example of such an antenna is the “NADS” developed for the 3Cat-4 satellite, which can be seen in Figure 1.2.

In addition, NASA has proposed designing a Ka-Band Parabolic Deployable Antenna that would allow a CubeSat to achieve extremely high gains. Such an antenna would provide a 10,000 times increase in data communication rates over an X-band patch antenna and a 100 times increase over state-of-the-art S-band parabolic antennas.

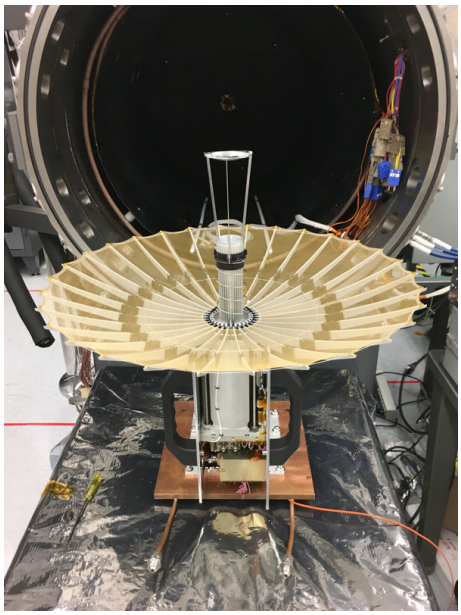

Figure 2.11: NASA’s Ka-Band Parabolic Deployable Antenna. [19]

2.3.4. Ground station antennas

The antennas of the Ground station, where satellite communications will be received, are extremely important because they are not limited by the size, weight, and power constraints as the satellites do. That is why a significant amount of resources are dedicated to these antennas. Due to their high gain characteristics, dish antennas are utilized in the ground segment of satellite links. The concept of these antennas is based on using a large parabolic-shaped ”dish” to reflect and capture the waves at the focus of the parabola. Therefore, the larger the size of the dish, the higher the gain will be.

Figure 2.12: S-Band antenna installed at the OAdM. [20]

2.4. CubeSat Control systems & actuators

An actuator is an attitude control device that, by some mechanisms, allows one to control the satellite's orientation. Actuators have the same objective but can be built with completely different technologies and they are selected depending on the application. Some typical satellite actuators are reaction or momentum wheels, thrusters or magnetic actuators.

2.4.1. Magnetic actuators

Nano-satellites are too small to include powerful thrusters, which is why almost all use magnetic actuators. These devices are used due to their size advantages and low power consumption. Nowdays, almost all of them use 'Magnetorquers' which will be described in the section 2.4.1.2.. Nevertheless, there are other types of magnetic actuators used in CubeSats wich also will be described.

2.4.1.1. Passive Magnetic Attitude Control (PMAC)

The attitude control of satellites, specifically the Passive Magnetic Attitude Control (PMAC), relies on the utilization of passive magnetic actuators such as hysteresis rods and permanent magnets. Passive magnetic actuators are not the most commonly employed type in CubeSats due to the significant dependence of their final outcome on the manufacturing process, as well as the inherent difficulty in theoretically predicting the ultimate result. Nevertheless, these types of solutions have already been tested in orbit, primarily in use for very small satellites (typically 1U to 3U CubeSats, see figure 2.4), owing to their limited capacity for generating dipole moments.

They are referred to as passive attitude stabilization devices because they do not require any power input to perform their actuation tasks, which is their main advantage. Additionally, another significant advantage of PMAC systems is their low mass requirement, which

is a crucial characteristic when designing a CubeSat.

Hysteresis rods are a type of passive magnetic actuator. Typically, it is necessary to combine these attitude-damping systems with permanent magnets, which will be described later, as hysteresis rods alone are not sufficient to efficiently perform these manoeuvres.

These rods are constructed with a material that has high magnetization capabilities (hysteresis magnetic material). This material, under the influence of an external magnetic field, becomes magnetized and stores this magnetic energy. If separated from this external field, the rod remains magnetized and continues to produce its own magnetic field, albeit weaker than the initial external field.

When there is a variation in the Earth's magnetic field, as is the case in a low Earth orbit (LEO) satellite, these rods generate a torque that can effectively reduce its oscillations. However, they are not very precise in orienting the satellite.

On the other hand, a permanent magnet does not require an external magnetic field to magnetize it. They are materials that are strongly magnetized and can generate magnetic fields indefinitely. Their magnetic field is produced by the magnetic dipoles within the material generated by the spin property of subatomic particles.

These magnets are efficient in controlling the satellite's orientation. This orientation control is achieved through the interaction between the magnet's field and the Earth's field. However, these implementations have significant limitations, as permanent magnets have a limited orientation capability.

An effective combination of hysteresis rods and magnetic magnets can result in good attitude control for small satellites, as long as the pointing limitations are not too significant.

Below is a typical configuration of passive magnetic actuators in a 3U satellite.

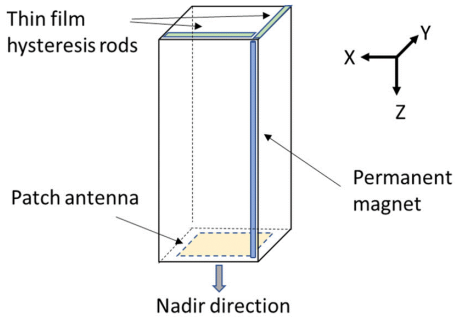

Figure 2.13: PMAC actuators configuration in a 3U CubeSat satellite. [21]

Since hysteresis rods are not commonly used, there are no commercial solutions readily available for this issue. However, permanent magnets are not exclusively designed for space applications, making them easily accessible in the market.

2.4.1.2. Magnetorquers

Magnetorquers are basically electromagnets (coils). When a current passes through the copper cable they are built with, these actuators exert a force that interacts with the surrounding Earth's magnetic field, leading to a reverse mechanical torque around the ship's centre of mass.

The advantages of magnetorquers over PMACs are as follows:

- Greater actuation capability: Magnetorquers can generate significantly higher torques.
- Full control of actuation intensity: Depending on the current input, magnetorquers can generate more or less dipole moment.
- Simpler design process: Magnetorquers have a simpler design compared to PMACs.

However, magnetorquers also have some disadvantages:

- Power consumption: Magnetorquers require power to operate, which can lead to the consumption of battery resources.
- Increased weight: The use of additional cables for magnetorquers results in a higher overall weight.

There are mainly two configurations of magnetorquers: torque rods and air core coils. The rods have a more elongated shape, while coils are more flattened and enclose larger areas as can be seen in the figure 2.15. Torque rods usually contain magnetic alloys that amplify the generated magnetic field for increased performance.

(a) Schematic of a coil magnetorquer.

(b) Schematic of a rod magnetorquer.

Figure 2.14: Magnetorquer types.

As they are the most widely used actuators in the market, there are multiple commercial options available for both coil and rod-type magnetorquers, although the latter are predominantly used.

(a) ISISPACE Magnetorquer Board (iMTQ) first view

(b) ISISPACE Magnetorquer Board (iMTQ) second view

Figure 2.15: ISISPACE Magnetorquer board. [22]

2.4.2. Other actuators

Although magnetic actuators are predominantly used in nanosatellites, traditional actuators such as reaction wheels have also been adapted to the size constraints of CubeSats. Furthermore, new ideas are being put into practice, such as electric thrusters. The following section describes these two types of actuators.

2.4.2.1. Reaction Wheels

Reaction Wheels, also known as momentum wheels, are attitude control devices used in satellites of all types, including CubeSats. They consist of a rotating wheel mounted on an axis. By generating angular momentum in the wheel, the satellite will start to rotate in the opposite direction due to the conservation of angular momentum. It is this principle that allows for the control of the satellite's attitude.

These are the most commonly used actuators in satellites. This type of actuator allows for precise and stable orientation of the satellite, which is essential for conducting scientific experiments that require accurate pointing, such as Earth observation or communications. However, they have a relatively short lifespan due to the wear of their mechanisms.

Reaction Wheels are the most commonly utilized actuators in satellites. They enable highly precise and stable satellite orientation, which is crucial for conducting scientific experiments that require accurate pointing, such as Earth observation or communications.

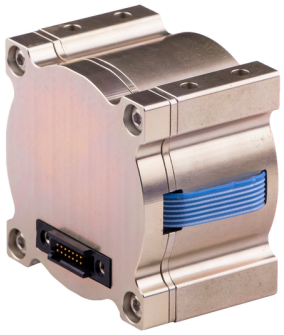

Figure 2.16: CubeSpace GEN1: CubeWheel. [23]

CHAPTER 3. COMMUNICATION SYSTEM

In this chapter, an analysis of the communication subsystems in the UHF, S, and X bands is conducted. A study of the links and their characteristics is performed for each band. The analysis includes calculating the Signal-to-Noise Ratio (SNR) for various elevation angles. Based on the results of this analysis, the appropriate antenna type for the X-Band subsystem will be selected, and a design for the S-band antenna will be developed.

3.1. Space communications analysis

Space communications is a specific branch within the field of communications that presents unique challenges compared to traditional radio links. The primary purpose of space communications is to receive scientific data collected by the satellite on Earth through the ground station and transmit Telemetry, Tracking and Command (TT&C) data from and to the satellite. Additionally, in manned missions such as trips to the International Space Station, communications are crucial for maintaining contact with the astronauts.

Unlike conventional radio links, satellite communications involve transmitting signals through space and the atmosphere. One of the main challenges is the long distances that the waves must travel to reach the ground station. To mitigate these issues, high transmitted powers, high-gain antennas, advanced modulation and coding techniques, as well as proper planning of the satellite-to-ground station connections, are required. Another challenge is signal attenuation due to propagation through the atmosphere, interference from other electromagnetic sources, and the presence of noise in communication links.

All aspects necessary to understand the communications link between the 3Cat-8 satellite and the Ground Station (GS) will be detailed below.

3.1.1. Orbits introduction & the 3Cat-8 orbit

In order to design a communication link between Earth and a satellite, it is necessary to have a detailed understanding of how a satellite behaves in orbit. This section aims to provide a brief introduction to orbits, specifically focusing on the orbit of 3Cat-8, which is relevant to this work.

3.1.1.1. Kepler's Laws

In 1619, Kepler enunciated his third law. The three laws described by the German scientist describe the geometry and kinematics of the orbits of planets around the Sun and provide a mathematical description of these orbits. Years later, Isaac Newton published the Law of Universal Gravitation, which states that all objects in the universe attract each other with a force proportional to their masses and inversely proportional to the square of the distance between them. Kepler's laws are fundamental in the understanding of orbits, and their meanings are as follows:

1. **Law of orbits**: Planets revolve around the Sun, following elliptical orbits. The Sun is located at one of the foci of the ellipse.

2. **Law of areas**: This law states that planets, while in orbit, sweep out equal areas in equal times. This implies that a planet moves faster when it is closer to the Sun (at perihelion, the point closest to the Sun in the orbit) and slower when it is farther away (at aphelion, the point farthest from the Sun in the orbit).

3. **Law of periods**: This law states that the square of the orbital period of a planet (the time it takes to complete one orbit around the Sun) is proportional to the cube of the semi-major axis of the orbit (half the distance between the perihelion and aphelion). In other words, the greater the average distance of a planet from the Sun, the longer it will take to complete its orbit.

$$T^2 \propto a^3 \tag{3.1}$$

Currently, orbits are defined using a set of parameters known as "Keplerian elements". These elements are a set of parameters that perfectly describe the orbit of an object in space. The Keplerian elements include the following: Semi-major axis (a), Eccentricity (e), Inclination (i), Argument of periapsis (ω), Right ascension of the ascending node (Ω), Mean anomaly (M).

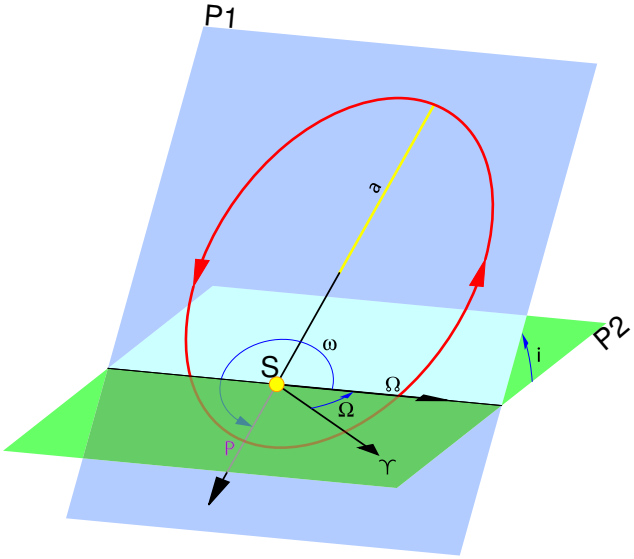

Figure 3.1: Keplerian elements. [25]

These Keplerian elements provide a comprehensive description of the orbit of an object and are commonly used in orbital mechanics and astrodynamics to analyze and predict the motion of satellites and other celestial bodies.

The Keplerian elements are part of the information that a satellite must transmit to the ground station. These parameters are transmitted within a data package called Two-Line Element (TLE). TLE files contain precise information about the orbital trajectory, position, and velocity of a satellite at a given moment. The main purpose of these files is to provide accurate and up-to-date information about the orbital trajectory of satellites. They are primarily used for satellite navigation but are also useful for determining the satellite's position at a certain time and pointing the ground station antenna to optimize the link characteristics. These files are part of the data encompassing the Telemetry, Tracking, and Command (TTC) information.

3.1.1.2. Geocentric orbit types

Indeed, an object with sufficient velocity can orbit the Earth, and it will follow Kepler's laws. However, the possibilities that Kepler's laws present are countless. Multiple types of orbits can manifest, and as a result, orbits can be classified in various ways. Orbits can be classified according to their altitude, inclination, or the shape of their orbit (elliptical or circular).

Classifying orbits according to their altitude, three main types can be distinguished: Low Earth Orbit (LEO), Medium Earth Orbit (MEO), and High Earth Orbit (HEO). The first type includes all satellites below 2,000 km of altitude. Satellites ranging from 2,000 to 36,000 km are classified as MEO, and those above that limit are defined as HEO. Additionally, an additional type called Geosynchronous Earth Orbit (GEO) can be added. This is a type of orbit whose period coincides with the rotation period of the Earth. The *Syncom 2*, launched in 1963 by NASA, was the first geosynchronous satellite in history. Geostationary orbits are a type of geosynchronous orbit with a ground track that is a single point, meaning the satellite always remains over the same point. Satellites in these orbits are very common and are used for communication services such as television.

A Sun-synchronous orbit is a type of orbit around the Earth in which a satellite maintains a constant angle relative to the Sun. This means that the satellite passes over any given point on the Earth's surface at the same local solar time during each orbit. Sun-synchronous orbits are often used for Earth observation applications. Sun Synchronous Orbits require a specific inclination, with a typical value around 97°, which depends on their orbital altitude.

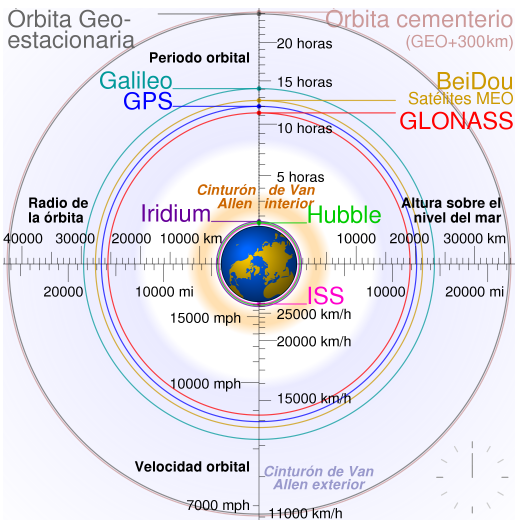

Figure 3.2: Diferent satellite constellations and orbit ranges. [26]

For the classification based on inclination, polar orbits and equatorial orbits are included. It is common to find scientific satellites in polar orbits because, due to their flight path, the satellites pass over different geographic areas in each orbit and can provide complete coverage of the Earth's surface. This makes them very convenient for remote sensing applications. Additionally, if they are low-altitude orbits, they are very fast, allowing a satellite to make multiple revolutions in a day.

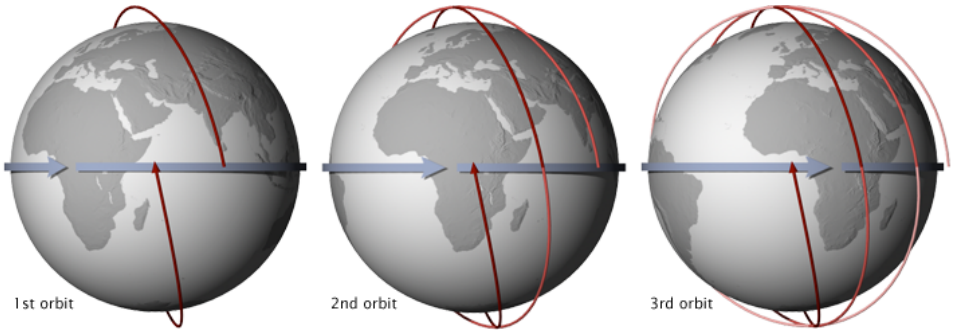

Figure 3.3: Polar Orbiting satellite. [27]

3.1.1.3. The 3Cat-8 orbit

One of the payloads of the 3Cat-8 satellite aims to study the polarization of the auroras borealis, which makes it necessary for the satellite to have a Sun-synchronous, and therefore polar, orbit. Additionally, this orbit will be a LEO with an altitude known to be between 450 and 600 km. The exact flight parameters of 3Cat-8 will be determined by the launch authority closer to the launch date. In the meantime, it will be assumed that the satellite will be in a 600km Sun-Synchronous Orbit, as this value is the most restrictive in terms of the communication links. The following is a 3D simulation of the 3Cat-8 satellite in orbit.

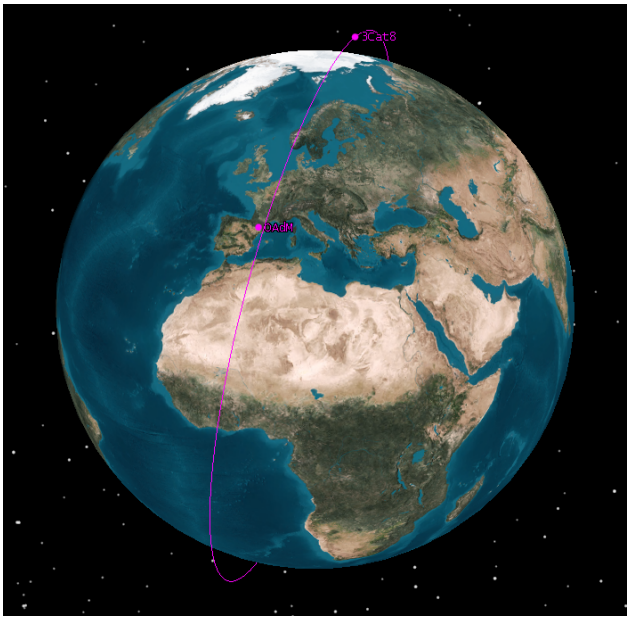

Figure 3.4: STK 3D simulated 3Cat-8 Orbit.

The TLE files for 3Cat-8 will not be generated until the satellite is in orbit. To visualize the ground track of 3Cat-8, a polar orbit with a TLE file has been simulated and plotted on a map of the Earth. The characteristics of the simulated orbit are an inclination of 97° and an altitude of 600 km. The ground track of a satellite is the path it follows on the Earth's surface. It can be determined by imagining a straight line between the satellite and the center of the Earth and plotting the coordinates where the line intersects the Earth's surface.

Due to the characteristics of a polar LEO orbit, we can obtain relevant information for the link. It can be deduced that the satellite's velocity will be very high, requiring a frequency tracking device called a Phase Locked Loop (PLL) to mitigate the effects of Doppler shift. Additionally, the orbital period will be very short, allowing the satellite to pass over the ground station multiple times a day, as shown in the following figure.

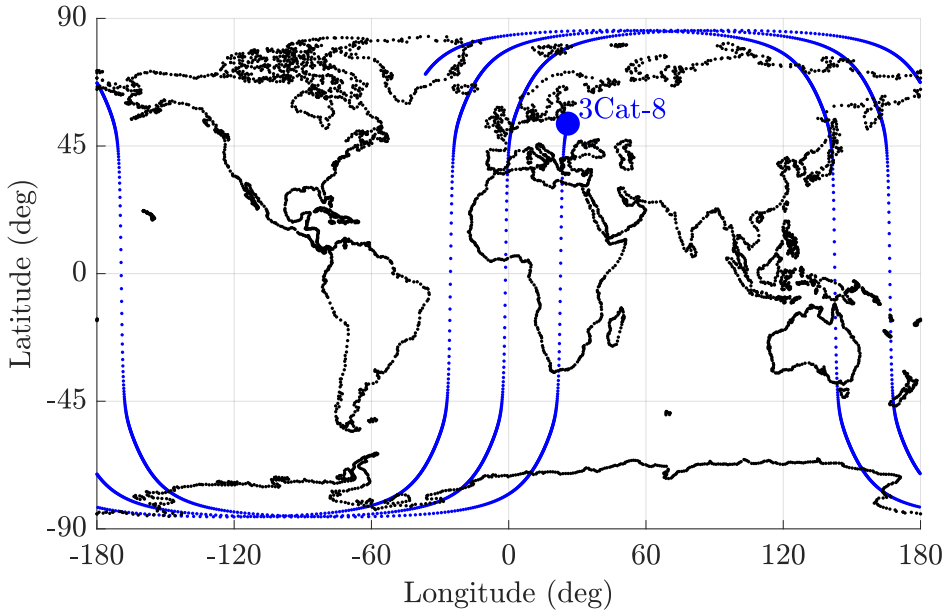

Figure 3.5: Simulated ground track of the 3Cat-8 satellite.

Certain relevant calculations for the link will be carried out below. First, the orbital period and the number of orbits per day will be calculated. The orbital period can be determined using the following formula:

$$T = 2\pi\sqrt{\frac{a^3}{GM}} \quad [s] \tag{3.2}$$

Assuming a circular orbit and an orbital altitude of 600 km, the semi-major axis (*a*) is obtained by adding the altitude to the radius of the Earth (6,371 km). *G* is the universal gravitational constant ($6.674E-11\left[\frac{m^3}{Kg\cdot s^2}\right]$), and *M* is the mass of the central object, which in this case is the Earth ($5.972E24\,[Kg]$). Finally, the orbital period is 5792.5 seconds, which is equivalent to 1 hour and 36 minutes. Therefore, the satellite completes 14.9 orbits around the Earth per day. 15 orbits per day represent a significant number of potential passes over the ground station (located in Montsec).

3.1.2. Introduction to radio links & link budgets

The link budget is a powerful tool used in the design of various types of radio links. It involves a theoretical analysis aimed at evaluating and calculating the feasibility of a radio

link. This involves simulating the conditions and characteristics of the link and calculating the quality of the received signal to determine if it meets the requirements of the link. The link budget helps optimize the configuration of parameters and devices involved in the link. It allows for estimating coverage, signal quality, and other applications.

Satellite links are highly sensitive due to the significant losses experienced by waves while traveling between the transmitter and receiver. To mitigate these losses, a thorough analysis and appropriate selection of the components comprising the transmission and reception chain are required, including antennas, among others. The devices typically used in these applications are often expensive due to the high requirements of the link.

In the link budget, multiple parameters must be taken into account, such as transmitted power, antenna gain, etc. All of these parameters will be detailed below, followed by the calculation of the three bands.

The link budget is primarily based on a power calculation, from the transmitted power to the received power, taking into account all the gains and losses experienced by the electromagnetic wave during its journey. These gains or losses can be due to the antenna, amplifiers, cables at the receiver, etc. The essence of the link budget can be seen in the following formula.

$$P_{RX} = P_{TX} \cdot \frac{\prod_{i=1}^{N} G_i}{\prod_{j=1}^{M} L_j} \quad [W] \tag{3.3}$$

This same expression can be translated into decibels. Decibels are a measure of the ratio between quantities that, in communications, are used as power ratios. Due to logarithmic properties, what was previously a multiplication now becomes an addition, which greatly simplifies the calculation.

$$P_{RX} = P_{TX} + \sum_{i=1}^{N} G_i - \sum_{j=1}^{M} L_i \quad [dBW] \tag{3.4}$$

Knowing the characteristics of the orbit, it is possible to perform a comprehensive analysis of this link. The following illustration shows a simple diagram of the link and some parameters that will be taken into account.

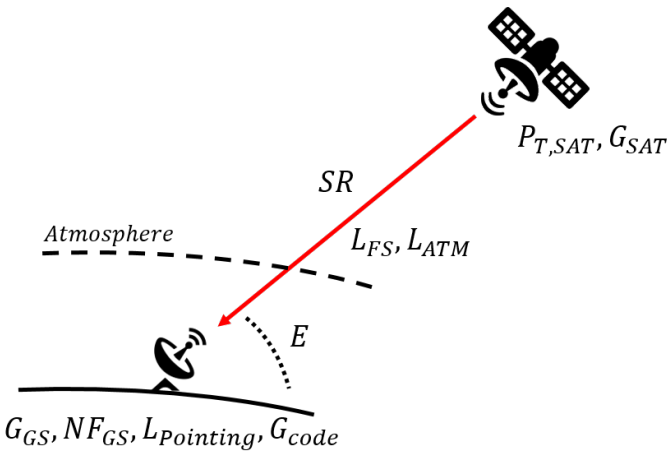

Figure 3.6: 3Cat-8 simulated ground track.

As mentioned, it is important to make the most of each satellite pass over the Ground Station (Observatorio Astronómico del Montsec), and therefore an analysis of the Signal to Noise Ratio at the receiver will be conducted based on the satellite's elevation angle (E). An important factor is the distance between the satellite and the receiver, specifically calculating this distance as a function of the elevation angle. This distance is referred to as the *"Slant Range"*.

3.1.2.1. Slant Range

The Slant Range is the oblique distance between a transmitter and a receiver, in the case of a satellite link, it refers to the distance between the satellite and the ground station. This distance is crucial for calculating free space losses or atmospheric losses. The following diagram illustrates how to determine the Slant Range.

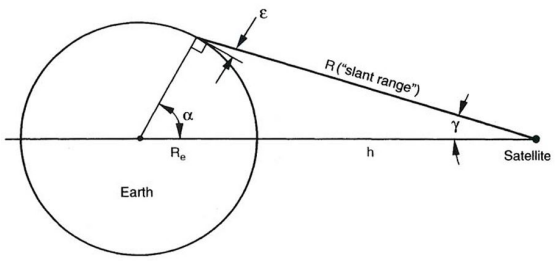

Figure 3.7: Slant range. [28]

The formula to calculate the Slant Range is:

$$SR = \sqrt{(R_e + h)^2 - (R_e \cdot \cos E)^2} - R_e \cdot \sin E \quad [m] \tag{3.5}$$

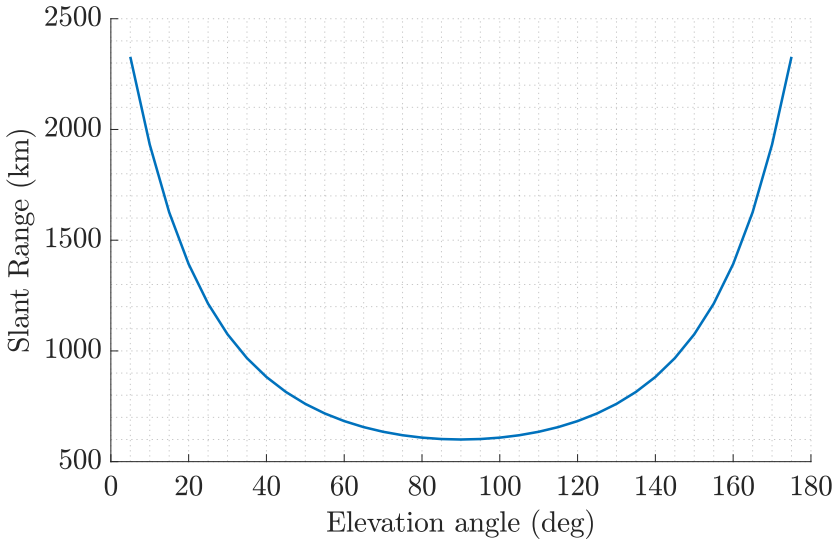

Figure 3.8: Slant Range vs elevation angle.

3.1.2.2. Electromagnetic waves

The main element used in telecommunications is electromagnetic waves. These waves form the basis for the transmission of signals over long distances. In 1864, the British physicist James Clerk Maxwell formulated Maxwell's equations, which unified the phenomena of electricity and magnetism. These equations describe the behavior of electric and magnetic fields and their interactions with sources. They lead to the conclusion that a varying electric field can generate a magnetic field, which in turn can generate another electric field. This feedback between the two fields results in an electromagnetic wave with a speed of $c = 3 \times 10^8 \left[\frac{m}{s}\right]$, the speed of light. Later on, Heinrich Hertz demonstrated that electromagnetic waves could be generated by oscillating electric charges and propagate through space.

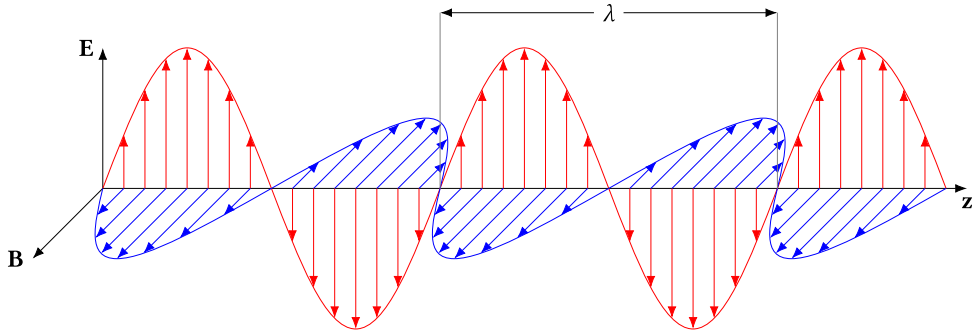

Figure 3.9: Electromagnetic waves. [29]

These electromagnetic waves can be configured or modulated in a desired manner to transmit information. Initially, analogue modulation was used, where the signal itself carried the information. Later, digital modulation was introduced, where the information (bits) was encoded in the waveform.

Electromagnetic waves have two components: the electric field $\vec{E}$ and the magnetic field $\vec{H}$. However, in the field of communications, power is measured in watts or, equivalently in dBW or dBm which are the equivalent units for Watts and milliwatts in a logarithmic scale.

3.1.3. Gain

Any type of power amplification in the transmission-reception chain is considered as gain. Gain is a power ratio and, therefore, is dimensionless. If the gain, in linear terms, is less than one, it means that the power is being reduced. In order to improve the characteristics and performance of a system, it is ideal to maximize the gains.

Therefore, the gain due to a particular system (such as an antenna, amplifier, etc.) is the difference between the input power and the output power. It is usually expressed in dB.

$$G = 10\log_{10}\left(\frac{P_{out}\,[W]}{P_{in}\,[W]}\right) \quad [dB] \tag{3.6}$$

The relevant gains in the proposed Link Budget for the communication links of 3Cat-8 will be described below.

3.1.3.1. Antenna gain

One of the main elements that provide power gains in a telecommunications system are antennas. The antenna is the device that transforms electrical signals into electromagnetic waves and vice versa. In this process, the signal can be amplified due to the characteristics of the antenna.

In the case of ground segment antennas, which are parabolic or “dish antennas”, the gain can be calculated using the effective area of the antenna. This effective area is a portion of the antenna’s total area that correctly reflects and radiates electromagnetic waves, and the relationship between them is called antenna efficiency. This inefficiency can be caused by different effects such as defocus or misalignment.

$$G_R = \frac{4\pi}{\lambda^2} A_{eff} \tag{3.7}$$

Being a circular aperture antenna, its physical or total area is the area of a circumference. Therefore, the effective area will be the efficiency multiplied by the total area of the antenna.

$$A_{eff} = \eta \cdot A_{phy} = \eta \cdot \pi \left(\frac{D}{2}\right)^2 \tag{3.8}$$

The Half Power Beam Width (HPBW) of an antenna is the angle at which the antenna gain is reduced by half. In parabolic antennas, it can be calculated as follows. This data will be relevant in the next section.

$$HPBW = \theta_{3dB} = 70 \left(\frac{\lambda}{D}\right) \tag{3.9}$$

3.1.3.2. Code Gain

The code gain is a virtual gain. Code gain occurs when a coding scheme, such as *Reed-Solomon (225,233)* coding, is implemented on the signal. This coding introduces redundant and parity bits within the transmitted messages, enabling error correction at the receiver if there have been any decoding errors. By employing this coding scheme, the system can tolerate a lower signal quality (measured in terms of E_b/N_0 and Signal to Noise Ratio (SNR)) while maintaining the same Bit Error Rate (BER). This difference is interpreted as a gain, hence referred to as code gain. The code gain can be interpreted as a gain of the Signal to Noise Ratio (SNR) or a reduction in the minimum required SNR.

The code gain can be obtained by analyzing the Bit Error Rate (BER) vs. E_b/N_0 curves and finding the E_b/N_0 required for the same BER used in the system. In this link, *Reed-Solomon (225, 233)* coding will be used. For the downlink links, the BER must be less than or equal to 10^{-5}. By searching for these values on the graphs, we can determine the code gain. This code gain can be computed as the difference between the minimum SNR of an uncoded signal and a coded signal.

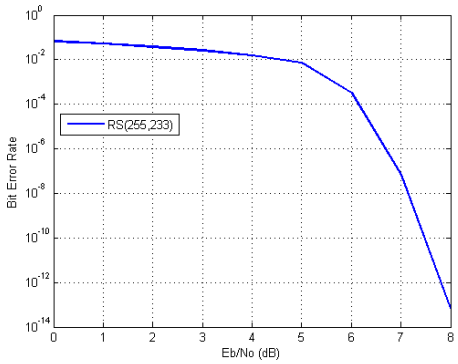

(a) RS(255,233) coded signal BER vs E_b/N_0 curve. [30]

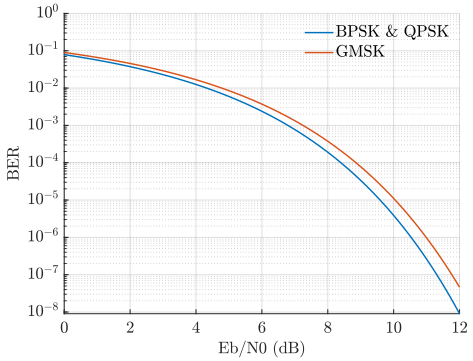

(b) BER vs E_b/N_0 for different uncoded modulated signals (BPSK is equal to QPSK).

Figure 3.10: BER vs E_b/N_0 curves.

The BER-E_b/N_0 curve of a BPSK signal is defined by the following function.

$$BER = P_b = \frac{1}{2} erfc\left(\sqrt{\frac{E_b}{N_o}}\right) \tag{3.10}$$

Based on both graphs and considering the corresponding values, the code gain can be calculated with the following formula.

$$G_{code} = [E_b/N_0(BER)]_{Uncoded} - [E_b/N_0(P_b)]_{RS(255,233)} \quad [dB] \tag{3.11}$$

The different code gains for the different analyzed cases are collected in the following table.

	BER	Code gain G_c (dB)
Uplink (BPSK & QPSK)	10^{-7}	4.31
Uplink (GMSK)	10^{-7}	4.77
Downlink (BPSK & QPSK)	10^{-5}	3.2
Downlink (GMSK)	10^{-5}	3.6

Table 3.1: Code gain for the different cases.

3.1.3.3. Receiver Gain

In this analysis, it will not be necessary to use the receiver gain, even if it is known. This is because the receiver amplifies both the signal power and the noise power equally, and when calculating the SNR, it does not introduce any change. The proof is provided below.

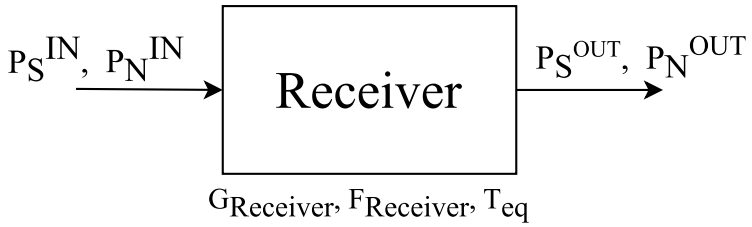

Figure 3.11: Receiver schema.

$$SNR_o = \frac{P_s^{OUT}}{P_N^{OUT}} = \frac{P_s^{IN} \cdot G_{Receiver}}{k(T_A + T_e q)BW \cdot G_{Receiver}} = \frac{P_s^{IN} \cdot}{k(T_A + T_e q)BW} \tag{3.12}$$

3.1.4. Losses

The losses in a radio link are the complete opposite of gain. They represent a decrease in signal power during its propagation. Losses, in decibels, are negative gains, but they are expressed as positive values.

$$L_i = -G_i \quad [dB] \tag{3.13}$$

3.1.4.1. Free Space Losses

As the waves propagate through space, they also experience attenuation. This power loss is directly proportional to the square of the distance travelled. Additionally, these losses also increase with the square of the frequency. Free space losses are calculated using the following formula.

$$L_{FS} = 20 \cdot \log_{10}\left(\frac{4\pi \cdot SR(E)}{\lambda}\right) \tag{3.14}$$

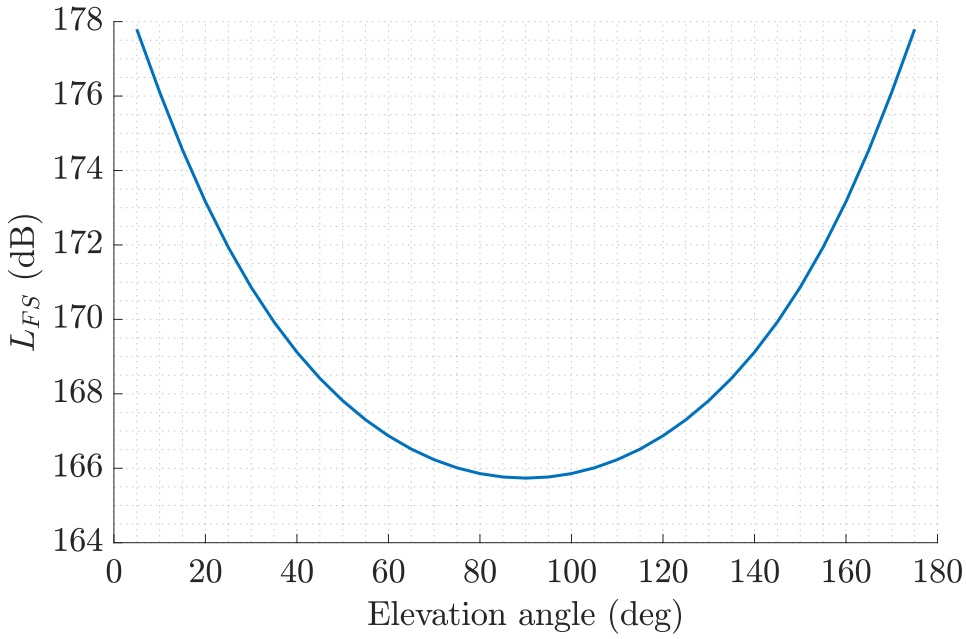

Figure 3.12: Free Space Losses vs elevation angle.

3.1.4.2. Atmospheric attenuation

Atmospheric losses are primarily caused by the absorption of electromagnetic waves by gases in the atmosphere (such as oxygen, water vapor, etc.). These losses are extremely difficult to estimate as they strongly depend on the atmospheric conditions at the time. They become significant starting from 10 GHz frequency. There are various models that can be used to estimate these losses, and the model specified by the ITU-R in Recommendation P.676-13 is utilized. This recommendation provides a mathematical model that allows for the calculation of the effects of atmospheric gas absorption (oxygen and water vapor) up to a frequency of 1000 GHz. The input variables for this mathematical model are temperature, atmospheric pressure, and water vapour density.

Given that the ground station is located in Montsec, the values will be chosen accordingly. The U.S. Standard Atmosphere ([31]) provides a mathematical model for calculating pressure at different altitudes (3.15). According to this model, atmospheric pressure is maximum at sea level (101.325 kPa) and decreases with altitude, reaching 83.43 kPa at an altitude of 1568 m, which is the altitude of Montsec.

$$P = P_o \cdot e^{-\left(\frac{a}{T}\right)\cdot z} \quad [kPa] \tag{3.15}$$

When temperatures are colder, absorption is higher. According to the historical temperature data in the Montsec area, the average of the daily minimum temperatures is 3ºC. Therefore, this value will be used to calculate these losses.

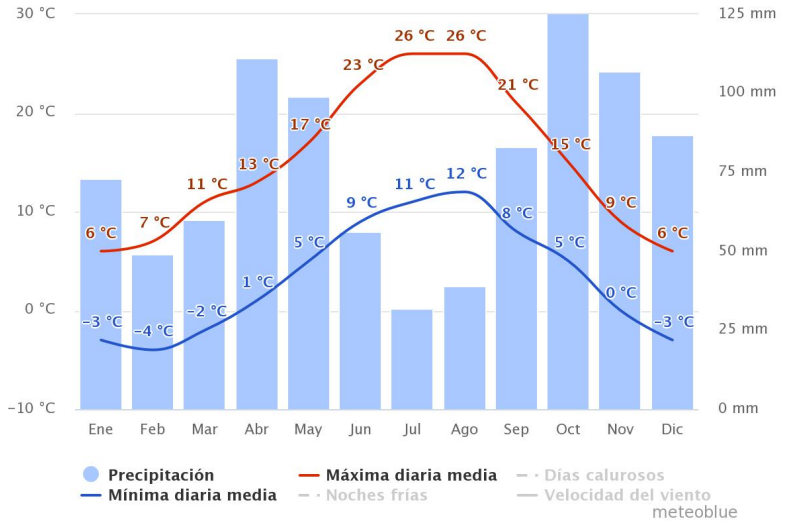

Figure 3.13: Historical record and model of temperatures at Montsec site. [32]

In addition, according to the book *"Microwave Radar and Radiometric Remote Sensing"* ([33]), a water vapour density of $15 g/m^3$ is quite restrictive. Therefore, this value will be used to calculate the atmospheric losses. With these three data points, it is now possible to calculate the specific attenuation due to gases. These specific attenuations were calculated using the "gaspl" function in MATLAB, which calculates them based on the model provided by ITU-R. The following figure shows that there is a peak at 60 GHz, which corresponds to the molecular resonance frequency of O_2. At this frequency, the molecule absorbs a greater amount of electromagnetic radiation. The frequencies relevant to this work are stated in section 1.6.2.5.. In the S and UHF bands, these losses are negligible. However, in the X band, these attenuations are significant enough to be taken into account.

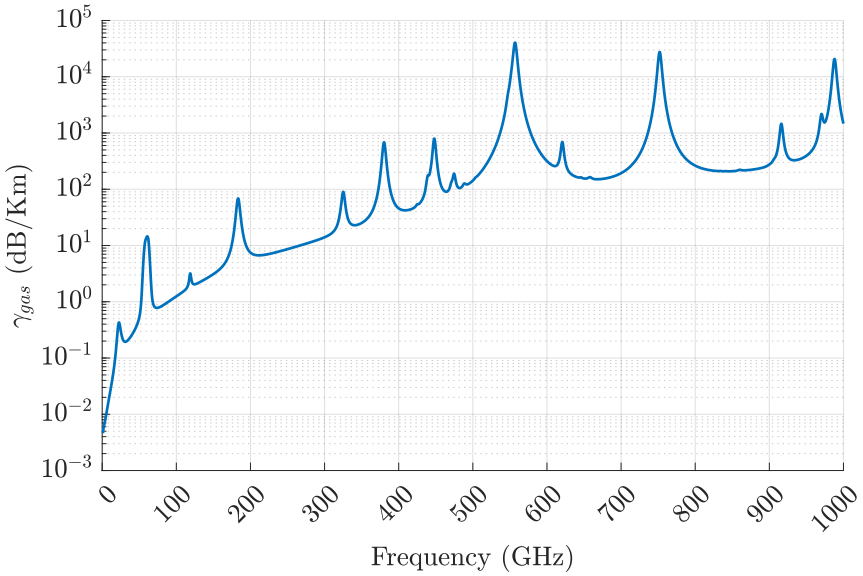

Figure 3.14: ITU-R P.676-13 specific attenuation by atmospheric absorption of gases. [34]

Having the specific attenuation due to atmospheric gas absorption ($0.017 dB/km$), it is only necessary to multiply it by the thickness as a function of the elevation angle to calculate the atmospheric losses.

$$L_{ATM} = (\gamma_{ox} + \gamma_{wv}) \cdot w_{ATM}(E) = \gamma_{Tot} \cdot w_{ATM}(E) \quad [dB] \tag{3.16}$$

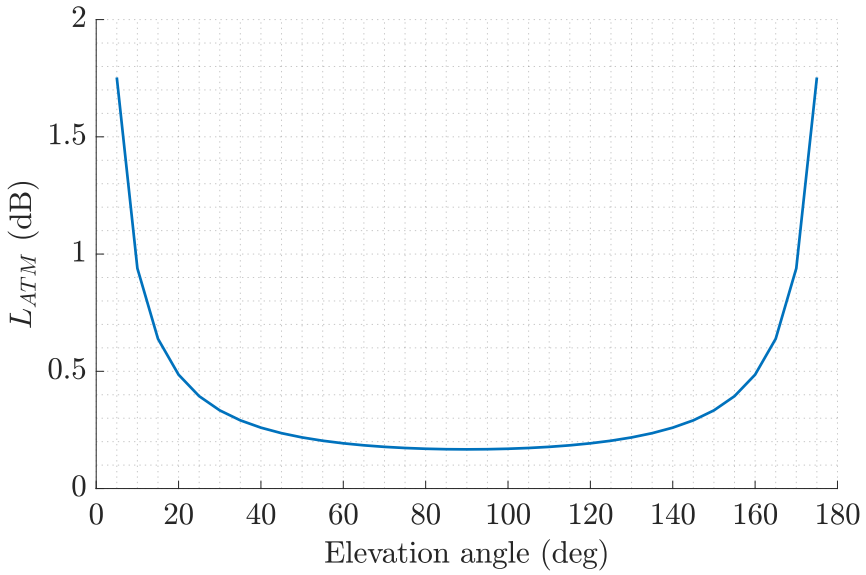

Figure 3.15: Atmospheric losses vs elevation angle.

3.1.4.3. Rain and cloud attenuation

To determine the attenuation due to rain and clouds, it is necessary to study the climatic history of the Montsec area. Referring to the data from *Meteoblue* ([32]), rainfall in this area is scarce throughout the year and of low intensity. Additionally, a weak cloud cover is present only about 20% of the year. The location of the OAdM was chosen because it is one of the areas with the highest percentage of clear skies in Catalonia. For these reasons, the losses due to rain and cloudy atmosphere will be negligible and will not be taken into account in the link analysis.

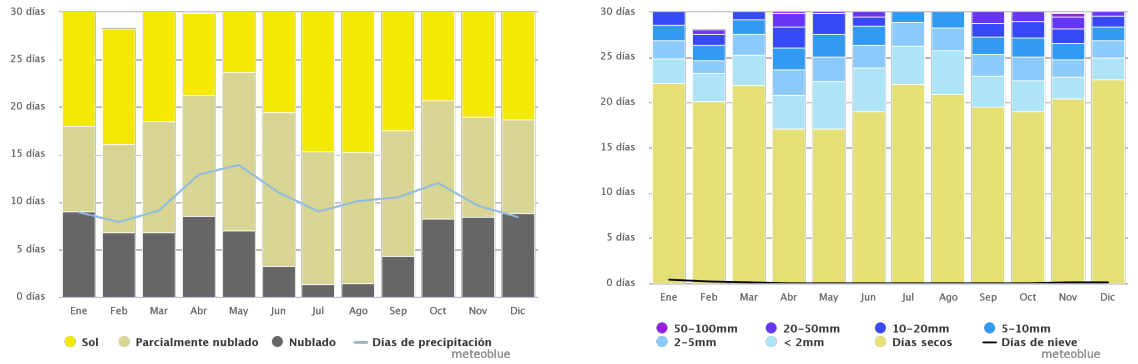

(a) Cloud cover in the montsec.

(b) Rainfall in Montsec.

Figure 3.16: Meteorological data of the Montsec.

3.1.4.4. Polarization losses

Polarization losses are losses caused by the mismatch between the polarization of the signal and the receiving antenna. The polarization of an electromagnetic wave refers to the plane in which the electromagnetic field of the wave oscillates. There are three main types of polarization: linear (horizontal and vertical), circular, and elliptical.

Polarization losses can also occur due to different factors, such as improper antenna alignment, depolarization through reflection, and so on.

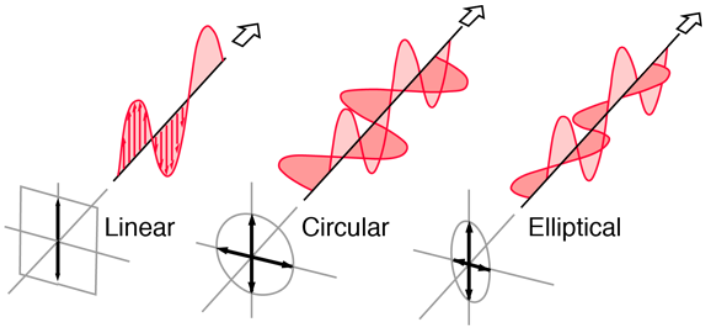

Figure 3.17: Electromagnetic wave polarization types.

The Polarization Loss Factor (PLF) is a metric that quantifies the polarization losses. It can be calculated as the square of the absolute value of the product of the polarization vectors of the incident wave ($\hat{\rho}_i$) and the receiving antenna ($\hat{\rho_a}$), or as the square of the cosine of the angle between them.

$$\hat{\rho} = \frac{\vec{E}}{\left|\vec{E}\right|} \tag{3.17}$$

$$PLF = |\hat{\rho}_i \cdot \hat{\rho_a}|^2 = \cos^2\theta \tag{3.18}$$

To obtain the losses in decibels (dB), it can be used the following formula:

$$L_{POL} = 10 \cdot \log_{10}(PLF) \quad [dB] \tag{3.19}$$

In the case of UHF, the polarization losses are at least 3 dB. These losses are due to the difference in antennas. The antenna installed on the spacecraft is a monopole, which emits waves with linear polarization, while the antenna at the ground station is a *WIMO X-Quad*, an antenna with X-shaped dipoles that has circular polarization.

For the S and X bands, the polarization losses will also be 3 dB due to the effects of the atmosphere on the polarization of the waves. The atmosphere, by affecting some polarizations more than others, causes the signal to transition from circular polarization to elliptical polarization, resulting in these losses.

3.1.4.5. Pointing Losses

Pointing losses are the losses due to misalignment of the receiving antenna with the satellite. This is caused by the directional characteristics of the antenna. The losses become significant when the angular error in pointing exceeds the half-power beamwidth (HPBW) (θ_{3db}). For parabolic antennas with larger dish diameters, the HPBW can be reduced to even less than one degree. In the simulations, a pointing error of 0.75 degrees will be considered. Since UHF antennas are omnidirectional, pointing losses are not taken into account.

$$L_{Pointing} = 12\left(\frac{\theta}{\theta_{3db}}\right)^2 = 12\left(\frac{Error\ angle}{HPBW}\right)^2 \quad [dB] \tag{3.20}$$

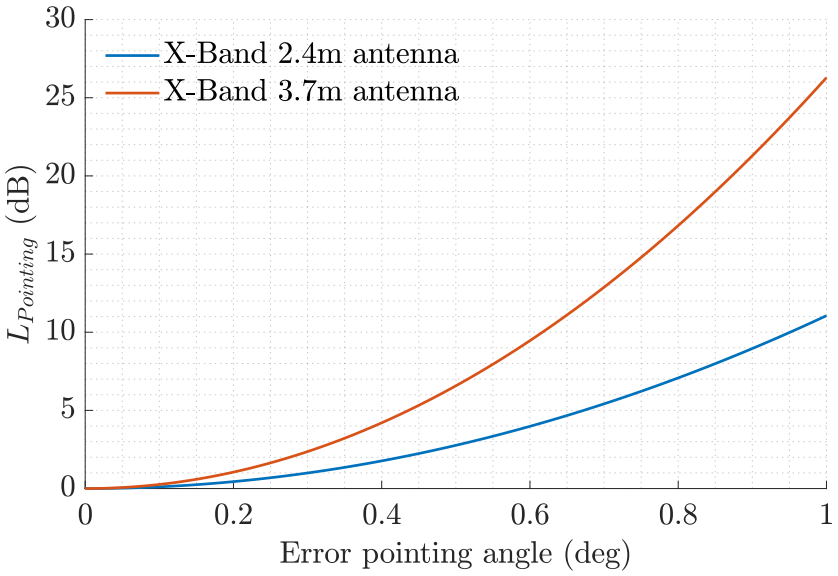

Figure 3.18: Pointing Losses vs error pointing angle.

3.1.5. Noise

Noise is an important factor to consider when designing a telecommunications link. It refers to any interference or unwanted signal that reaches the receiver, deteriorating the quality of the desired signal. A high level of noise can result in poor signal interpretation at the receiver. Noise can have various sources, such as noise generated by the electronic devices of the receiver (Johnson-Nyquist noise) or external radiations within the same frequency band.

The power of the noise can be calculated using the following formula, where k is the Boltzmann constant $(1.38 \cdot 10^{-}23J/K)$, T_{sys} is the system temperature, and BW is the receiver bandwidth. This temperature is a way to quantify noise and does not represent an actual temperature.

$$P_N = k\, T_{Sys}\, BW \quad [W] \tag{3.21}$$

The noise figure (F) is a measure of the amount of noise introduced to a signal by an electronic device. It is calculated using the following formula.

$$F = \frac{P_N^{OUT}}{P_N^{IN}} \tag{3.22}$$

The system temperature is the sum of T_0 and T_{eq}. The first term represents the antenna temperature, which is the noise captured by the antenna and depends on its pointing direction. The second term represents the receiver equivalent temperature, which is the noise temperature that is equivalent to the noise introduced by the receiver.

$$T_{SYS} = T_A + T_{eq} = T_A + T_0 \cdot (F-1) \quad [K] \tag{3.23}$$

The figure of merit is a ratio between the antenna gain and the receiver system temperature. It is a commonly used measure in space applications as it takes into account both the antenna gain and the noise added by the antenna and the receiver to the signal.

$$G/T = \frac{G_{Antenna}}{T_{Sys}} \quad \left[K^{-1}\right] \tag{3.24}$$

3.1.5.1. Signal to noise ratio (SNR)

The signal-to-noise ratio (SNR) is a measure of the signal quality relative to the level of noise. It represents the ratio of signal power to noise power. A higher SNR indicates a clearer signal and makes it easier to demodulate the information.

$$SNR = \frac{P_S}{P_N} \tag{3.25}$$

The minimum required Signal to Noise Ratio (SNR) for demodulating the signal depends on the transmission rate, bandwidth, and E_b/N_0. This parameter will be calculated to perform the link budget analysis.

$$SNR_{MIN} = \frac{E_b}{N_o} \cdot \frac{R_b}{BW} = \frac{E_b}{N_o} \cdot log_2(M) \tag{3.26}$$

Considering E_b/N_0 as the Energy per bit to noise power spectral density ratio, R_b as the bit transmission rate, BW as the bandwidth of the transmitted signal, and M as the number of symbols in the modulation.

3.1.5.2. Energy per bit to noise power spectral density ratio (E_b/N_0)

The E_b/N_0 is another measure of signal quality, different from the Signal to Noise Ratio. It is commonly used to evaluate the performance of a communication system. It represents the relationship between the energy per bit transmitted (Eb) and the noise power spectral density, measuring the ratio between the signal energy and the noise introduced by the channel.

3.1.6. Modulation

A modulation is a modification of the signal with the purpose of introducing certain information that needs to be transmitted. Nowadays, digital modulations are commonly used.

In the case of the X-band, due to the limitations of the link, only BPSK modulation can be used. In this modulation, the phase of the received signal indicates the information bits, and it only uses two states: 0 or 180 degrees.

In the case of UHF and S bands, it is possible to use BPSK, QPSK, and GMSK modulations. BPSK modulation distinguishes its bits between two phases (0 and π radians), thus having two symbols. QPSK modulation differentiates between four phases. GMSK modulation is similar to BPSK, but it distinguishes its bits by slight frequency shifts, using a Gaussian pulse response to smooth these changes in the pulses.

3.1.7. Transmission equation

Once all the factors that influence the link, such as gains, losses, or noise, have been studied, it is necessary to establish the transmission equation that obtains the desired parameter, the SNR in this case. This equation has been previously stated as (3.3), however, we are trying to calculate the SNR and not the received power. By using this equation together with formula 3.25 and 3.21, we can obtain the transmission equation for the proposed satellite link. The following are the transmission equations in both linear and decibel forms.

$$SNR = \frac{P_S^{IN}}{k(T_A + T_{eq})BW} \cdot \frac{\prod_{i=1}^{N} G_i}{\prod_{j=1}^{M} L_j} \tag{3.27}$$

$$SNR = P_{TX} + \sum_{i=1}^{N} G_i - \sum_{j=1}^{M} L_i - 10log_{10}\left(k(T_A + T_{eq})BW\right) \quad [dB] \tag{3.28}$$

Here are the equations for the uplink (UL) and downlink (DL) in each band. Please note that, for brevity, only the linear form equations are provided here, but the actual calculations were performed using the equations in decibel form. It is important to emphasize that these equations are fully equivalent.

3.1.7.1. UHF-Band Transmission equations

$$SNR_{DL}^{UHF} = \frac{P_T^{SAT} \cdot G_{SAT} \cdot (G/T)_{GS} \cdot G_{Code}}{L_{FS} \cdot L_{POL} \cdot k\,BW} = \frac{P_T^{SAT} \cdot G_{SAT} \cdot \frac{G_{GS}}{T_A + 290(F_{GS}-1)} \cdot G_{Code}}{L_{FS} \cdot L_{POL} \cdot k\,BW} \quad (3.29)$$

$$SNR_{UL}^{UHF} = \frac{P_T^{GS} \cdot G_{GS} \cdot (G/T)_{SAT} \cdot G_{Code}}{L_{FS} \cdot L_{POL} \cdot k\,BW} = \frac{P_T^{GS} \cdot G_{GS} \cdot \frac{G_{SAT}}{T_A + 290(F_{SAT}-1)} \cdot G_{Code}}{L_{FS} \cdot L_{POL} \cdot k\,BW} \quad (3.30)$$

3.1.7.2. S-Band Transmission equations

$$SNR_{DL}^{S} = \frac{P_T^{SAT} \cdot G_{SAT} \cdot (G/T)_{GS} \cdot G_{Code}}{L_{FS} \cdot L_{POL} \cdot L_{Pointing} \cdot k\,BW} \quad (3.31)$$

$$SNR_{UL}^{S} = \frac{P_T^{GS} \cdot G_{GS} \cdot (G/T)_{SAT} \cdot G_{Code}}{L_{FS} \cdot L_{POL} \cdot L_{Pointing} \cdot k\,BW} \quad (3.32)$$

3.1.7.3. X-Band Transmission equations

Since X-Band will only be used for data download from scientific experiments (mainly 3Cat-Gea), only the downlink will be implemented.

$$SNR_{DL}^{X} = \frac{P_T^{SAT} \cdot G_{SAT} \cdot G_{GS} \cdot G_{Code}}{L_{FS} \cdot L_{ATM} \cdot L_{POL} \cdot L_{Pointing} \cdot P_N} \quad (3.33)$$

3.2. Link Budget statement

In the previous section, all the important parameters to consider in the communication links of the 3Cat-8 satellite are detailed. In this section, the values of the key parameters for each communication subsystem are indicated, and if necessary, additional explanation is provided.

3.2.1. UHF-Band Characterisation

In this section, the values used in the calculation of the UHF band are presented. The Bit Error Rate (BER) is different for the uplink and downlink because the uplink will mainly be used for Telemetry, Tracking and Command (TT&C) transmissions, which are very delicate transmissions that require ensuring the correct transmission of data. TT&C transmissions involve sending very small packets, so large bandwidths are not necessary for transmitting

them. The transmission power of the Ground Station (GS) antenna is fixed at 4 W. Pointing losses due to atmospheric absorption are negligible. The Noise factor of the satellite and the base station are provided by the 3Cat-8 NanoSat Lab team. The bandwidth and transmission power of the satellite are the variables intended to be clarified with this analysis. Additionally, the parameters of the GS used are different from those published on the website ([35]) due to more recent testing data.

Parameter	Value	Unit
Physiscal parameters		
Downlink Frequency (f_c^{DL})	438	MHz
Uplink Frequency (f_c^{UL})	440	MHz
Bandwidth (BW)	TBD	MHz
Uplink Bit Error Rate (BER_{UL})	10^{-7}	-
Downlink Bit Error Rate (BER_{DL})	10^{-5}	-
Code Gain (G_c)	3.2	dB
Satellite parameters		
Transmitted Power (P_T^{SAT})	TBD	dB
Antenna gain (G_A^{SAT})	1.2	dBi
Antenna temperatura (T_A^{SAT})	300	K
Receiver Noise Factor (NF_{SAT})	3	dB
Ground segment parameters		
Transmitted Power (P_T^{GS})	4	W
Antenna gain (G_A^{GS})	15	dBi
Antenna temperatura (T_A^{GS})	38	K
Receiver Noise Factor (NF_{GS})	8.8	dB
Losses		
Polarisation losses (L_{POL})	3	dB
Free Space Losses (L_{FS})	Equation 3.14	dB

Table 3.2: UHF-Band Link budget parameters.

3.2.2. S-Band Characterisation

In the case of the S band, pointing losses are taken into account. Once again, the acceptable BER is lower for the uplink due to the reasons explained earlier. The antenna gain has been selected using the commercial antenna *"EnduroSat"* ([36]). Additionally, since the S-band downlink will be used for scientific data download, the bandwidth will need to be significantly wider, on the order of megahertz. The uplink will also be used for TTC transmissions or even software updates if necessary. Atmospheric absorption losses are below 1 dB and are considered negligible.

Parameter	Value	Unit
Physiscal parameters		
Downlink Frequency Range	2200 - 2290	MHz
Uplink Frequency Range	2025 - 2110	MHz
Bandwidth (BW)	TBD	MHz
Uplink Bit Error Rate (BER_{UL})	10^{-7}	-
Downlink Bit Error Rate (BER_{DL})	10^{-5}	-
Code Gain (G_c)	3.2	dB
Satellite parameters		
Transmitted Power (P_T^{SAT})	TBD	dB
Antenna gain (G_A^{SAT})	7	dBi
Antenna temperatura (T_A^{SAT})	300	K
Receiver Noise Factor (NF_{SAT})	5	dB
Ground segment parameters		
Transmitted Power (P_T^{GS})	4	W
Antenna Diameter (D_A^{GS})	3	m
Antenna Efficiency (η_A^{GS})	0.5	-
Pointing error angle (θ_{Error}^{GS})	0.75	deg
GS merit factor G/T_{GS}	9	dBK^{-1}
Losses		
Free Space Losses (L_{FS})	Equation 3.14	dB
Pointing Losses ($L_{Pointing}$)	Equation 3.20	dB
Polarisation losses (L_{POL})	3	dB

Table 3.3: S-Band Link budget parameters.

3.2.3. X-Band Characterisation

For the X band, the implementation of the uplink will not be carried out. The type of antenna for the satellite still needs to be decided. The options are a single-patch antenna (lower gain, higher HPBW) and a 2x2 patch array antenna (higher gain, lower HPBW). Additionally, the ground station antenna has not been installed yet, so there are two commercial options available: one with a 2.4m diameter and another with a 3.7m diameter. Finally, in X band, atmospheric losses are not negligible.

Parameter	Value	Unit
Physiscal parameters		
Frequency (f_c^{DL})	8400	MHz
BER	10^{-5}	-
Code Gain (G_c)	3.2	dB
Bandwidth (BW)	TBD	MHz
Satellite parameters		
Transmitted Power (P_T^{SAT})	TBD	dB
Antenna gain (G_A^{SAT})	6/10	dBi
Ground segment parameters		
Antenna Diameter (D_A^{GS})	2.4 / 3.7	m
Antenna Efficiency (η_A^{GS})	0.5	-
Pointing error angle (θ_{Error}^{GS})	0.75	deg
Antenna temperatura (T_A^{GS})	38	K
Receiver Noise Factor (NF_{GS})	7	dB
Losses		
Free Space Losses (L_{FS})	Equation 3.14	dB
Atmospheric Losses (L_{ATM})	Equation 3.16	dB
Pointing Losses ($L_{Pointing}$)	Equation 3.20	dB
Polarisation Losses (L_{POL})	3	dB

Table 3.4: X-Band Link budget parameters.

3.3. Link Budget results

In this section, the results of the analysis of the proposed links are detailed. The objective is to maximize the data transmission rate and minimize the transmitted power of the satellite.

3.3.1. UHF-Band results

As expected, the results for the UHF band are good. This is due to the low attenuation experienced by the waves at this frequency and the fact that the type of antenna used does not cause pointing losses, as its radiation pattern is omnidirectional.

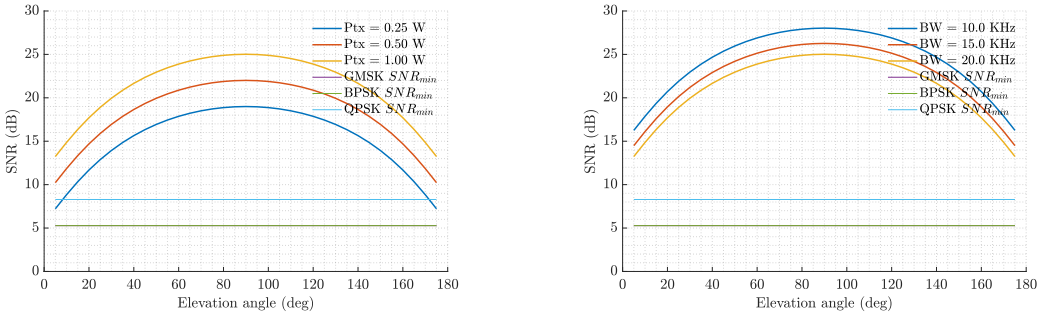

(a) SNR vs elevation angle for a fixed bandwidth of 1 MHz.

(b) SNR vs elevation angle for a fixed transmitted power of 1 W.

Figure 3.19: UHF-Band link budget uplink results.

The downlink, as usual, is the most restrictive link. This is primarily because the GS has the capability to transmit at higher powers, 4W in this case. The UHF band is a link with favorable characteristics that allows for precise transmission and reception. Since the purpose of this band is to transmit TT&C messages, it does not require large bandwidths. This protects it from the effects of noise. For this band, the goal will be to minimize the transmitted power in order to allocate it preferably to the other bands.

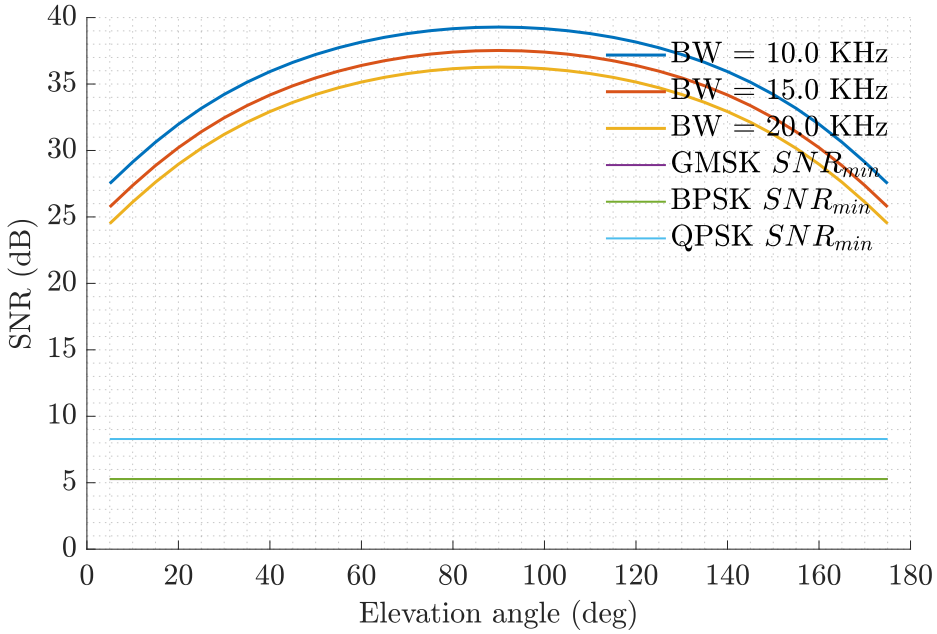

Figure 3.20: UHF-Band link budget uplink results.

3.3.2. S-Band results

Given that the S-band operates at a higher frequency than UHF, it represents a more challenging scenario. However, the results are satisfactory. It can be observed that the downlink, being the most restrictive link, achieves SNRs of up to almost 20 dB in some cases. At certain times, it will be possible to use QPSK modulation, which greatly improves the bit rate. In this case, using a power of 1 W, a bandwidth of 1 MHz, and QPSK modulation is the best option as it covers a decent range of elevation angles during which data can be downloaded at high speeds thanks to the modulation upgrade.

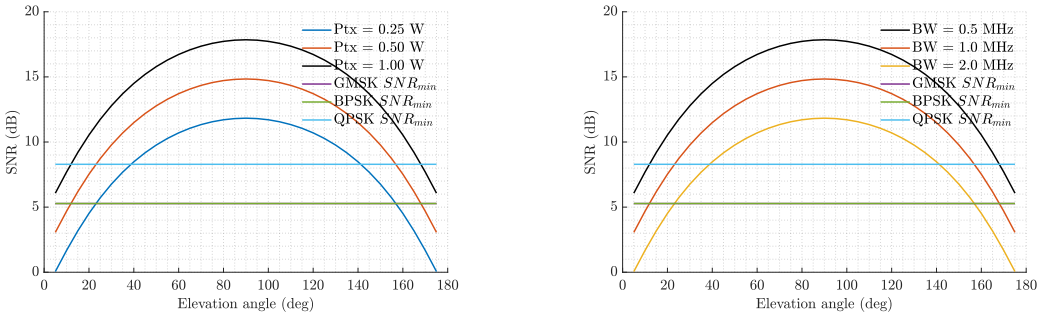

(a) SNR vs elevation angle for a fixed bandwidth of 0.5 MHz.

(b) SNR vs elevation angle for a fixed transmitted power of 1 W.

Figure 3.21: S-Band link budget uplink results.

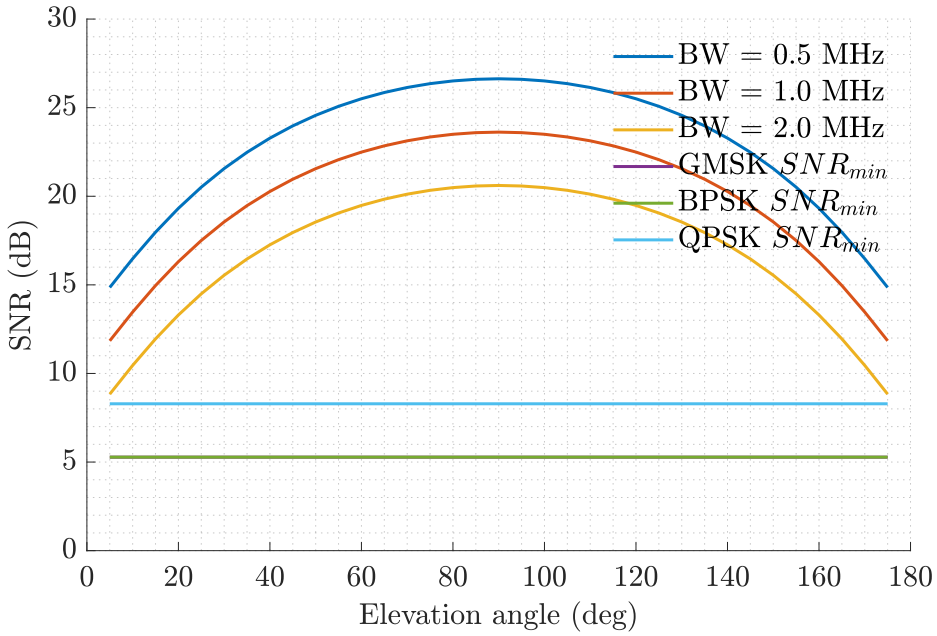

Figure 3.22: S-Band link budget uplink results (Transmitted power = 4W).

3.3.3. X-Band ground station antenna

Before continuing with the result of the link budget for the X-band, it is necessary to select the GS antenna. As mentioned earlier, the NanoSat Lab still has X-band facilities at the Observatorio Astronómico del Montsec, so it is necessary to choose the antenna to be purchased for this purpose. The NanoSat Lab has two options for commercial parabolic antennas with different possible diameters: 2.4 meters ([37]) and 3.7 meters ([38]).

To select the antenna, a balance of the "effective" or "real" gain has been performed, taking into account the losses caused by pointing errors. Since this error originates from the pointing mechanism, for the same error, we look at the effect that the antenna diameter has on the final gain. This is done by subtracting the values obtained using equations 3.7 and 3.20.

$$G_{final} = G_A(D_{GS}) - L_{Pointing} \quad [dBi] \tag{3.34}$$

By plotting the gain against the antenna diameter, it can be observed that when considering a pointing error angle of 0.75 degrees, it is better to use an antenna with a smaller diameter. This will result in a wider beamwidth and fewer pointing losses. Therefore, the 2.4-meter diameter antenna will be used for the X-band link.

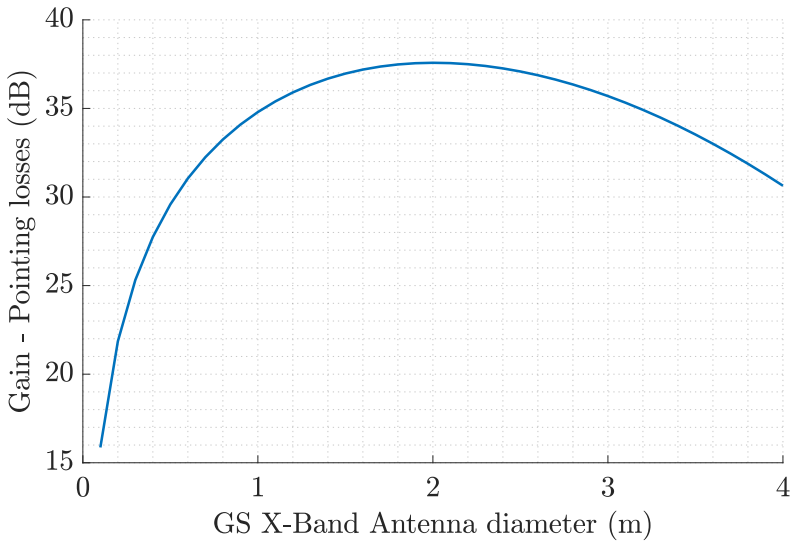

Figure 3.23: X-Band link budget results.

Antenna diameter (m)	$G_A - L_{Pointing}(dB)$
2.4	37.26
3.7	32.45

Table 3.5: Relevant values for selecting the X-Band GS antenna.

3.3.4. X-Band results

The main purpose of the X-band link analysis is to determine which type of antenna is more favourable to install on the satellite based on its characteristics. The two options are a single patch antenna and a 2x2 patch array antenna.

The X-band scenario is the most challenging of all due to the effects caused by the operating frequency.

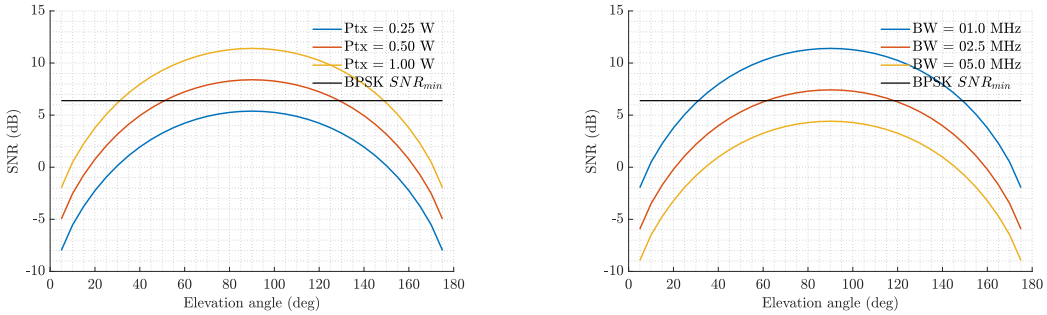

(a) SNR vs elevation angle for a fixed bandwidth of 1 MHz.

(b) SNR vs elevation angle for a fixed transmitted power of 1 W.

Figure 3.24: X-Band link budget results with a single patch satellite antenna.

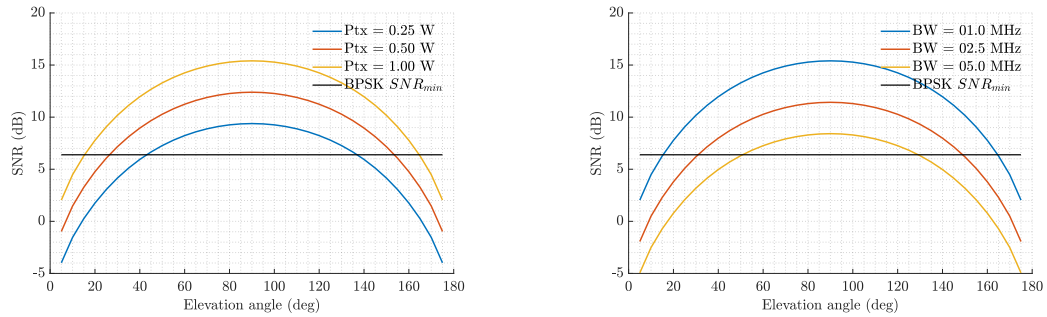

(a) SNR vs elevation angle for a fixed bandwidth of 1 MHz.

(b) SNR vs elevation angle for a fixed transmitted power of 1 W.

Figure 3.25: X-Band link budget results with a 2x2 patch array satellite antenna.

As can be seen in the figures, the X-band link is more limited due to higher losses, which restrict the signal acquisition to higher elevation angles compared to other bands. However, the single patch antenna configuration shows worse cases that would result in a significant reduction of available elevation angles. It is important to note that this analysis assumes perfect pointing towards the GS by the satellite. If perfect pointing is achievable, the array configuration would yield better results. However, if precise pointing is not possible, the single patch antenna may provide better performance due to its wider Half Power Beam Width.

Using the X-band patch array, an appropriate parameter configuration could be a transmitted power of 1 W and a bandwidth of 2.5 MHz, which would enable faster data download

within an elevation angle range of 140 to 140 degrees.

3.4. S-Band satellite patch antenna

The design of this antenna, as part of the development of this Bachelor's thesis, has been carried out for educational purposes. The main objective is to understand the process of designing a microstrip antenna for a CubeSat and to learn how to use and handle the commonly used tools such as High-Frequency Structure Simulator (HFSS) and CST Studio Suite for the development of such devices.

3.4.1. Microstrip technology and microstrip antennas

Microstrip technology is a type of microwave and Radio Frequency (RF) circuit construction that is commonly used in the communications industry. It is favored for its low cost, simplicity of fabrication, ease of integration into more complex systems, and its ability to operate over a wide range of frequencies, from Radio Frequency to microwave. This technology allows for the production of various circuits such as filters, hybrids, amplifiers, and more.

This technology is based on a planar structure that consists of a ground plane, a dielectric substrate, and a metalized trace on top, which forms the circuit. The structure follows the following configuration.

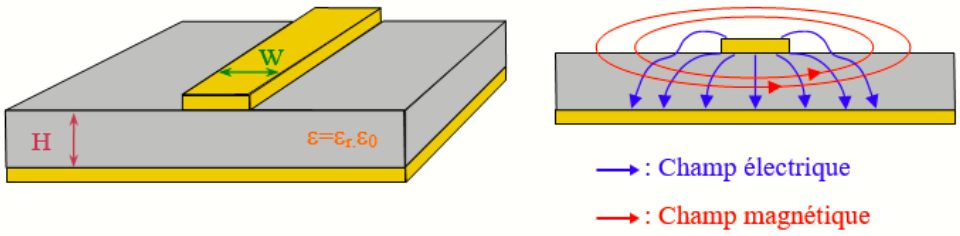

Figure 3.26: Microstrip Technology. Electric (blue) and magnetic (red) fields. [39]

Patch antennas or microstrip antennas are commonly used antennas due to the advantages offered by this technology, as mentioned earlier. These antennas are composed of a ground plane, a dielectric substrate, and a metalized patch that serves as the radiating element. The main advantage of this technology is the ability to compact circuits into very small dimensions, which is perfect for satellite applications where space is a crucial factor. To radiate effectively, the patch must adhere to the rules of microstrip technology. This involves specific dimensions such as substrate height, patch height, antenna thickness, and more.

A typical microstrip antenna has the following architecture.

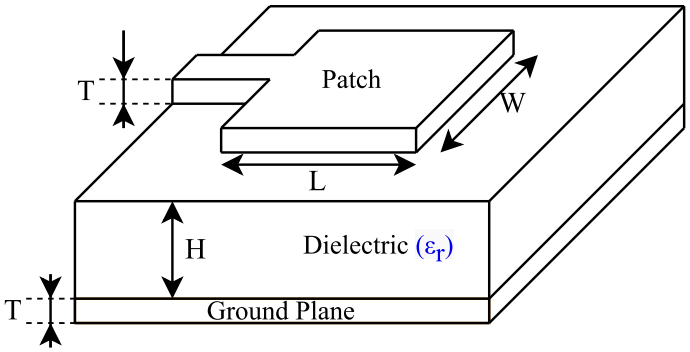

Figure 3.27: Microstrip antenna architecture.

3.4.2. Antena characteristics

The following are the basic principles of antennas that are described to understand their design.

3.4.2.1. Far-field radiation pattern

The main objective of an antenna is to radiate the electrical signal that is input to it. The antenna is the element that transforms the electrical signal into an electromagnetic wave. Depending on the geometry of the antenna, it will radiate in a certain way. The mathematical expression of the electric field radiated typically by a patch antenna is as follows.

$$\vec{E}(\theta,\phi) = \frac{sin\left(\frac{kWsin\theta sin\varphi}{2}\right)}{\left(\frac{kWsin\theta sin\varphi}{2}\right)} cos\left(\frac{kLsin\theta cos\varphi}{2}\right) cos\varphi \tag{3.35}$$

The far-field radiation pattern is a graphical representation of the distribution of radiated power from an antenna in all directions of space. It is calculated using the formula below. It is a mathematical computation of how well the antenna radiates in different directions.

$$t_p(\theta,\phi) = \frac{\vec{E}(\theta,\phi)}{|\vec{E}(\theta,\phi)|^2_{MAX}} \tag{3.36}$$

The radiation pattern depends on several factors, such as the geometry of the conducting patch and the size of the ground plane relative to the patch. The radiation pattern of patch antennas is highly characteristic, featuring a main lobe with moderate gain. The radiation pattern in the horizontal plane is typically wide and symmetrical with respect to the direction of maximum radiation.

3.4.2.2. Gain

The gain of an antenna is a measure of its ability to concentrate radiated energy in a specific direction compared to an isotropic antenna. Gain is the difference between the radiation in the direction of maximum radiation and what would be radiated by an ideal

isotropic antenna. An ideal isotropic antenna is one that radiates the same intensity in all directions.

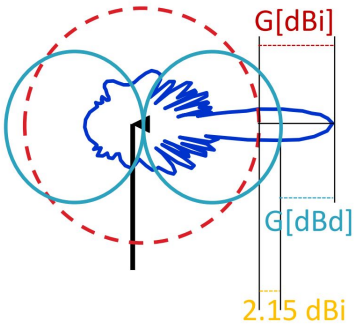

Figure 3.28: Antenna Gain.

The gain is calculated with the following formula. $U(\theta,\phi)$ is the radiation intensity of an isotropic antenna, $e_{Antenna}$ is the radiation efficiency that depends on multiple factors such as losses introduced by the substrate or antenna matching, P_T is the power of the signal that is introduced into the antenna to be transmitted, and $e_{Antenna}$ is the total efficiency of the antenna.

$$G(\theta,\phi) = \frac{U(\theta,\phi)}{\frac{P_T}{4\pi}} \cdot e_{Antenna} \quad [dBi] \tag{3.37}$$

The objective of the designed antenna is to achieve a gain close to 7, which is the typical gain of a commercial S-band antenna for CubeSats.

3.4.2.3. Polarization

The polarization of an electromagnetic wave has been explained in Section 3.1.4.4.. In this section, we will describe how circular polarization will be achieved in the patch antenna. Antennas used in space are predominantly circularly polarized because it allows for transmission and reception while in motion without causing losses.

There are different methods to achieve circular polarization in a patch antenna. The first method involves making two cuts in the corners of the patch (3.4.2.3.). The second method involves feeding the antenna from behind with two probes, where the probes have a phase difference of 90° (3.4.2.3.). After evaluating different prototypes, it was decided to use the second method as it proved to be compatible with antenna matching (3.4.2.5.).

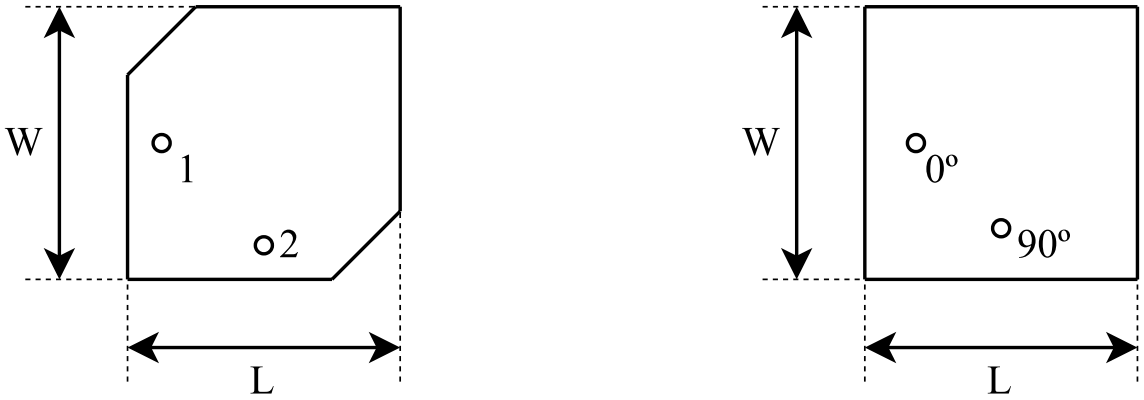

(a) Corner trimming method. Use port 1 for LHCP or port 2 for RHCP.

(b) Differential feeding method. Feed simltaneously ports 1 and 2 with 90 degree difference.

Figure 3.29: Circular polarization methods for a patch antenna.

In order to use the second method, it is strictly necessary for the antenna to be square rather than rectangular, as is typical for a patch antenna. Additionally, due to structural constraints of the satellite, it is required that the antenna be fed from behind, meaning that the probe is inserted from the ground plane through the dielectric layer to reach the patch.

3.4.2.4. Axial Ratio

The Axial Ratio (AR) is a parameter used to characterize the polarization of an antenna. It is a measure of the ratio of the radiated electric field in the axes perpendicular to the axis of wave propagation. If an antenna radiates with a high Axial Ratio, it means that the wave has elliptical polarization. If the value is extremely high, it can be considered practically linear. If the Axial Ratio value is 0, it means that the amplitude of the electric field in both axes is equal, indicating a completely circular polarization.

$$AR = 20\log\left(\frac{\vec{E}_{Mayor\,axis}}{\vec{E}_{Minor\,axis}}\right) \quad [dB] \tag{3.38}$$

The objective, as mentioned in the previous section, is to achieve a polarization that is as circular as possible, in other words, an Axial Ratio (AR) value close to zero.

3.4.2.5. Antenna matching & S-Parameters

The matching of an antenna is one of the most important factors in antenna design. It is a significant factor that primarily influences antenna efficiency and, consequently, the radiated power.

The impedance of the antenna (Z_A) is a combination of its resistance and reactance, expressed in complex terms. A mismatch in impedance between two RF systems results in a reflection effect on the incoming waves at the antenna. These reflected waves do not reach the antenna, leading to a loss of radiated power. The reflection efficiency of the antenna

(e_{red}) can be calculated using the reflection coefficient (ρ_A), which primarily depends on the antenna impedance (Z_A) and the reference impedance of the system (Z_o).

$$e_{ref} = 1 - |\rho_A|^2 = 1 - \left|\frac{Z_A - Z_o}{Z_A - Z_o}\right|^2 \tag{3.39}$$

The matching of an antenna is the process of adjusting the electrical parameters of an antenna to minimize the aforementioned reflection effects. The adaptation process involves equalizing the input impedance of the antenna (or equivalent impedance) to the impedance of the rest of the system. In microstrip technologies, this is achieved using matching networks, which are essentially circuits that equalize the impedance between the antenna and the rest of the system.

To characterize and adapt circuits, S-parameters are commonly used. They are a common way of describing the behaviour of a Radio Frequency (RF) or microwave network. These parameters are used to characterize the transmission and reflection properties of a network of electronic devices, such as antennas, amplifiers, filters, and other components. The S-parameters provide information about the impedance matching of the ports of a circuit and its frequency response. They also provide information about the power flow relationship between different ports.

The parameter relevant to antennas is the S-parameter S_{11}, which happens to be the reflection coefficient of the antenna. Since the antenna has two ports, the S_{11} parameter is used to match the first port, and the S_{22} parameter is used to match the second port. These two parameters indicate the amount of signal being reflected at the antenna input, and the goal is to minimize their values, ideally close to zero.

Another measure to indicate the adaptation is the Return Loss (RL). The higher the RL value, the better the antenna matching.

$$RL = -20 \cdot \log|\rho_A| = -20 \cdot \log|S_{11}| \quad [dB] \tag{3.40}$$

3.4.3. Antenna design

In this stage, the process followed to design the S-band patch antenna is described. The antenna was designed using the electromagnetic simulation software *CST Studio Suite*.

The usual calculations for this type of antenna are provided below. However, these calculations are intended for rectangular patch antennas fed with a microstrip line. Due to the specific requirements of the 3Cat8 antenna (square patch, Right Handed Circular Polarization, and back-fed), it will not follow the typical design. Therefore, these calculations will be used as an initial estimate, and through iterations, the optimal size of the antenna that optimizes its matching will be determined.

- 1^{st} **step:** Compute the patch width.

$$W_{Patch} = \frac{c}{2f_0 \cdot \sqrt{\frac{\varepsilon_r+1}{2}}} \quad [m] \tag{3.41}$$

- 2^{nd} **step:** Compute the effective dielectric constant (Relative permittivity).

$$\varepsilon_{eff} = \frac{\varepsilon_R + 1}{2} + \frac{\varepsilon_R - 1}{2} \cdot \left[\frac{1}{\sqrt{1 + 12 \cdot \left(\frac{h}{W}\right)}} \right] \tag{3.42}$$

- 3^{rd} **step:** Compute the length of the patch.

$$L_{patch} = L_{eff} - 2 \cdot \Delta L \quad [m] \tag{3.43}$$

$$L_{Patch} = \frac{c}{2 f_0 \cdot \sqrt{\varepsilon_{eff}}} - 0.824h \cdot \frac{(\varepsilon_{eff} + 0.3) \cdot (\frac{W}{h} + 0.264)}{(\varepsilon_{eff} - 0.258) \cdot (\frac{W}{h} + 0.264)} \quad [m] \tag{3.44}$$

- 4^{th} **step:** Iterate, using the patch length and changing the delta parameter, until the antenna is matched.

$$L = L_{Patch} + \delta \quad [m] \tag{3.45}$$

3.4.3.1. Dielectric

The substrate used is the *Rogers RT/duroid 5880*, which is a high-quality substrate. This substrate will allow the antenna to have very low losses, which are crucial for the proper functioning of the communication system and the energy-saving of the satellite.

Parameter	Value
Dielectric constant (ε_r)	2.2
Dissipation Factor ($tan\ \delta$)	0.001

Table 3.6: Rogers RT/duroid 5880 design properties. [40]

3.4.3.2. Antenna dimensions

The dimensions of the antenna were chosen according to the space constraints of the satellite and taking as a reference the measurements of a commercial S-band antenna. This antenna is the S-band antenna from Endurosat ([36]).

Parameter	Value	Unit
Copper cladding thickness (T)	35	μm
Dielectric height (H)	3.5	mm

Table 3.7: Antenna dimensions.

3.4.3.3. 90 degrees hybrid

To introduce the same signal with a 90-degree phase shift into the antenna, a device called a hybrid will be used. It is a component used in RF and microwave systems to split a signal into two outputs, maintaining a 90-degree phase separation between them. It is a 4-port device, where the input signal is introduced through port 1, which will exit through ports 3

(through) and 4 (coupled), while a 50 Ωload will be connected to port 2 to dissipate the entire signal.

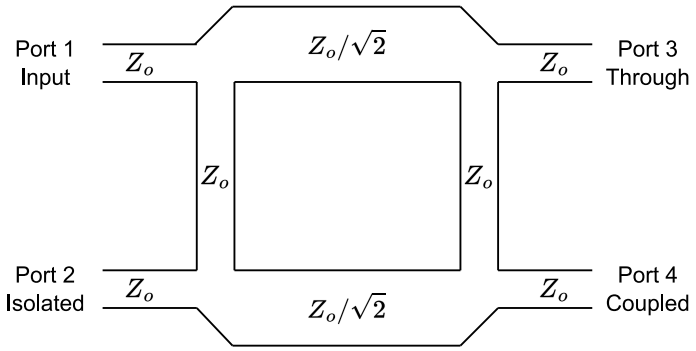

Figure 3.30: 90 degrees hybrid.

The hybrid that will be finally installed is the *QCS-312+* from *Mini-Circuits*, which has very compact dimensions and is a cost-effective product ([41]).

3.4.3.4. Antenna connectors

The connectors that will be soldered to the antenna and placed at the back will be *HUBER+SUHNER* connectors ([42]).

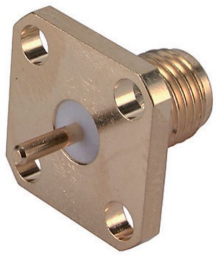

(a) Antenna connector model.

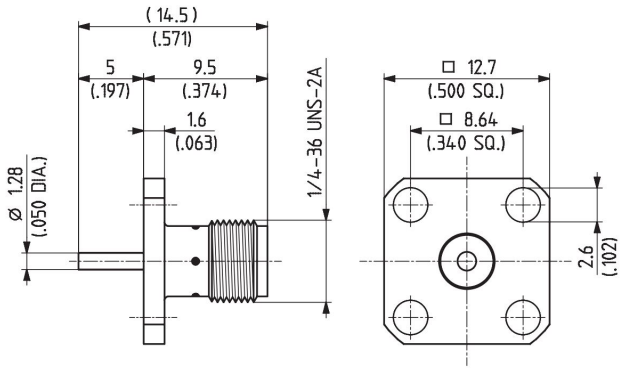

(b) Antenna connector dimensions.

Figure 3.31: HuberSuhner antenna connector.

To these connectors, the cables will be connected, which will later be connected to the 90-degree hybrid.

3.4.4. Antenna final design & results

The final result of the designed antenna is the following one.

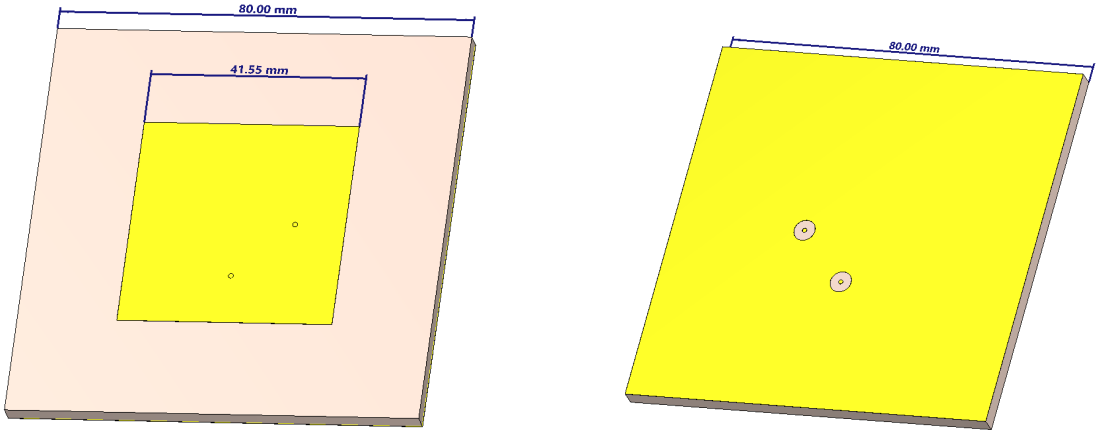

(a) Front view of the antenna.

(b) Back view of the antenna.

Figure 3.32: Prototype antenna model.

The results for the parameters S_{11} and S_{22} are exceptionally good, with return losses for both being approximately -18 dB. This indicates that most of the power would enter the antenna for radiation. Such high return losses are a very desirable characteristic for this antenna prototype. To determine the antenna bandwidth, we need to find when the threshold drops by -3 dB. In this case, the bandwidth is 230 KHz.

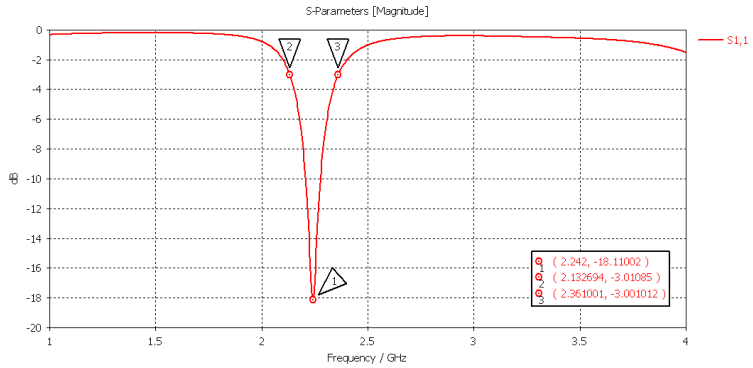

(a) Antenna $S_{11}(dB)$.

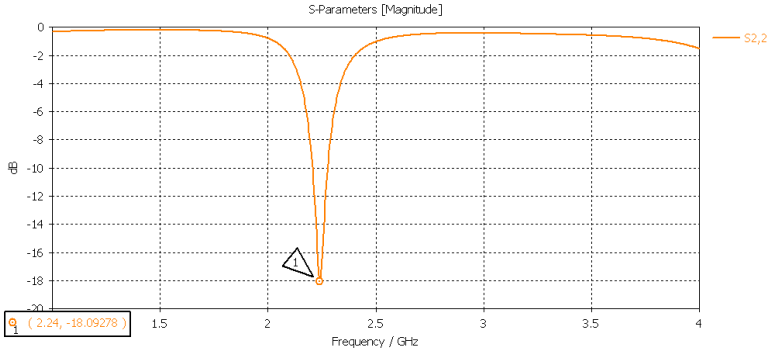

(b) Antenna $S_{11}(dB)$.

Figure 3.33: Antenna S paremeters.

The next feature to analyze is the radiation pattern and gain. The maximum antenna gain

is 7.51 dB, which is not very high but falls within the expected values for an antenna of this type. Additionally, the direction of maximum radiation is almost perpendicular to the patch, which means that there are no pointing inefficiencies.

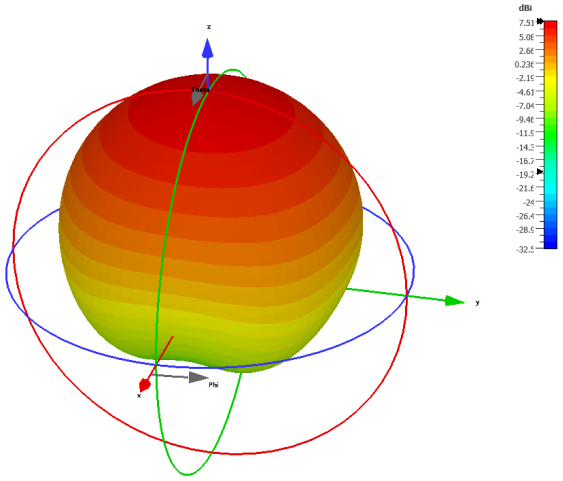

Figure 3.34: Antenna Gain.

Next, in more detail, are shown two cuts of this radiation pattern. The cuts used are for $\phi = 90$ degrees and $\phi = 0$ degrees while varying θ. As can be seen in the following figure.

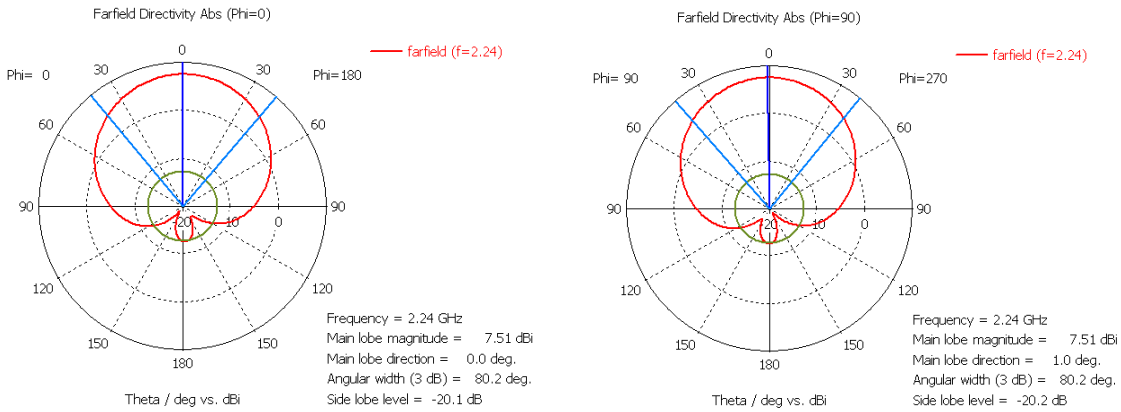

(a) Antenna Farfield cut for $\phi = 0$ degrees.

(b) Antenna Farfield cut for $\phi = 90$ degrees.

Figure 3.35: Farfield cuts.

Finally, the Axial Ratio needs to be checked to determine if the antenna would be radiating RHCP. As can be seen in Figure 3.36, the AR of the radiated waves does not exceed 0.6 dB. This means that the polarization is practically circular.

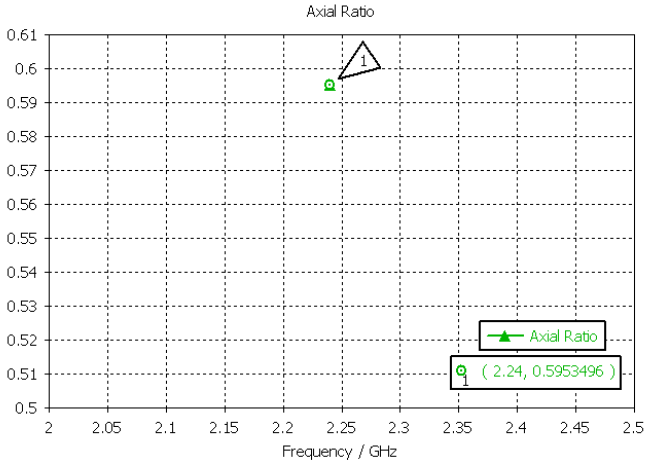

Figure 3.36: Axial Ratio.

These are mostly good values for the simulated antenna. However, it is important to note that this is a simulation. Simulating the antenna in an electromagnetic simulation software does not take into account manufacturing errors or potential inefficiencies that may arise once the antenna is constructed. To truly verify these values, it would be necessary to manufacture the antenna and measure its characteristics in a laboratory setting using an anechoic chamber and a network analyzer.

3.4.5. Antenna comparison

The objective of this section is to compare the characteristics of the designed antenna with other commercial antennas from different companies. The main antennas used for comparison are the antenna from *EnduroSat* ([36]) and the antenna from *ISISPACE* ([43]).

	EnduroSat antenna	**ISISPACE antenna**	**Prototype**
Parameter	**Value**	**Value**	**Value**
Frequency range (MHz)	2400-2450	2200-2290	2133-2361
Maximum Gain (dBi)	8.3	6.5	7.51
HPBW (degrees)	71	100	80
Return Losses (dB)	-	> 13	18
Polarization	LHCP	RHCP	RHCP
Axial Ratio (dB)	-	< 3	0.6

Table 3.8: Antenna comparison.

The prototype antenna exhibits significantly better values compared to the commercial antennas except for the bandwidth. One can observe the trade-off between gain and HPBW, where an increase in one parameter leads to a decrease in the other. The bandwidth of the designed antenna is smaller compared to the other antennas. The utilization of differential feeding to achieve circular polarization proved to be a highly efficient method. In summary, with a few modifications for mass production, the designed S-band antenna could be a competitive product compared to other market options.

3.5. Conclusions & future work

In this section, the conclusions drawn from the work conducted throughout this chapter are presented. Furthermore, potential implementations or pending tasks, which could not be carried out due to time constraints, are discussed.

Firstly, it can be stated that the link results are satisfactory, and they can be considered feasible. The theoretically obtained Signal to Noise Ratio is sufficient for transmitting and receiving messages in different frequency bands, with acceptable ranges of elevation angles. However, this analysis assumes the existence of a control mechanism that enables the satellite to constantly point towards the ground station. As depicted in Figure 3.5, the satellite will not always pass directly over the ground station. Additionally, the selection of the X-band antenna for the satellite is entirely dependent on the Ground Station pointing. Considering the range of elevation angles that allow transmission in the X-band and comparing the two potential antennas to be implemented, it can be declared that, if the pointing mode to the Ground Station is achievable, the selected antenna for the satellite in the X-band will be a 2x2 patch array antenna. This issue will be analyzed in the next chapter, which involves the design and manufacture of an Engineering Model of magnetic actuators to control the satellite's attitude and provide it with the ability to point towards the ground station when necessary.

Furthermore, it will be necessary to perform a data budget. The main objective would be to compare whether it is more beneficial to increase the bandwidth, thus reducing the transmission time (due to the reduction of elevation angles with communication feasibility), or whether it would be better to decrease the bandwidth, allowing for longer data upload and download periods. Considering the characteristics of the links presented in this Bachelor's thesis, the access times between the satellite and the Ground Station would be calculated using the *Ansys Systems Tool Kit*. Then, the required bit rate would be calculated, taking into account the SNR computed in this analysis. With the bit rate and access time data, the amount of data transferred in each case could be calculated, and the best option could be chosen.

Regarding the antenna, designing an antenna has been an extremely educational exercise that has allowed me to become familiar with antenna simulation and design tools, as well as to gain a deeper understanding of antenna operation and both microstrip and stripline technologies. The next step would be to manufacture the antenna using a substrate board and the appropriate chemical processes. After that, the suitable connector would be installed, and the return losses would be measured using a network analyzer to confirm that it is well-matched. Finally, in an anechoic chamber, the radiation pattern and the Axial Ratio would be measured.

Moreover, during the design process, various ideas were considered to improve the antenna's characteristics. One of these designs would involve integrating a 90-degree hybrid using stripline technology behind the antenna's ground plane. With this solution, the need for external cables and a 90-degree hybrid that is not securely attached to the satellite's structure could be eliminated. This approach would enhance performance by mitigating the impact of vibrations caused by the launch vehicle during liftoff.

CHAPTER 4. CONTROL SUBSYSTEM

The main objective of this chapter is to design the actuators for the control system of the 3Cat-8 mission. The importance of this design stems from the need to point towards the Ground Station (GS) to make feasible the X and S-Band links.

This section focuses solely on the design of the Z-axis magnetorquer, which is the largest and requires the highest actuation power, making it the most restrictive one. This magnetorquer will be located around the polarized lens of the 3Cat-Gea camera (1.6.1.1.). This can be seen in detail in the image below.

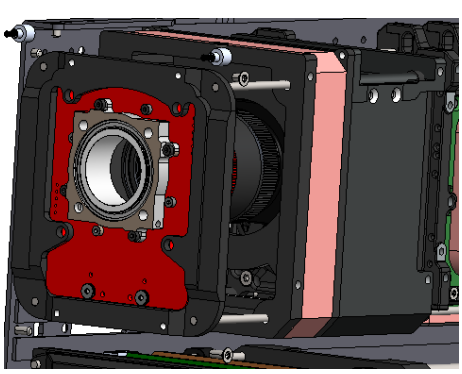

(a) Detailed view of the Z-axis magnetorquer and the 3Cat-Gea camera.

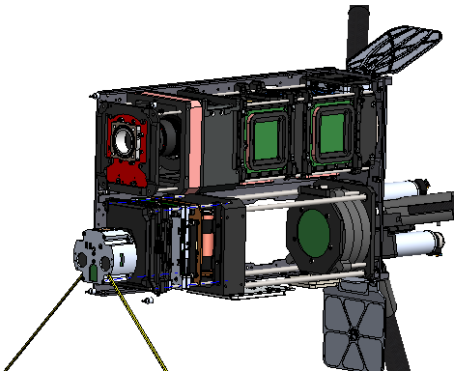

(b) Overall view of the Z-axis magnetorquer and the 3Cat-Gea camera.

Figure 4.1: Magnetorquer Z Computer-aided Design (CAD).

4.1. ADCS subsystem description

The Attitude Determination and Control System of a satellite is one of the most critical subsystems of a space mission. It is responsible for controlling the attitude and orientation of the satellite in orbit. This system encompasses the sensors that determine the state, the control algorithms that determine the actuator input power based on the information measured by the sensors, and the actuators themselves that exert forces in the appropriate direction to provide control over the satellite.

In satellites, sensors such as gyroscopes, magnetometers, solar sensors, etc., are used. These sensors allow the satellite to determine its state. The sensors transmit the collected information in the form of electrical signals to the On-Board Computer (OBC), which is responsible for collecting that information. Through pre-programmed control algorithms, the OBC calculates the required actuator effort to orient the satellite correctly. The actuators, as detailed in Section 2.4., are responsible for performing the physical effort.

4.1.1. Control Algorithms

The control algorithms are programs that enable the control of the system's attitude. They can be implemented in both hardware and software. In satellite applications, these algorithms are predominantly implemented in software. They are introduced into the satellite's

OBC. These programs process the information obtained from the sensors and, through mathematical operations, generate commands for the actuators.

An example of a satellite control algorithm is the *Bdot* or *B-dot* control algorithm. This algorithm is implemented in the control system of 3Cat-8. It is used to measure and control the rate of change of the magnetic field around the satellite.

4.1.2. Control & Pointing modes

In this section, some of the control modes that will be implemented in the 3Cat-8 satellite are described.

The “detumbling” control mode is used when the satellite is in an initial uncontrolled state, experiencing a high spin rate, or with an unknown orientation. The objective of this mode is to reduce the satellite’s spin rate and stabilize its attitude using available actuators such as reaction wheels or magnetorquers.

The pointing modes are modes that aim to make the satellite point in a specific direction or location, such as the center of the Earth (Nadir) or the GS.

“Nadir Pointing” is a control mode whose main objective is to orient a specific face of the satellite towards the center of the Earth. This mode has applications in remote sensing or Earth observation.

Sun pointing is a mode whose purpose is to align the solar panels located on the exterior of the satellite towards the sun. This mode is utilized when the satellite is experiencing low battery levels.

The *Ground station pointing* mode is the mode that concerns this Bachelor’s thesis. It is a control mode that aims to point the satellite’s antennas towards the ground station located at the Observatorio Astronómico del Montsec. The purpose is to optimize the communication link characteristics to enable the proper exchange of data and commands.

4.2. Active Magnetic Actuators (Magnetorquers)

In this section, the main concepts necessary for the design of magnetic actuators or magnetorquers are described.

A magnetorquer is essentially an electromagnet. An electromagnet is a device that generates a magnetic field when an electrical signal, specifically a current, is introduced to it. It consists of a coiled wire.

In 1820, Ørsted discovered that a compass was affected by the presence of a nearby wire through which an electrical signal was passing. This experiment laid the foundation for connecting electricity and magnetism. Building upon this discovery, the French physicist André-Marie Ampère formulated Ampère’s laws. According to Ampère’s law (4.1), an electric current generates a magnetic field around it. In physics, a field is a spatiotemporal distribution of a physical quantity. In 1831, Faraday demonstrated electromagnetic induction, which states that a changing magnetic field can induce a current in a circuit.

$$\oint_C \vec{B} \cdot \vec{dl} = \mu_0 \cdot I \tag{4.1}$$

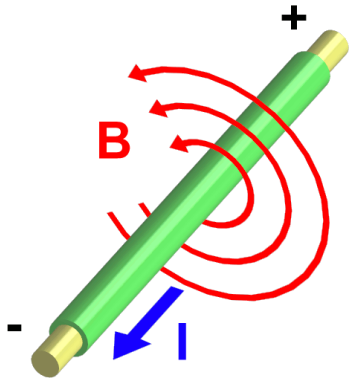

Figure 4.2: Magnetic field generated by a wire conductor. [44]

The American scientist Joseph Henry discovered that by winding a wire into a coil, the field lines generated by the different segments of the wire interfere constructively, resulting in a much stronger magnetic field inside the coil. This coil, which has the ability to generate large magnetic fields, was named electromagnet.

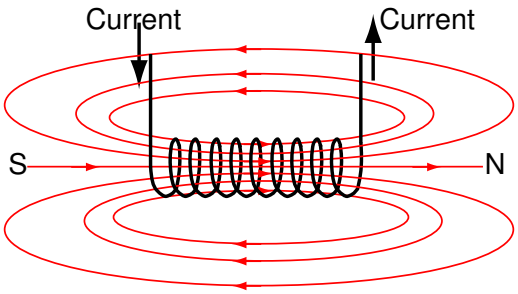

Figure 4.3: Magnetic field generated by a wire conductor. [45]

The magnetic moment of a coil is a quantity that measures the intensity and orientation of a magnetic field. This measurement is used in the design of electromagnets, generators, and other devices. The magnetic moment of an electromagnet depends on the current passing through it and the area enclosed by its geometry. The magnetic moment of a coil can be calculated using the following formula, where 'I' represents the current passing through the coil (in Amperes), 'N' is the number of turns of the coil, 'A' represents the area of one loop, and 'n' is the vector perpendicular to the coil's surface.

$$\vec{m} = I \times \sum_{i=0}^{N} \hat{n} \cdot A_i \quad [A \cdot m^2] \tag{4.2}$$

In the case that all the coils had the same area, the formula could be simplified by obtaining the commonly used formula:

$$\vec{m} = I \cdot N \cdot A \quad [A \cdot m^2] \tag{4.3}$$

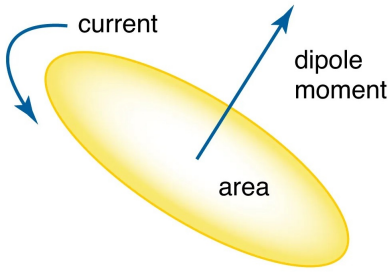

Figure 4.4: Dipole moment of a single turn. [46]

The magnetic moment, in the presence of an external magnetic field, tends to align itself. The magnetic moment can be interpreted as the intensity with which an electromagnet aligns itself with the external magnetic field, in the case of a satellite, the Earth's magnetic field. This alignment can be measured as the torque generated by the electromagnet. The following formula computes the torque generated by a magnetorquer, where τ is the torque, 'm' is the magnetic moment, and 'B' is the Earth's magnetic field.

$$\vec{\tau} = \vec{m} \times \vec{B} \quad [N \cdot m] \tag{4.4}$$

These are the physical concepts that will allow the 3Cat-8 to control its attitude and point the antennas towards the ground station.

Another important concept regarding control systems and actuators is the saturation point, which represents the physical limit of actuation for the device. In the case of a magnetic actuator, saturation refers to the maximum magnetic moment that the magnetorquer can generate.

4.2.1. Power supply of the magnetorquers

The attitude determination and control subsystem's workflow can be summarized in 3 stages: The sensors read the attitude of the satellite; the OBC reads the data from the sensors, compares the desired attitude with the current attitude and computes the necessary inputs for the actuators; finally, the actuators receive the power input (from the OBC) and partially correct the attitude of the satellite. This section focuses on describing in detail what happens in the third of the mentioned stages.

The first step is the description of the waveform that feeds the magnetorquers. It is called Pulse Width Modulation (PWM). This signal is commonly used to control the speed of a motor, in this case, a magnetorquer. It consists of a rectangular pulse of current or voltage (current in this case) that is repeated at a certain frequency that changes the duty cycle depending on the needs of the moment. The duty cycle is the parameter that the OBC must constantly determine. As the duty cycle increases, the power input the actuators also increases, which translates into more torque generated by them.

The OBC that will finally be installed in the 3Cat-8 is the Alen space TRISKEL. The main parameters are obtained from its datasheet:

- Current amplitude: 1000 mA
- Pulse repetition frequency: 250 kHz

In the figure below three cases of the PWM signal are represented.

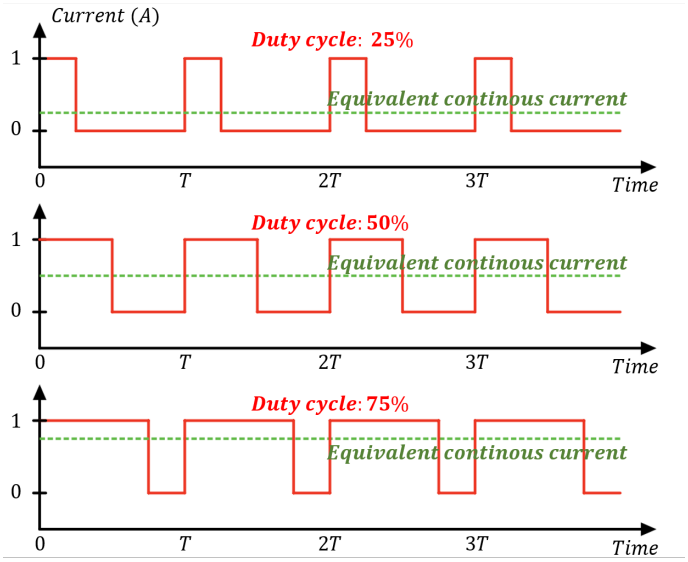

Figure 4.5: PWM Signal waveform.

As shown in Figure 4.4, the dipole moment generated by the magnetorquers depends on the direction of the current passing through them. To properly control the satellite, it must be able to generate moment in both directions, which requires the ability to introduce current in both directions as well. This polarity inversion, which allows the magnetorquers to exert torque in one direction or the other, is achieved through a circuit called an H-bridge. The H-bridge consists of 4 transistors and 4 protection diodes whose configuration allows for the desired result. The H-bridge circuit is shown in the figure below. The two different operating configurations where the magnetorquers are active in the H-bridge circuit are also provided in the figure.

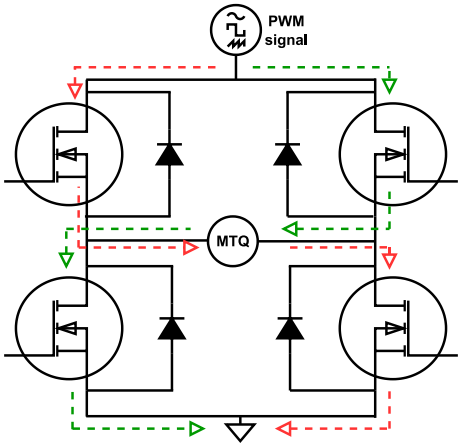

Figure 4.6: H-Bridge circuit. In red, the first configuration of the feeding of the MTQ (first direction of actuation), in green, the second configuration (second direction) [47].

However, it will not be necessary to develop a PCB board that contains this circuit since the satellite's OBC, IENAI's TRISKEL itself, which has been exclusively developed for nanosatellites, already includes this system. Each axis (X, Y, and Z) has 2 current outputs for both directions, as shown in the diagram below (Figure 4.7).

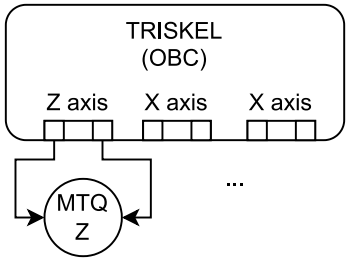

Figure 4.7: Triskel's Magnetorquer feeding scheme. [48]

4.2.2. Electrical model of a magnetorquer

The electrical model of a magnetorquer consists of a resistance and an inductance, as can be observed below.

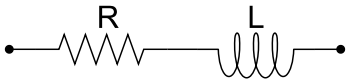

Figure 4.8: Theoric electrical model of a magnetorquer.

Therefore, the complete impedance of the model will have a real part (resistance) and an imaginary part (reactance). The way to calculate it is as follows.

$$Z = R + j \cdot X = R + j \cdot \omega \cdot L \quad [\Omega] \tag{4.5}$$

Being Z the impedance, R the resistance, X the reactance, ω the angular frequency of the signal feeding the magnetorquer, and L the value of the inductance.

The real part of the magnetorquer impedance, that is, the resistance (R), comes from the resistance of the wire itself. This resistance is the resistance of the wire to the flow of electrons (current). This resistance can be calculated using the following formula. Where ρ represents the wire's material resistivity (Ω/m), l the length of the wire (m), A the cross-sectional area of the wire (m^2), and r the radius of the wire's cross-sectional area (assuming it is a circle).

$$R = \rho \cdot \frac{l}{A} = \rho \cdot \frac{l}{\pi \cdot r^2} = \rho \cdot \frac{l}{\pi \cdot (d/2)^2} \quad [\Omega] \tag{4.6}$$

Once the resistance has been calculated, the next step is to determine the inductance. However, estimating this value, which strongly depends on the coil's geometry, is a quite challenging value to estimate, and there is no exact formula for its calculation. Wheeler's formulas ([49]) are available to calculate the inductance for certain cylindrical geometries, but they cannot be applied to the case of the magnetorquers of the 3Cat-8. Due to these

reasons, no prediction will be made regarding the inductance value. Instead, once the magnetorquers are constructed, the inductance will be measured using an inductance measuring instrument.

According to equation 4.5, the total power flowing through the magnetorquer consists of both a real and an imaginary part. The total power is referred to as apparent power (S, in Volt-Amperes), the real part as active power (P, in watts), and the imaginary part as reactive power (Q, in Volt-Amperes Reactive):

$$S = R + j \cdot Q \quad [V \cdot A] \tag{4.7}$$

The phase of this power can be calculated as:

$$\theta_z = \arctan\left(\frac{\omega \cdot L}{R}\right) \quad [rad] \tag{4.8}$$

With this, the apparent power can be calculated, and we can arrive again at formula 4.7:

$$S = \frac{|V_e f f|}{|Z|} \cdot e^{j \cdot \theta_z} = |I|^2 \cdot |Z| \cdot e^{j \cdot \theta_z} \quad [V \cdot A] \tag{4.9}$$

However, the useful power, the power that the magnetorquer uses to generate a dipole moment, is solely the active power (P). The reactive power (Q) does not contribute energy. For this reason, the active power is the one that will be used to assess the power consumed by the magnetorquers. The instantaneous active power consumed can be computed as:

$$P = I^2 \cdot R \quad [W] \tag{4.10}$$

Where 'P' represents the power consumed in Watts, 'I' is the instantaneous current passing through the coil in Amperes and R is the resistance.

However, if two identical magnetorquers are connected in parallel instead of one, the dissipated power will be halved while the generated torque remains the same, as the current passing through both magnetorquers is the same. The simplified electrical model (considering only the active power, the real part of the apparent power) would be as follows:

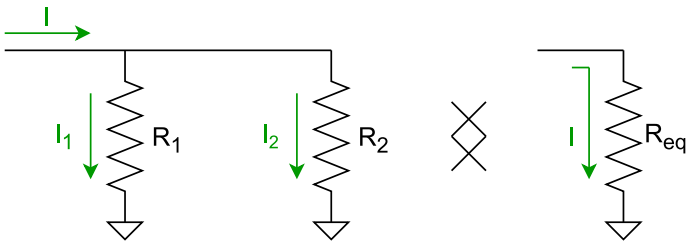

Figure 4.9: Electrical model (Only real part of the impedance) of two parallel magnetorquers.

Being:

$$R_{eq} = \frac{R \cdot R}{R+R} = \frac{R^2}{2 \cdot R} = \frac{R}{2} \quad [\Omega] \tag{4.11}$$

Taking into account this circuit, the power consumed by the magnetorquers can be calculated using two different methods: using a current divider or using the equivalent resistance. Both cases are equivalent, so the result is the same. The first demonstration is by using Equation 4.11 and substituting it into Equation 4.10, we obtain:

$$P = I^2 \cdot R_{eq} = I^2 \cdot \frac{R}{2} \quad [W] \tag{4.12}$$

The second demonstration involves summing up the powers consumed by each magnetorquer. To do this, we need to determine the current passing through each magnetorquer, which can be obtained using a current divider:

$$I_1 = I_2 = I \cdot \frac{R_2}{R_1 + R_2} = I \cdot \frac{R}{2 \cdot R} = \frac{I}{2} \quad [A] \tag{4.13}$$

Therefore:

$$P_{TOT} = P_{MTQ1} + P_{MTQ2} = \left(\frac{I}{2}\right)^2 \cdot R + \left(\frac{I}{2}\right)^2 \cdot R = \frac{I^2 \cdot R}{2} \quad [W] \tag{4.14}$$

Therefore, it is demonstrated that the power consumed by two identical magnetorquers is half of the power consumed by one for the same current. For this reason, it has been decided to manufacture two magnetorquers per axis.

However, it is not the case for the generated magnetic moment. To calculate the moment, the moments generated by each magnetorquer should be summed using Equation 4.2.

$$M_{TOT} = M_{MTQ1} + M_{MTQ2} = N \cdot A \cdot \frac{I}{2} + N \cdot A \cdot \frac{I}{2} = NAI = M_{MTQ} \quad [A \cdot m^2] \tag{4.15}$$

4.3. Objective

The goal, as described earlier, is to design the magnetorquers that will allow pointing the S and X-band communication antennas, which in turn will enable the download of data obtained from scientific experiments. To achieve this, the main parameters to be determined are the diameter of the wire to be used for winding the Magnetorquer (MTQ) and the number of turns required for the device to generate the magnetic moment.

To select these parameters, an approximate calculation will be performed in order to generate the required moment with the minimum number of turns possible. This approach aims to minimize the number of tests conducted and expedite the design process.

4.4. Requirements & restrictions

The first step to start designing the magnetorquers is to gather the constraints that limit the design. Below are detailed all the requirements of the different subsystems of the mission that need to be met for the satellite to be feasible.

4.4.0.1. Size and allocation requirements

One of the main concerns when designing technologies for a nanosatellite is the available space and weight. Space is a variable that takes great importance in the design of magnetic actuators since the generated momentum depends directly on the area described by the coils. The mission's structural design team is in charge of sizing and locating all the elements of the satellite in order to optimize the space in it and ensure its structural integrity. This team is also able to locate the centre of mass of the 3Cat-8 which is a piece of very important information to design the control system of the mission.

To fit all the pieces and optimize the space inside the satellite, there are some guide rods on the edges of the structure. These rods do not allow the magnetorquer to be square, so they will have to be octagonal.

Also, due to volume issues, coil-type magnetorquers are the ones that will be implemented for the 3Cat-8 satellite.

The figure below shows the maximum dimensions that the wiring of the MTQ can have.

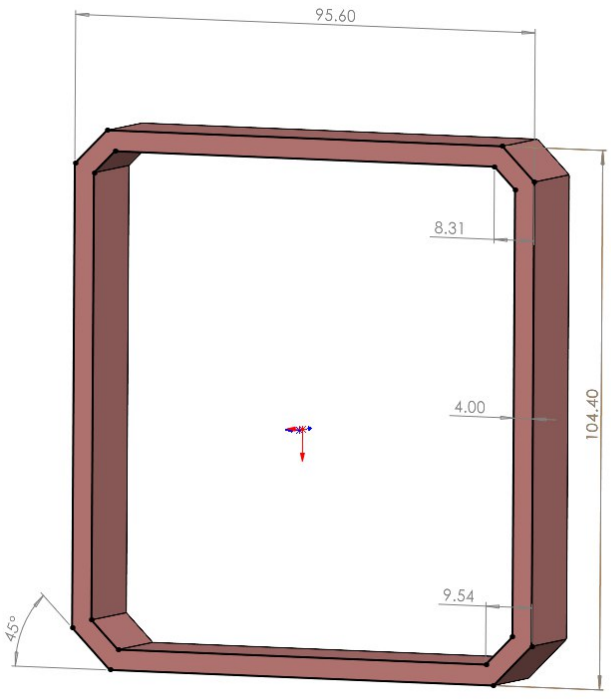

Figure 4.10: Z magnetorquer dimensions.

4.4.0.2. Actuating requirements

The AOCS team of the 3Cat-8 mission can determine the necessary saturation (Maximum momentum) in order to effectively control the satellite and therefore, provide the ability to target the base station. With a simulator of the satellite and its control algorithms developed in Matlab, the ADCS team of the 3Cat-8 subsystem has determined that the needed maximum magnetic moment with an input current of 1 Ampere must be bigger than 1.5 Amperes per square meter. This means that the saturation of the magnetorquer must be above that threshold.

4.4.0.3. Power Requirements

Power consumption is another decisive factor in the design of devices for satellite systems. The satellite has limited energy and must ensure the power feeding of all its subsystems. For this reason, the Electric Power Subsystem (EPS) team of the 3Cat8 have determined that the maximum consumed instantaneous power of the magnetorquer should be below 6 W per axis. This means that the consumption of both magnetometers of the Z axis must be below 6 Watts.

4.4.0.4. Material requirements

The choice of cable for winding the magnetorquer is also an important factor to consider during manufacturing. For convenience and easy availability, copper wires of the American Wire Gauge (AGW) standard will be used. The AGW standard is a system for parameterizing and standardizing cables based on their diameters, facilitating their manufacturing, nomenclature, and commercial use. These cables can be purchased in various formats. The format chosen will be enamelled solid-core wire, ensuring that there is no contact between the different turns when it is wound into a coil, allowing the current to pass through all of them.

In addition, the material used for the structure of the MTQ must be identified, as metallic materials can act as ferromagnetic cores and affect the performance of the device. Initially, the structure for the Engineering Model will be 3D printed using plastic, which does not have a magnetic effect on the magnetorquer's performance. However, for the Flight Model (FM) of the magnetorquer, the structure that houses it will be constructed using aluminum. Aluminum is a non-ferromagnetic material, and its relative magnetic permeability is equal to that of air, so it will not affect the magnetic performance of the actuator. In fact, aluminium is commonly used to protect antennas due to this particular characteristic.

4.5. Design procedure

The objective of the magnetorquer design is to determine the diameter of the cable to be used for winding and the required number of turns, based on the stated requirements (required dipole moment, power consumption, etc.). This section describes the design process undertaken to determine these parameters and proceed to the manufacturing stage.

To obtain the necessary data, the goal was to create a plot that shows the generated dipole moment (y-axis) as a function of the number of turns (x-axis), and a similar plot showing power consumption as a function of the number of turns.

To solve these two unknowns, a MATLAB code has been developed to generate these plots based on the design variables.

The design variables are as follows:

- Diameter of the used cable
- Maximum available current
- Magnetorquer dimensions (Will be defined in section 4.5.1.)

4.5.1. Magnetorquer sizing and winding geometry

Due to the size constraints of the satellite, the magnetorquer needs to be an irregular octagon. Therefore, fully defining its dimensions and accurately calculating the area for each turn is not a trivial task.

The shape of the magnetorquer, specifically the Z-axis magnetorquer, is depicted in the figure below. To define its maximum dimensions, they will be labeled as follows:

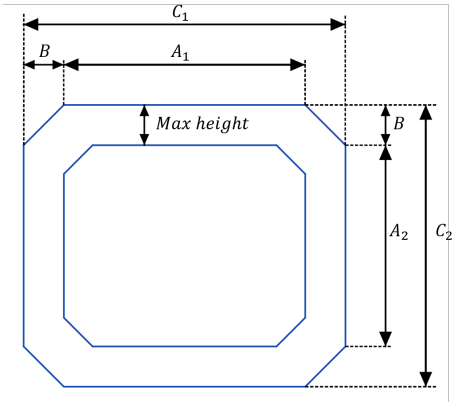

Figure 4.11: Z magnetorquer dimensions definition.

Furthermore, as a simplification, it has been assumed that the sides labelled *"B"* are always completely equal and their value is the average of the 4 sides. This way, the polygon is easier to characterize.

Thus, the area enclosed by the outer octagon is calculated by using the area of the square and subtracting the triangular areas of the corners:

$$A = C_1 \cdot C_2 - 2 \cdot B^2 \quad [m^2] \tag{4.16}$$

Its perimeter, necessary to calculate the length of a turn and thus the resistance of the cable, can be calculated as follows:

$$P = 2 \cdot A_1 + 2 \cdot A_2 + 4 \cdot \sqrt{2 \cdot B^2} \quad [m] \tag{4.17}$$

The structure that will accommodate the magnetorquers also has defined dimensions. For this reason, it will be necessary to estimate the number of turns that fit within the structure, that is, the number of circumferences that fit within one section of the structure (See Figure 4.12).

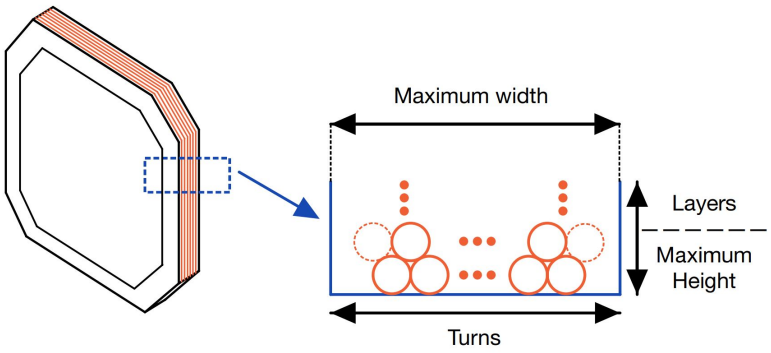

Figure 4.12: MTQ structure section dimensions.

Estimating the width and height occupied by a section of the magnetorquer will be difficult to determine as the winding of the turns will never be done ideally. There are two ideal ways to compact the turns, which are shown in the image below.

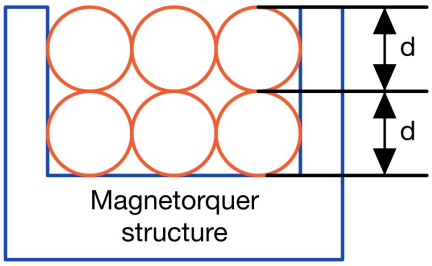

(a) Magnetorquer first wire accumulation case.

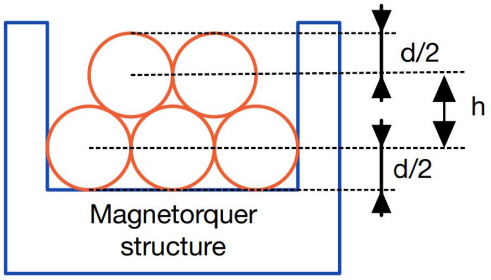

(b) Magnetorquer second wire accumulation case.

Figure 4.13: Wire accumulation cases.

In Figure 4.13(b), a method is shown that minimizes the vertical space used, but the generated moment will be slightly lower as the compactness is higher and, consequently, the enclosed area is smaller. The other case, Figure 4.13(a), is the opposite, with poorer compactness but larger enclosed areas. Neither of these cases is an exact representation of reality, but in order to simulate and obtain an approximation of the required number of turns, an average of both cases will be used.

Furthermore, the previously defined perimeter and area (equations 4.16 and 4.17) will not always remain the same due to the accumulation of turns on top of each other. This is something that the code will take into account. If we hypothetically start winding the Magnetorquer from the outer layers, the subsequent layers will have reduced area and perimeter because they must be contained within the perimeter defined by the previous layer.

Additionally, when reducing a layer using the compact model shown in Figure 4.13(b), the dimensions detailed in Figure 4.11 will be reduced by the cable diameter. In the case of Figure 4.13(a), they will be reduced by a distance *"h"* (defined in the same figure) that depends on the cable diameter used. This distance can be calculated as follows.

$$h = \frac{\sqrt{3}}{2} \cdot d \quad [m] \tag{4.18}$$

Therefore, each time the code needs to change to a new layer, it should reduce the dimensions C_1 and C_2 by twice the distance h, as this amount is reduced on both sides of the magnetorquer. In the defined geometry, the measurement B will always be a proportion of the measurement C_1, so we will use this proportion to calculate the new measurements A_1 and A_2. This is detailed in Figure 4.14.

$$F = \frac{B^{MAX}}{C_1^{MAX}} \tag{4.19}$$

With this factor F, it is possible to calculate the characteristic dimensions of the next layer ($n = 2$) with those of the previous layer ($n = 1$). The formulas to calculate the dimensions are as follows:

$$C_{1,2}^{n=2} = C_{1,2}^{n=1} - 2 \cdot h \quad [m] \tag{4.20}$$

$$B^{n=2} = C_{1,2}^{n=2} \cdot F \quad [m] \tag{4.21}$$

$$A_{1,2}^{n=2} = C_{1,2}^{n=2} - B^{n=2} \quad [m] \tag{4.22}$$

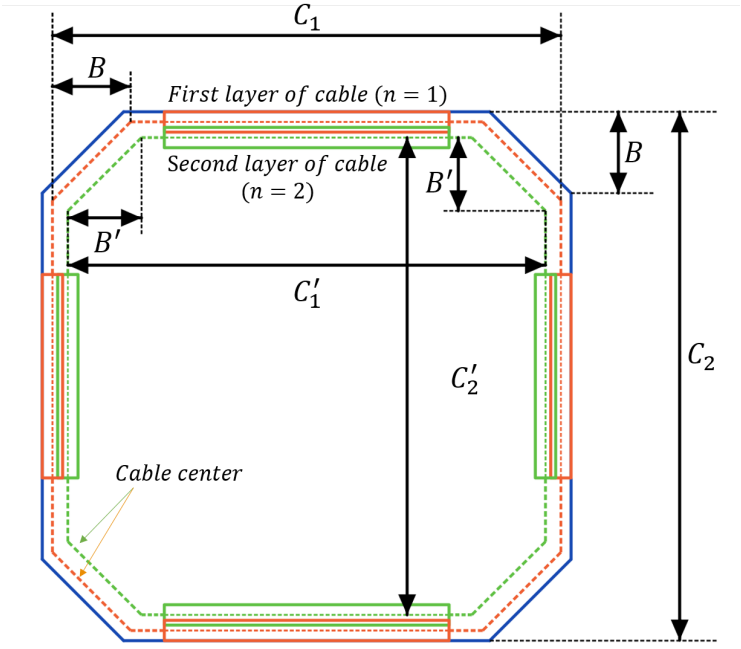

Figure 4.14: MTQ layer geometry definition.

4.5.2. Code workflow

The following image is a flowchart of the process followed by the MATLAB code to generate the required plots for the design of the actuators.

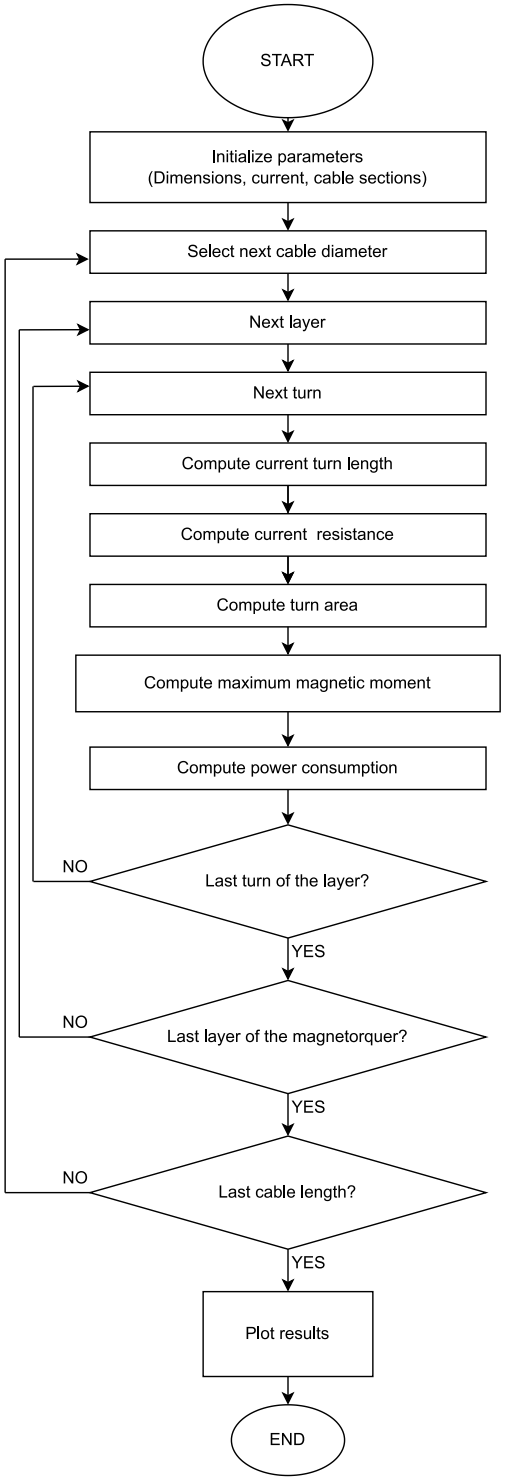

Figure 4.15: Magnetorquer (MTQ) code flowchart.

The code starts by initializing the design parameters, such as the different diameters to simulate, the maximum current, and the maximum dimensions of the MTQ. After that, a

loop begins in which the length of the coil (4.17), its resistance (4.6), the enclosed area (4.16), the magnetic moment (4.2), and the power consumed (4.10) are calculated. The loop iterates through all the coils of the layer until the available space is exhausted, and then continues with the next layer. This process continues until the available space defined by the ”Maximum height” distance (Figure 4.11) is exhausted.

4.5.3. Final results

Once the code is finished, the necessary plots are obtained to select the design variables of the magnetorquer. It is worth noting that the plots represent the magnetic moment and power consumed by two parallel magnetorquers with the same characteristics (same cable, same number of turns). As can be seen, as the cable diameter increases, the power consumed decreases significantly (due to the fact that the cable resistance is inversely proportional to its cross-sectional area, as per the formula 4.6). However, the same does not apply to the magnetic moment, which decreases to a lesser extent. For this reason, we will try to choose the thickest possible diameter that meets the performance and power consumption requirements.

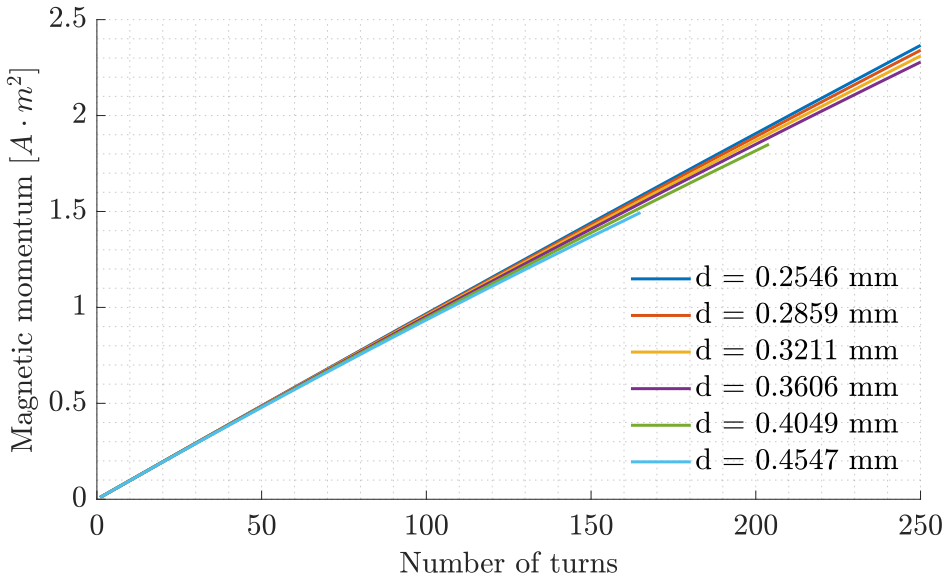

Figure 4.16: MTQ Z Magnetic moment ($I_{max} = 1A$).

As can be seen from the previous figure, there is only one cable diameter that would not meet the performance requirements, which is the 0.46 mm diameter cable, the thickest one. To meet this requirement, it would need more turns than can fit in the magnetorquer structure. However, the cable with a diameter of 0.4 mm (caliber 26 in the AWG standard) does meet this requirement. With 170 turns, the magnetorquers would exert a magnetic moment of 1.57 Amperes per square meter. Now let’s see if this diameter meets the power conditions.

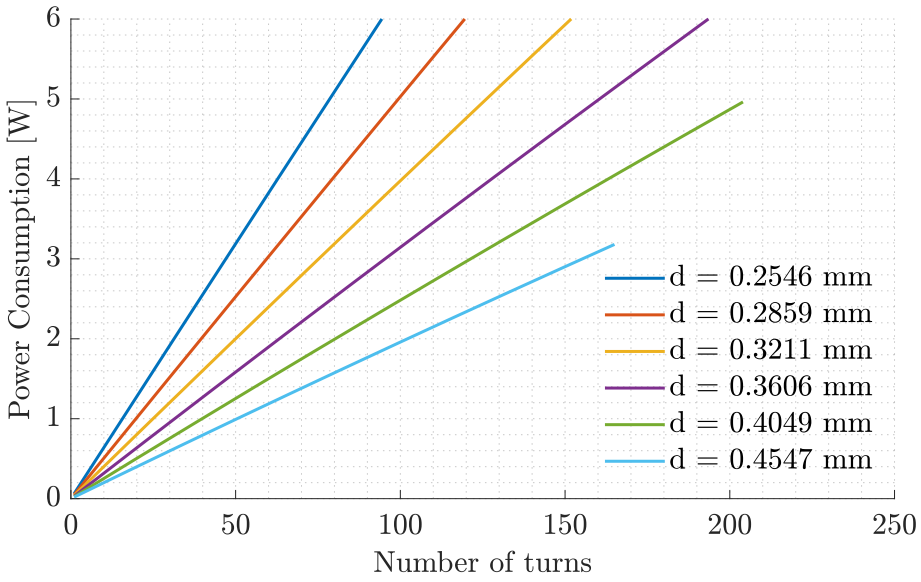

Figure 4.17: MTQ Z power consumption.

By analyzing the power plot, it can be observed that the MTQ (two in parallel) also meets the power requirement. Specifically, for two magnetorquers in parallel operating at a total current of 1 Ampere, the power consumed is 4.19 Watts.

These aforementioned data indicate that the construction of the magnetorquers would allow for satellite control.

Below is a table summarizing the key parameters of the MTQ that will be manufactured as an Engineering Model to verify that these characteristics are suitable in practice. If these requirements are met in the EM, the design will be finalized and we will be able to proceed with the Flight Model manufacturing stage.

Magnetorquer Z characteristics		
Parameter	**Value**	**Units**
Cable Diameter	0.405	mm
Number of turns	170	-
Theoretical Resistance	8.37	Ω
Total area ($\sum_{i=0}^{N} A_i$)	1.57	m^2
Theoretical magnetic moment ($I = 1A$)	1.57	$A \cdot m^2$
Theoretical power consumption	4.19	W

Table 4.1: Magnetoquer Z design values.

4.6. Manufacturing

Once the design process is complete, the manufacturing stage begins. In this stage, an Engineering Model (EM) of the magnetorquer was constructed to verify the hypothetical results obtained in the design phase. This section describes the complete manufacturing process.

The first step in building the EM is to create the component's model where the MTQ will be installed. Since this is a simulation to verify the design, the component will be 3D printed using plastic. It is important to note that the final Flight Model will be manufactured using aluminum. Below, you will find a photo of the piece during the printing process and another photo of the completed piece.

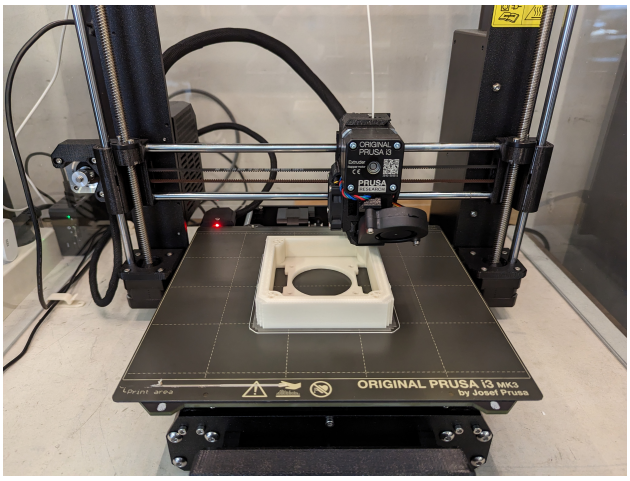

Figure 4.18: Printing process picture.

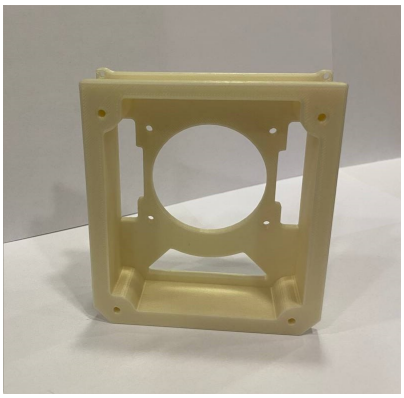

(a) First view of the winded Z magnetorquer.

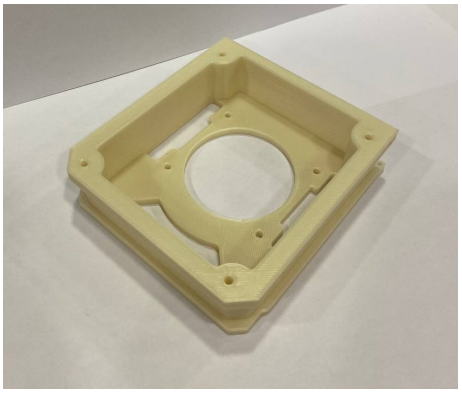

(b) Second view of the printed magnetorquer.

Figure 4.19: Printed Magnetorquer.

After that, it's time to start winding the magnetorquer. It's important to note that the printed structure (Figure 4.19) has space for two magnetorquers that will be connected in parallel, as specified in section 4.2.2.. This information is particularly relevant when interpreting the data obtained during the testing phase (section 4.7.), as the power consumed will be

double what was calculated. To facilitate and expedite the winding process, the following setup was used. Since there were two winding machines available, both were utilized to increase efficiency. First, the machines were positioned facing each other. One machine held the copper wire spool, while the MTQ was placed in front of the other machine. The end of the wire was tied to the MTQ. As the MTQ began to rotate, the wire was tensioned, causing the machine holding the copper wire spool to also rotate. During this process, the wire was unwound from the spool and wound onto the Magnetorquer's structure. It was necessary to guide the wire to ensure optimal placement. Fortunately, the winding machines had a built-in turn counter, so it wasn't necessary to manually keep track of the number of turns during the process. Below is an image of the setup.

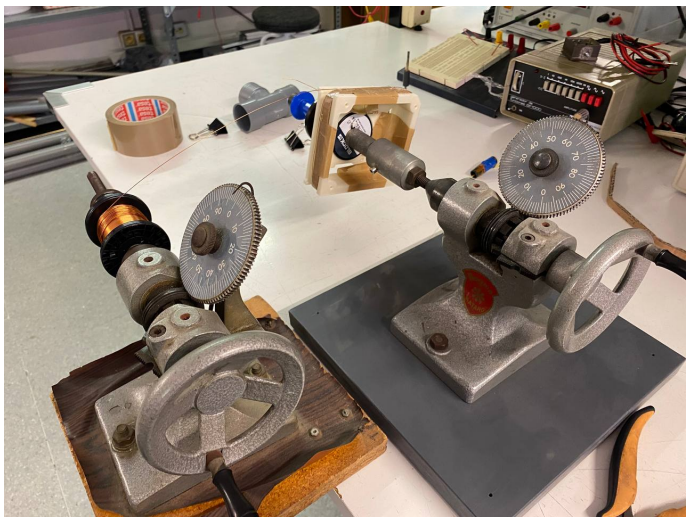

Figure 4.20: Magnetorquer manufacturing setup.

The described process involved introducing 170 turns into the structure of the Z-axis magnetorquer.

Once the winding process was completed, the result is as follows:

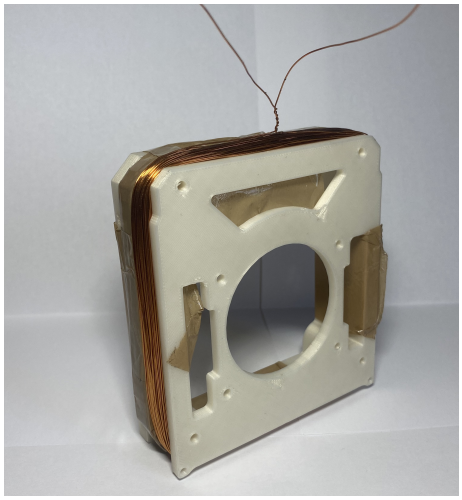

(a) First view of the magnetorker Z winding.

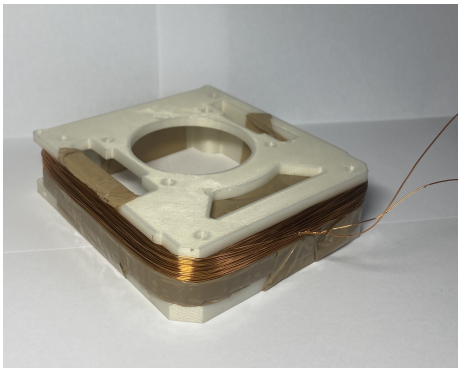

(b) Second view of the magnetorker Z winding.

Figure 4.21: Manufactured magnetorquer Engineering Model (EM).

4.7. Testing

In this section, we describe all the tests that were conducted to characterize and analyze the feasibility of the magnetorquer and to verify its functionality. Firstly, an impedance analysis was performed to characterize its electronic model as outlined in Section 4.2.2.. Additionally, a measurement of the magnetic field generated by the magnetorquer was also conducted. All of these tests are described in detail in the following sections.

4.7.1. Impedance characterisation

The first test conducted was the impedance test. This test is performed to characterize the impedance and electronic model of the magnetorquer based on empirical data collected. Its main purpose is to make a decision regarding the frequency of the Pulse Width Modulation (PWM) signal. Two main tests were carried out, one in Direct Current (DC) and another in Alternating current (AC). By observing the change in impedance with frequency, a more accurate electrical model can be defined compared to the one previously stated (4.2.2.).

Firstly, the impedance test was performed in DC, which means at zero frequency. This test primarily serves to verify that the resistance calculation performed during the design stage aligns with the actual value (4.6). A voltmeter was used for this experiment. The resistance of the MTQ was measured to be 8.3 ohms, a value closely matching the analytically calculated value during the design process (4.5.3.).

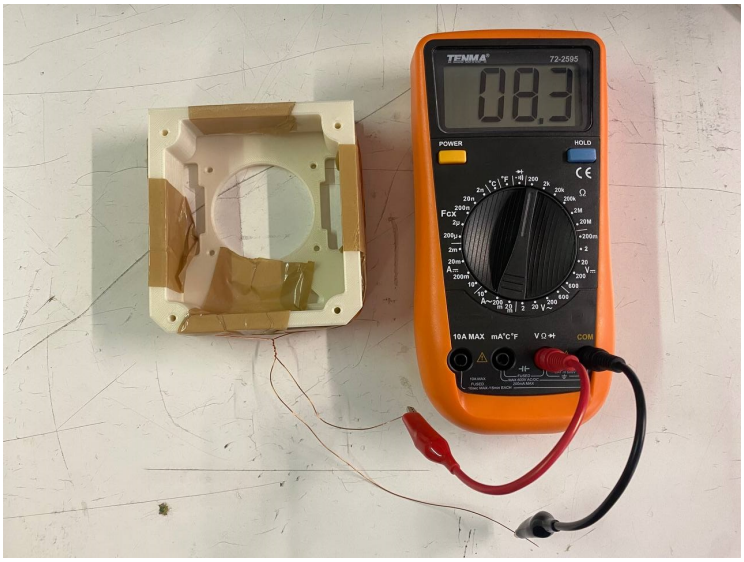

Figure 4.22: Magnetorquer (MTQ) DC impedance.

The second test, in Alternating current (AC), was conducted using an *HP Precision Impedance Analyzer (4294A)* located in the research laboratory of the *Grup d'Instrumentació, Sensors i Interfícies (ISI)* (aula 020B) at the Escola d'Enginyeria de Telecomunicació i Aeroespacial de Castelldefels (EETAC). The following image depicts the moment when the test was being performed.

Figure 4.23: Impedance analyzer.

Since it is an old instrument that does not support screen captures, it was necessary to manually record the data and plot it using *MATLAB*. The following plot displays the results obtained.

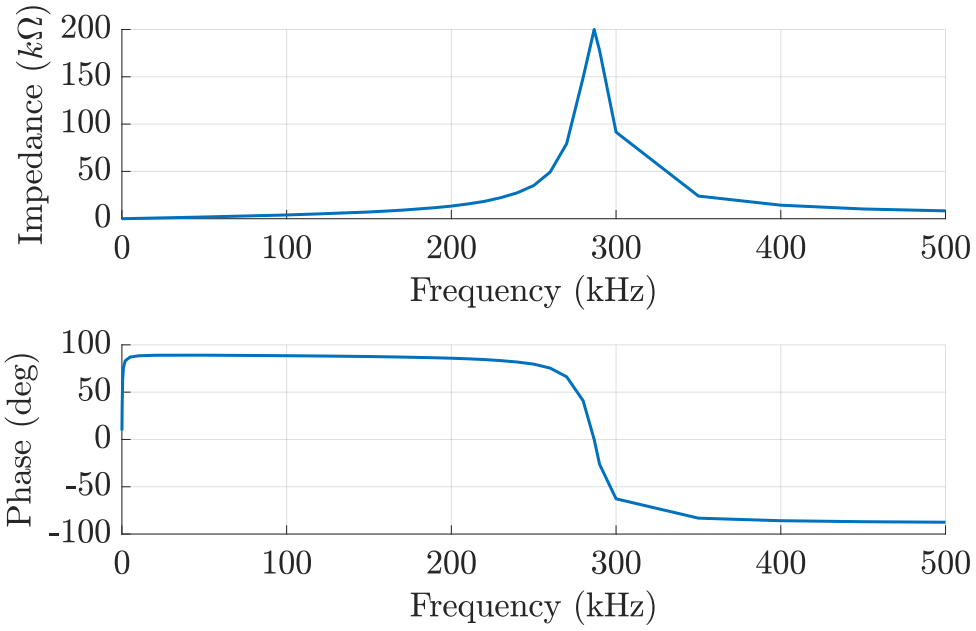

Figure 4.24: Magnetorquer impedance (module and phase) vs frequency.

As observed in the plot, there is a resonance at $286.7kHz$ where the impedance reaches a maximum of $200k\Omega$. Additionally, the phase is zero. This phenomenon suggests that the

magnetorquer contains two reactive elements that are resonating. A model that fits this frequency response is a series resistance with an inductance and, in parallel, a capacitance.

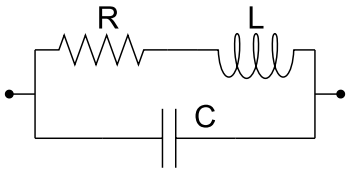

Figure 4.25: Magnetorquer (MTQ) empiric electrical model.

This model simulates the impedance response across the frequency spectrum, with the resonance frequency being:

$$f_0 = \frac{1}{2\pi \cdot \sqrt{L \cdot C}} \quad [Hz] \tag{4.23}$$

Below is a table of values along the frequency axis to provide a quantitative overview of the impedance values:

Frequency	**Impedance module**	**Impedance's phase (degrees)**
0 Hz	8,3 Ω	0
100 Hz	8,976 Ω	22.60
1 kHz	35,752 Ω	76.44
10 kHz	343,962 Ω	88.42
100 kHz	3.95 kΩ	88.52
250 kHz	35.06 kΩ	79.61
286.7 kHz	200 kΩ	0

Table 4.2: Some impedance measurements.

To decide the pulse repetition frequency of the PWM signal, two factors must be taken into account. The frequency should be low enough so that the input impedance of the magnetorquer is not excessively high, and it should be high enough for the satellite to have a fast response to attitude disturbances. By evaluating both factors and seeking a balance between them, a pulse repetition frequency of 100 Hz could be suitable. This frequency exhibits a very low impedance, similar to the impedance in DC, and has a pulse period of 10 ms, resulting in 100 pulses per second. Having 100 pulses per second would enable a quick response to rapid attitude changes of the satellite.

$$T = \frac{1}{f} = \frac{1}{100\,Hz} = 0.01\,s = 10\,ms \tag{4.24}$$

$$N = \frac{1s}{0.01s} = 100\,pulses\,per\,second \tag{4.25}$$

4.7.2. Magnetic field measurement

The next test conducted was the measurement of the magnetic field generated by the electromagnet. This test was carried out in laboratory D4-213 at the Campus Nord of UPC.

The purpose of this test is to confirm that the designed and constructed magnetorquer truly meets the performance requirements and power consumption (based on the current applied and the exerted magnetic moment). It aims to verify if the device will allow the spacecraft to control its attitude and point towards the GS.

Different tests were conducted with various configurations due to the issues that arose during the testing campaign. To simulate flight conditions as realistically as possible, it would be ideal to use an H-Bridge circuit to introduce the PWM signal to the Magnetorquer. However, this circuit was not available for testing. Additionally, at the time of the tests, it was not known that the PWM signal frequency of the TRISKEL OBC ([48]) was adjustable between 1 Hz and 250 kHz. This information was provided by the company Alén Space after the ADCS team of 3Cat-8 inquired. When conducting the first test, the results of the impedance study from the previous section were already known. Therefore, introducing a 250 kHz signal caused most of the power to not be utilized in generating a magnetic field since the impedance at that frequency is practically imaginary (Section 4.2.2.).

Initially, the magnetic test was performed using a precision magnetometer used in aircrafts and spacecrafts ([50]). However, the purpose of this type of magnetometer is to accurately measure the Earth's magnetic field, which is relatively small compared to the fields generated by a magnetorquer of this nature. This implies that the dynamic range of this device is too small ($\pm 60\,\mu T$). Finally, the magnetometer installed in an *iPhone 11* was used, along with the *"Physics Toolbox Sensor Suite"* application, which allows real-time measurement of the magnetic field around it. The magnetometer in the iPhone is not as precise as the *Billingsley* magnetometer, but it does allow for measuring a wider range of magnetic fields.

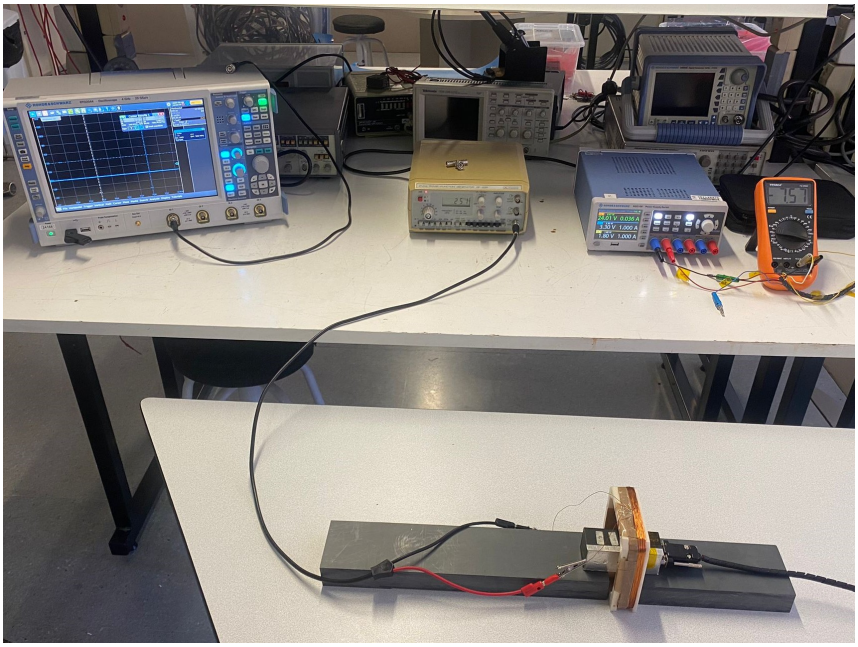

Figure 4.26: First magnetic field test with the Billingsley sensor.

For the reasons mentioned earlier, the magnetic field test was conducted as follows: A DC power supply was used, connected directly to the Magnetorquer, and the voltage was gradually increased. As the voltage increased, so did the introduced current, and with it, the generated magnetic field. Additionally, the power supply allowed for monitoring the current passing through the magnetorquer at all times, enabling a more in-depth analysis.

The following photo shows the setup for measuring the generated magnetic field. It's worth noting that the iPhone's magnetometer is located in the upper-left corner, and to measure the magnetic field generated by the coil, the magnetometer should be placed in the center of the coil.

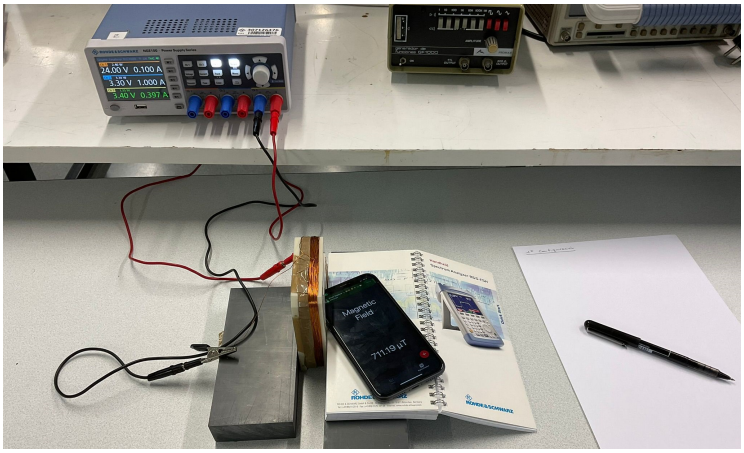

Figure 4.27: Final magnetic field test.

When collecting the magnetic field data, there were other magnetic fields that influenced the measurement, such as the Earth's magnetic field or the magnetic field from the phone's speaker magnets. To mitigate their impact, each time a data point was taken, a measurement was also taken with the MTQ turned off. This way, the readings could be subtracted later to obtain only the field generated by the actuator.

Firstly, current vs. voltage curves were plotted for the ideal data (4.5.3.) and the data obtained in the laboratory. As can be seen, as the voltage increases, the Magnetorquer stops admitting the expected current. This effect can be attributed to various factors, such as the heating of the wire due to Joule effect. At a certain point, the wire becomes unable to dissipate as much power and stops accepting current. Additionally, this characteristic curve perfectly follows Ohm's law, with its slope representing the inverse of the MTQ's resistance. The graph also shows the Magnetorquer's saturation point, which is the maximum point of magnetic field generation. Beyond that point, the MTQ ceases to accept current, and therefore, it does not generate stronger magnetic fields.

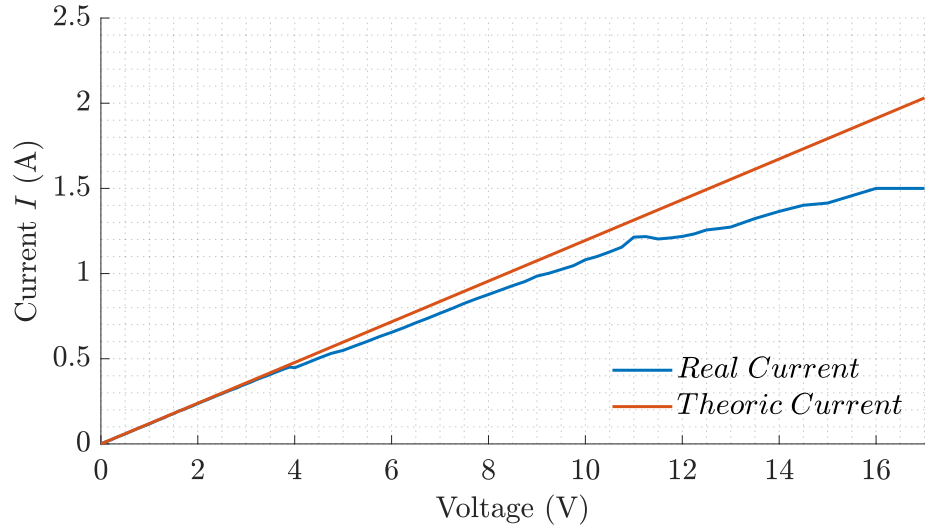

Figure 4.28: Voltage vs Current. Theorical and empirical values.

The generated magnetic field was also plotted as a function of current. Considering that the Earth's magnetic field values range between $\pm\, 25\, \mu T$ and $\pm\, 65\, \mu T$, the magnetic field generated by the MTQ is significantly more powerful. Furthermore, this graph provides a clearer view of the MTQ's saturation point, where it stops generating a stronger magnetic field. This point is approximately at 1.32 Amperes, which is higher than the maximum current that the TRISKEL OBC can provide. This is a highly satisfying result, as it indicates that the available current is being fully utilized. The magnetic field generated by a MTQ powered with 1 Ampere is 1753 μT.

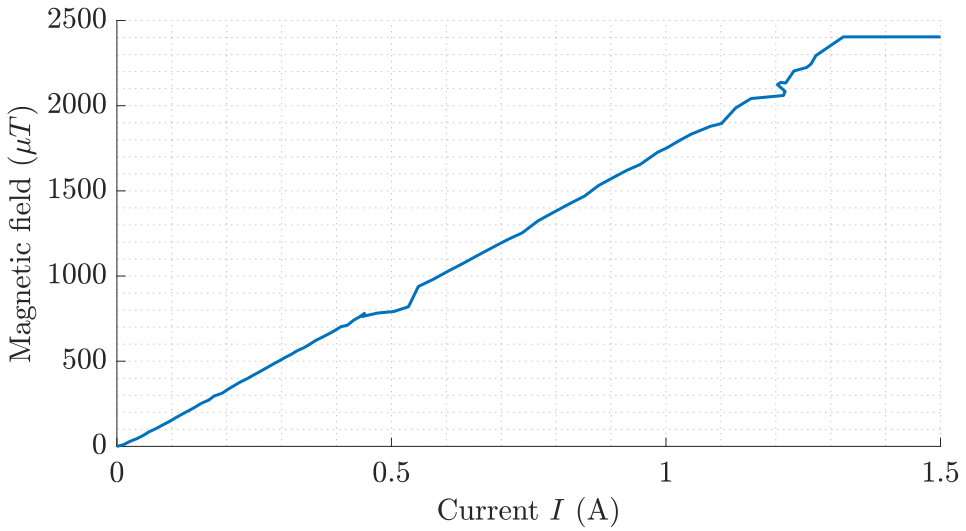

Figure 4.29: Magnetic field (μT) vs Current.

By using the physical parameters of the Magnetorquer (4.5.3.), the moment generated by it can be calculated using the formula 4.2. To do this, the current data obtained in the laboratory is multiplied by the total area of the MTQ (known because we know the number of turns) to obtain the generated moment. By plotting these data, we can obtain the magnetic moment generated by the Magnetorquer for different currents. The most important data point is the moment generated when a current of 1 Ampere is applied, which is equal to 1.574 $A \cdot m^2$. This value perfectly matches the theoretically calculated value. This indicates that the MTQ meets the performance requirements of the satellite.

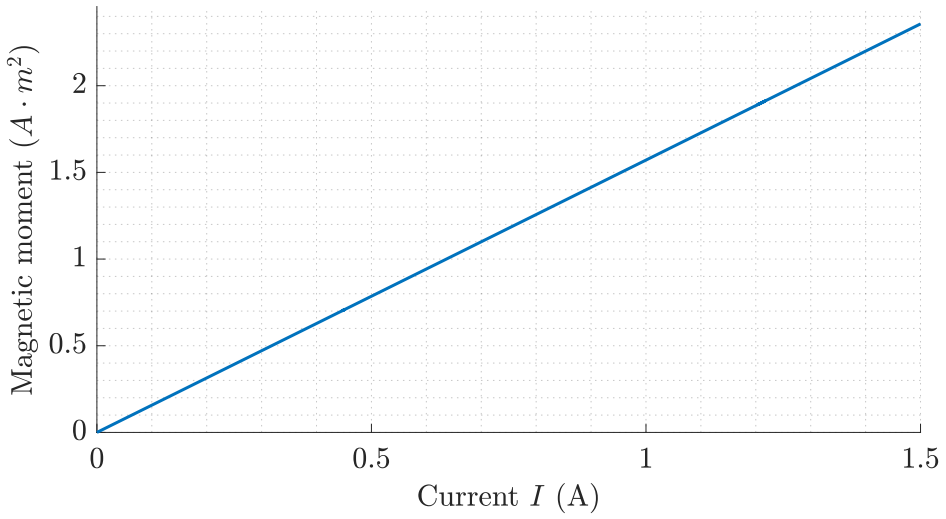

Figure 4.30: Magnetic moment ($A \cdot m^2$) vs Current.

Finally, it is necessary to verify if the power consumption requirements of the actuator are met. It is important to note that only one actuator is being measured, so the power consumption will be double when two magnetorquers are connected in parallel (4.14). However, this does not apply to the moment (4.15). The power consumption of the acr-shortmtq when a current of 1 Ampere is applied is 9.23 Watts. Half of this power is 4.6 Watts, which is higher than the theoretically calculated power. However, it still satisfies the power consumption requirements of the actuators.

Parameter	**Value**	**Unit**
Generated magnetic moment ($I = 1A$)	1753	$A \cdot m^2$
Generated magnetic field ($I = 1A$)	1.574	μT
Power consumption ($I = 1A$)	9.23	W

Table 4.3: Real MTQ values.

4.8. Conclusions & future work

In this section, the conclusions of the entire chapter are detailed, along with some tasks that can be carried out to continue the work done.

Firstly, as observed in the last section, the theoretical calculations align closely with the measurements obtained in the laboratory. This indicates that the tool developed for designing the MTQ of 3Cat-8 is truly useful and could be used in future missions. Regarding the designed magnetorquer, it is a solution that fulfills all the requirements for the 3Cat-8 satellite to properly control its attitude.

The next step is to wind the second MTQ and perform tests with both of them connected in parallel. Furthermore, to conduct a more realistic test that simulates the flight conditions, an H-Bridge circuit should be used to introduce the necessary current. Additionally, it is important to simulate the PWM signal at 100 Hz to make it even more appropriate.

Once the structural design team of 3Cat-8 has finished locating and sizing the MTQ for the X and Y axes, a similar analysis to the one conducted in this chapter should be performed.

Moreover, printing the aluminum structure of the magnetorquers and rewinding them will also be necessary. It is worth noting that when rewinding the MTQ in the final structure, a method for achieving greater compactness and rigidity is to use a Kapton film to insulate them from the structure and epoxy resin to gradually bond each turn to the film and the adjacent turns. This will allow for better cable compactness within the structure.

Once the design and assembly process of the 3Cat-8 mission is completed and all subsystems are mounted on the satellite structure, a simulated launch test should be conducted to verify that the satellite is capable of performing the detumbling maneuver (4.1.2.) using the simulated MTQ. This test will be carried out in the Helmholtz coils available in the NanoSat Lab facilities. These coils allow for simulating the magnetic field that the satellite would experience during several orbits and verifying if it successfully performs this maneuver. Additionally, at the center of these coils, there is a platform that can create a sense of weightlessness using compressed air, reducing friction and allowing the satellite to simulate the situation more closely to a real scenario.

CONCLUSIONS AND FUTURE WORK

This chapter concludes this Bachelor's thesis. The work encompasses and covers different areas of aerospace and telecommunications engineering, which are the degrees it aims to fulfil. Although the structure of the work is divided into different subsystems and may appear disconnected, this work cannot be understood without any of the chapters present. The initial objective, to develop an analysis of the communications of the 3Cat-8 satellite and design the S-band antenna and the satellite's actuators, has been successfully accomplished.

Throughout this work, the feasibility of the communication subsystems in the UHF, S, and X bands of the 3Cat-8 satellite was analyzed. Additionally, a preliminary design of the S-band antenna for the mission was carried out. Finally, a design and prototype of magnetic actuators were developed to ensure that the simulated communication analysis conditions are met. All of this has a common objective, which is to ensure that satellite communications are possible.

As mentioned in the previous paragraph, the first step was to conduct an analysis of the communication links. This analysis aimed to take into account all possible effects that could occur and hinder the proper functioning of these subsystems. In this process, several *MATLAB* codes were developed to simulate the Signal to Noise Ratio at different elevation angles. This code calculates all the aspects that were taken into consideration and presents the results in easily interpretable graphs. The results of these simulations are encouraging, as all the links appear to be viable initially. However, the initial conditions assume the existence of a pointing mechanism (an attitude control subsystem) that enables the satellite to align its antennas towards the ground station. This control subsystem would have devices called actuators that allow for this pointing movement. The objective of the fourth chapter of this work is to design these actuators.

Chapter four of this work focuses on the Attitude Determination and Control System and the design of magnetic actuators, also known as Magnetorquer (MTQ). In this chapter, the design and manufacturing of these devices are carried out to enable the satellite to perform the pointing towards the Ground Station. Throughout this chapter, a *MATLAB* code is developed to design the magnetorquers and determine the required number of turns and cable diameter. The structure of the MTQ is 3D printed with the assistance of a 3D printer, and the electromagnet is wound. Finally, appropriate tests are conducted to verify that the magnetorquer meets the requirements. The results of these tests confirm that the magnetorquers are capable of providing the necessary actuation power to enable the 3Cat-8 satellite to perform both detumbling and ground station pointing.

In addition, the design of an S-band antenna using microstrip technology was carried out. This design was performed using the electromagnetic simulation tool, CST Studio Suite. The results turned out to be very promising. However, due to time constraints, it was not possible to materialize this design and verify its functionality with an actual antenna prototype.

The main conclusion of this work is that, thanks to the design and implementation of the magnetorquers, the S-band and X-band communication subsystems will be feasible. Additionally, thanks to this implementation, the X-band antenna will be a 2x2 patch array that will improve the link conditions (section 3.3.4.). Furthermore, the code developed to simu-

late the magnetorquers proved to be highly accurate, showing a good agreement between theoretical and practical results. This code can be used in the future for different missions that require the implementation of such devices.

The work carried out can still be improved. Firstly, the design of the S-band antenna needs to be refined, manufactured, and its capabilities tested. Since it does not exist yet, it will be necessary to implement the X-band reception system and the antenna at the ground station (Observatorio Astronómico del Montsec). Additionally, the magnetorquers for the X and Y axes of the satellite need to be designed. Finally, flight models need to be constructed using aluminum structures and compacted as much as possible. This compactness can be achieved by bonding the magnetorquer turns with epoxy resin.

During the process of conducting this work, the complexity involved in the development of satellite systems was comprehended. These systems are meticulously designed to ensure precise functionality. Achieving this requires optimal coordination among all team members involved. Furthermore, working on a project of this magnitude entails a comprehensive understanding of the mission and its characteristics. In its entirety, working on space applications, specifically satellites, requires utmost dedication and concentration on the proposed tasks. One important lesson that this experience has taught me is that the development of a satellite does not solely entail aerospace engineering or telecommunications engineering but encompasses all engineering disciplines and necessitates their thorough knowledge and application.

BIBLIOGRAPHY

[1] Nanosats Database. *"Nanosatellite Launches"*. ix, 1

https://nanosats.eu

[2] NanoSat Lab UPC. *"3Cat-4"* ix, 4

https://nanosatlab.upc.edu/en/missions-and-projects/3cat-4

[3] Instituto de estudios espaciales de Cataluña (IEEC). *"C3SatP description"*. 6

https://www.ieec.cat/content/30/success-cases

[4] IENAI SPACE. *"ATHENA ionic Thuster"*. 7

https://ienai.space

[5] Sputnik 1. IDIS ix, 12

https://proyectoidis.org/sputnik-1

[6] Héctor Rodríguez. *"La Carrera Espacial paso a paso"*

https://www.nationalgeographic.com.es/llegada-del-hombre-a-la-luna/carrera-espacial-paso-a-paso_14369

[7] NASA. *"July 12, 1962: The Day Information Went Global"*. ix, 12

https://www.nasa.gov/topics/technology/features/telstar.html

[8] NASA. *"Voyager mission"*. 12

https://voyager.jpl.nasa.gov

[9] NASA. *"Voyager 2"*. ix, 13

https://es.wikipedia.org/wiki/Voyager_2

[10] CubeSat.org *"CubeSat Standard"*. 13

https://cubesat.org

[11] European Space Agency. *"ESA's Technology CubeSats"*. ix, 14

https://www.esa.int/Enabling_Support/Space_Engineering_Technology/Technology_CubeSats

[12] Alén Space. *"Basic guide for nanosatellites"*. ix, 14

https://alen.space/es/guia-basica-nanosatelites

[13] ISISPACE. *"CubeSat Antenna System for 1U/3U"*. 15, 16

https://www.isispace.nl/product/cubesat-antenna-system-1u-3u

[14] NanoAvionics. *"CubeSat UHF Antenna System"*. 15

https://nanoavionics.com/cubesat-components/cubesat-uhf-antenna

[15] NASA. *"PhoneSat 2.5"*.

https://www.nasa.gov/centers/ames/engineering/projects/phonesat

[16] Ahmed M. A. Sabaawi, Charalampos C. Tsimenidis. *"Circular truncated patch antennas for energy harvesting applications"* (Newcastle University, UK, 2013). ix, 16

https://www.nasa.gov/centers/ames/engineering/projects/phonesat

[17] Mehdi Hasan Chowdhury, Quazi Delwar Hossain, Md. Azad Hossain, Ray C.C. Cheung. *"Single Feed Circularly Polarized Crescent-Cut and Extended Corner Square Microstrip Antennas for Wireless Biotelemetry"*. (International Journal of Electrical and Computer Engineering, Vol. 9, No. 3, June 2019, pp. 1902 - 1909) ix, 17

https://www.researchgate.net/publication/330277091_Single_Feed_Circularly_Polarized_Crescent-Cut_and_Extended_Corner_Square_Microstrip_Antennas_for_Wireless_Biotelemetry

[18] EnduroSat. *"EnduroSat Antenna solutions"*. ix, 17

https://www.endurosat.com/products/#cubesat-antennas

[19] Jonathan Sauder, Nacer Chahat, Richard Hodges, Eva Peral Yahya Rahmat-Samii and Mark Thomson. *"Lessons Learned from a Deployment Mechanism for a Ka-band Deployable Antenna for CubeSats"* (NASA Glenn Research Center, May 16-18, 2018). ix, 18

https://esmats.eu/amspapers/pastpapers/pdfs/2018/sauder.pdf

[20] Nasa's Jet Propulsion Laboratory. *"NASA Adds Giant New Dish to Communicate With Deep Space Missions"*. ix, 19

Link

[21] Jin S. Kang, Jeffery T. King, Christopher R. Anderson, Michael H. Sanders. *"Performance Analysis of Passive Magnetic Pointing Method for Implementation of Directional Antennas on CubeSats"* (International Journal of Aeronautical and Space Sciences, March 2022). ix, 20

https://www.researchgate.net/publication/359300442_Performance_Analysis_of_Passive_Magnetic_Pointing_Method_for_Implementation_of_Directional_Antennas_on_CubeSats

[22] ISISPACE. *"iMTQ Board"*. ix, 21

https://www.isispace.nl/product/isis-magnetorquer-board/

[23] CUBESPACE. *"GEN1: CubeWheel"*. ix, 22

https://www.cubespace.co.za/products/gen-1/actuators/cubewheel/

[24] ENPULSION. *"NANO R³"*.

https://www.enpulsion.com/order/nano-r3/

[25] Wikipedia. *"Orbital elements"*. ix, 24

https://es.m.wikipedia.org/wiki/Archivo:Orbital_elements.svg

[26] Wikipedia. *"List of orbits and constellations"*. ix, 25

https://en.wikipedia.org/wiki/List_of_orbits

[27] NASA Earth Observatory. *"Catalog of Earth Satellite Orbits"*. ix, 26

https://earthobservatory.nasa.gov/features/OrbitsCatalog

[28] Princeton University. *"Space System Design course slides. Lecture 16: Telecommunications. Slide 5"*. ix, 29

http://www.stengel.mycpanel.princeton.edu/MAE342Lecture16.pdf

[29] Wikipedia. *"Electromagnetic radiation"*. ix, 30

https://commons.wikimedia.org/wiki/File:Electromagnetic_wave2.svg

[30] Wikipedia. *"Reed–Solomon error correction"*. 32

https://en.wikipedia.org/wiki/Reed-Solomon_error_correction

[31] National Aeronautics and Space Administration (NASA). *"U.S. Standard Atmosphere"*. (Washington D.C. October 1, 1976) 34

https://ntrs.nasa.gov/citations/19770009539

[32] David Long, Fawwaz Ulaby. *"Microwave Radar and Radiometric Remote Sensing"*. ix, 35, 36

https://ieeexplore.ieee.org/document/9100160

[33] Meteoblue. *"Datos climáticos y meteorológicos históricos simulados para el Montsec d'Ares"*. 35

https://www.meteoblue.com/es/tiempo/historyclimate/climatemodelled/el-montsec

[34] MATHWORKS *"gaspl: RF signal attenuation due to atmospheric gases"*. ix, 35

https://es.mathworks.com/help/phased/ref/gaspl.html

[35] NanoSat Lab UPC. *"Ground Segment"*. 42

https://nanosatlab.upc.edu/en/facilities-folder/ground-segment

[36] EnduroSat *"S-Band Patch Antenna"* 42, 54, 58

https://www.endurosat.com/cubesat-store/cubesat-antennas/s-band-patch-antenna/

[37] Antesky. *"2.4M X-band Antenna"*. Link. 47

[38] Antesky. *"3.7M X-band Antenna"*. Link. 47

[39] elliptika *"Microstrip technology"* x, 49

https://www.elliptika.com/en/case-studies/microstrip-technology/

[40] Rogers Corporation. *"RT/duroid 5880 Laminates"*. xii, 54

https://www.rogerscorp.com/advanced-electronics-solutions/rt-duroid-laminates/rt-duroid-5880-laminates

[41] Mouser Electronics *"QCS-312+"*. 55

Link.

[42] Mouser Electronics. *"Antenna connector model"*. 55

Link.

[43] ISISPACE. *"S-Band Antenna"*. 58

https://www.isispace.nl/product/s-band-patch-antenna/

[44] Wikipedia. *"Ampere's Law"*. x, 63

Link.

[45] Physics-SchoolUK *"Electromagnets"*. x, 63

Link

[46] Encyclopædia Britannica. *"Magnetic dipole"*. x, 64

https://www.britannica.com/science/magnetic-dipole

[47] Modular Circuits. *"H-Bridges – the Basics"*. x, 65

https://www.modularcircuits.com/blog/articles/h-bridge-secrets/h-bridges-the-basics/

[48] ALEN Space. *"TRISKEL"*. x, 66, 82

https://products.alen.space/products/triskel

[49] Harold A. Wheeler. *"Simple Inductance Formulas for Radio Coils"*. 66

https://ieeexplore.ieee.org/document/1669896

[50] Billingsley Aerospace and Defence. *"TFM65-VQS magnetometer"*. 82

https://magnetometer.com/products/fluxgate-magnetometers/tfm65-vqs/

[51] Ajinkya Phanse, Atharva Karaguppi, Onkar Murkewar, Shubham Thorat, Madhur Nalawade, Onkar Bhakare, Aman Gupta. *"Design, Implementation and Comparison of Power Electronic Circuits for Current Control through 3-axis Magnetorquer coils in a Satellite"* (College of Engineering, Pune, July 2019).

https://ieeexplore.ieee.org/document/8998925

[52] N. Jovanovic , B. Riwanto , P. Niemelä , M. Rizwan Mughal , and J. Praks. *"Design of Magnetorquer-Based Attitude Control Subsystem for FORESAIL-1 Satellite"*. (IEEE Journal on miniaturization for air and space systems, Vol. 2, No. 4, December 2021).

https://ieeexplore.ieee.org/document/9468712

[53] FENG Qian, LIU Yong, LI Lizhe, PAN Quan, ZHANG Chunming, YANG Guang. *"Optimal Design and Implementation of Coreless Magnetic Torque for Nano-satellites"* (Northwestern Polytechnical University. 2013, Xi'an, China).

https://ieeexplore.ieee.org/document/6640418

APPENDICES

APPENDIX A. GANT DIAGRAM

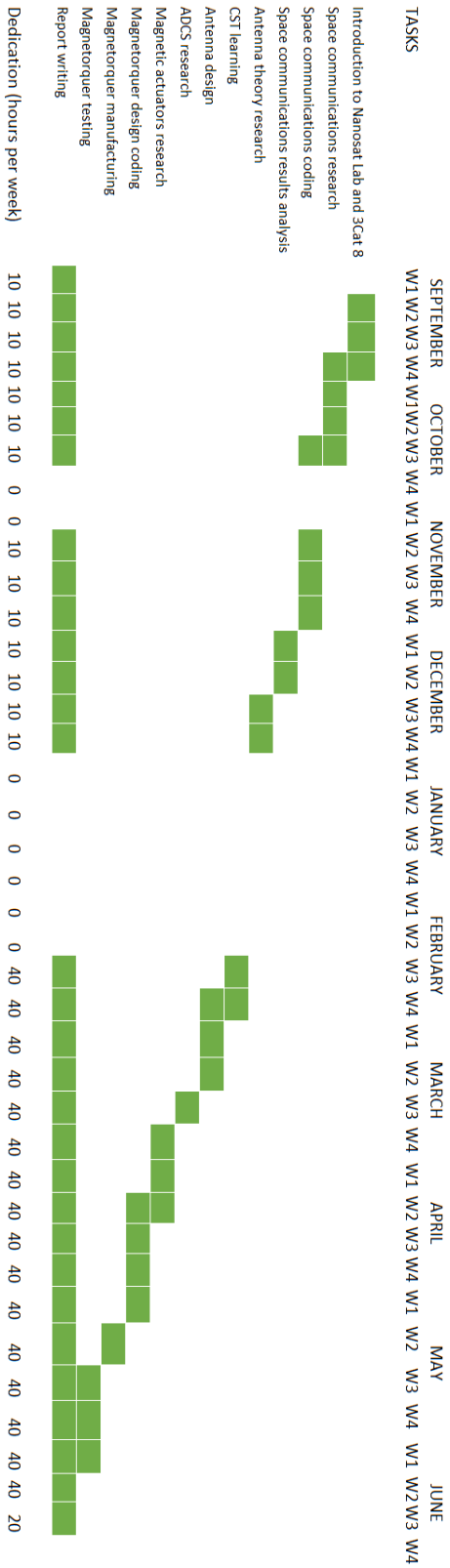

Figure A.1: Gantt diagram of this Bachelor's Thesis.

APPENDIX B. PROJECT BUDGET

Licenses

Item	Price	QTY.	Total
Matlab Student License	€69/year	1 year	€69
SolidWorks Student License	€90/year	1 year	€90
CST University License	€2.999/year	1 year	€2.999

Material

Item	Price/Quantity	QTY.	Total
3D printing	€90 (Min. price)	1	€90
AWG wire	€27/wire reel	2	€54

Wage

Item	Price/Quantity	QTY.	Total
Gross wage	€23.000/year	10 months	€19.167
IRPF taxes (15,22 %)	€3.500/year	10 months	€2.917
Other contributions	€1.621/year	10 months	€1.351
Net salary	€17.878/year	10 months	€14.899

Total			€18.200

Table B.1: Project Budget.

APPENDIX C. LINK BUDGET MATLAB CODE

This appendix includes the codes used to simulate the link budgets.

C.1. UHF-Band

```
clear;clc;close all;tit ='UHF-Band link budget';
%%%%%%%%%%%%%%%%%%%%%%%%%
% UHF -Band Link Budget %
%%%%%%%%%%%%%%%%%%%%%%%%%


%% CONSTANTS

% Propagation constants
f_UL = 438e6;            % Max frequency (Worst Lfs case) (Hz)
f_DL = 440e6;            % Max frequency (Worst Lfs case) (Hz)
c  = 3e8;                % Light speed (m/s)
lambda_UL = c/f_UL;      % Wave length
lambda_DL = c/f_DL;      % Wave length
k  = 1.38064852E-23;     % Boltzman's constant
T0 = 290;                % Temperatura (K)

% Orbit parameters
Re        = 6371E3;       % Earth radius (m)
h         = 600E3;        % Orbit height (m)

elev_deg = 5:5:175;           % Elevation angles (deg)
elev_rad = deg2rad(elev_deg);% Elevation angles (rad)

SR    = sqrt( (Re+h)^2 -(Re*cos(elev_rad)).^2 ) -Re*sin(elev_rad); % Satellite slant range

%% Link Budget initial constrains

% Transmission params
Pt_DL      = [0.25,0.5,1]; % Transmission power from cubesat (W)
Pt_UL      = 4;            % Transmission power from cubesat (W)

BW_DL    = [10,15,20]*1e3;      % RX Bandwidth
BW_UL    = [10,15,20]*1e3;      % TX Bandwidth

Mod_list  = ['GMSK';'BPSK';'QPSK'];
```

```
Mod_index = [2,2,4];

BER_DL      = 1E-5;      % Minimum bit error rate
BER_UL      = 1E-7;      % Minimum bit error rate

%% GAIN

% Antenna Gain
G_sat = 1.2;
G_GS  = 15;

% COMMS parameters
Gc = 3.2;  % dB Reed Solomon

%% LOSSES

% Free space losses
Lfs_DL = 20*log10(4*pi*SR/lambda_DL); % Downlinnk Free
   space losses (dB)
Lfs_UL = 20*log10(4*pi*SR/lambda_UL); % Uplink Free space
   losses (dB)

% Polarization losses in dB
Lpol = 3;

% Scintillation
Lsci = 0;

% Atmospheric losses
Latm = 0;

% Pointing losses
Lpointing = 0;

%% Noise

% Ground station G/T
NF_GS = 8.8; % dB
Ta_GS = 40;
Tsys = Ta_GS + T0*( 10^(NF_GS/10) - 1 );
GT_GS = G_GS -10*log10(Tsys)

% Satellite G/T
Ta_sat    = 300;        % K
NF_sat    = 3;          % dB
Tsys_sat = Ta_sat + T0*( 10^(NF_sat/10) - 1); % System
   temperature (Ts = Ta + Teq)
GT_sat    = G_sat   - 10*log10(Tsys_sat); % dBk^1
```

```
82
83
84  %% DOWNLINK
85
86  % Modulation parameters
87  BER_DL  = 1e-5; % Minimum bit error rate
88  Gc_BPSK_DL = 4.31;
89  Gc_GMSK_DL = 4.77;
90  a = 0.9;
91
92  EbN0_BPSK_DL =     (erfcinv(BER_DL*2))^2; EbN0_BPSK_DL =
       10*log10(EbN0_BPSK_DL)-Gc_BPSK_DL; EbN0_BPSK_DL = 10^((
       EbN0_BPSK_DL)/10);
93  EbN0_GMSK_DL = 1/a*(erfcinv(BER_DL*2))^2; EbN0_GMSK_DL =
       10*log10(EbN0_GMSK_DL)-Gc_GMSK_DL; EbN0_GMSK_DL = 10^((
       EbN0_GMSK_DL)/10);
94  EbN0_QPSK_DL =     (erfcinv(BER_DL*2))^2; EbN0_QPSK_DL =
       10*log10(EbN0_QPSK_DL)-Gc_BPSK_DL; EbN0_QPSK_DL = 10^((
       EbN0_QPSK_DL)/10);
95
96  EbN0_DL       = [EbN0_GMSK_DL,EbN0_BPSK_DL,EbN0_QPSK_DL];
97
98  for c=1:length(EbN0_DL)
99      SNRmin_DL(:,c) = 10*log10( EbN0_DL(c)*log2(Mod_index(c)
           ) );
100 end
101
102 % Calling Downlink
103 % ********** DOWNLINK **********
104
105 B = max(BW_DL); % Hz
106 Ptx = max(Pt_DL); % W
107
108 % Link budget for different transmitted powers
109 formatSpec ='%04.2f';
110
111
112
113
114 hfig = figure;
115 % title('UHF-Band LinkBudget Downlink')
116 % subtitle(['SNR vs elevation for different Transmitted
       Powers','(BW = ',num2str(B*1e-3),' KHz, BER = ',num2str(
       BER_DL),')']);
117 hold on;grid minor
118 xlabel('Elevation angle (deg)');xticks(0:20:180);xlim
       ([0,180]);
119 ylabel('SNR (dB)');yticks(0:5:30);ylim([0,30]);
```

```
120
121 for n=1:length(Pt_DL)
122
123         PIRE = 10*log10(Pt_DL(n)) + G_sat;
124
125         SNR_Pt(n,:) = PIRE + GT_GS - Lfs_DL - Lpol - 10*
               log10(k*B);
126
127 %          leg1(n,:) = ['Ptx = ',num2str(Pt_DL(n),formatSpec
    ),' W'];
128
129 %          plot(elev_deg,SNR_Pt(n,:))
130
131         plot(elev_deg,SNR_Pt(n,:),'-','LineWidth',1.5,'
               DisplayName',['Ptx = ',num2str(Pt_DL(n),
               formatSpec),' W'])
132
133 end
134
135 for n=1:1:length(Mod_index)
136
137 %      yline(SNRmin(n),'-',[Mod_list(n,:),'SNR min'])
138     plot(elev_deg,SNRmin_DL(n)*ones(1,length(elev_deg)),'-'
       ,'LineWidth',1,'DisplayName',[Mod_list(n,:),' $SNR_{
       min}$'])
139
140 end
141
142 % plot(elev_deg,SNRmin*ones(1,length(elev_deg)),'k-','
    LineWidth',1,'DisplayName',['BPSK $SNR_{min}$'])
143
144 % legend(leg1);legend('boxoff');legend('Location','
    northeast')
145
146 fname = 'UHFdownlink1';
147
148 picturewidth = 20; % set this parameter and keep it forever
149 hw_ratio = 0.65; % feel free to play with this ratio
150 set(findall(hfig,'-property','FontSize'),'FontSize',15) %
    adjust fontsize to your document
151
152 legend
153 set(findall(hfig,'-property','Box'),'Box','off') % optional
154 set(findall(hfig,'-property','Interpreter'),'Interpreter','
    latex')
155 set(findall(hfig,'-property','TickLabelInterpreter'),'
    TickLabelInterpreter','latex')
```

```
156 set(hfig,'Units','centimeters','Position',[3 3 picturewidth
        hw_ratio*picturewidth])
157 pos = get(hfig,'Position');
158 set(hfig,'PaperPositionMode','Auto','PaperUnits','
       centimeters','PaperSize',[pos(3), pos(4)])
159 print(hfig,fname,'-dpdf','-painters','-fillpage')
160 print(hfig,fname,'-dpng','-painters')
161 hold off;
162
163
164
165 % Link budget for different Bandwidths
166 formatSpec ='%04.1f';
167
168
169
170 hfig=figure;
171 % title('UHF-Band LinkBudget Downlink')
172 % subtitle(['SNR vs elevation for different Bandwidths','(
       Ptx = ',num2str(Ptx),' W, BER = ',num2str(BER_DL),')']);
173 hold on;grid minor
174 xlabel('Elevation angle (deg)');xticks(0:20:180);xlim
       ([0,180]);
175 ylabel('SNR (dB)');yticks(0:5:30);ylim([0,30]);
176
177 for n=1:length(BW_DL)
178
179     SNR_BW(n,:) = 10*log10(Ptx) +G_sat +GT_GS -Lfs_DL -Latm
            -Lpol -10*log10(k*BW_DL(n));
180
181 %     leg2(n,:) = ['BW = ',num2str(BW_DL(n)*10^-3,
       formatSpec),' KHz'];
182
183 %     plot(elev_deg,SNR_BW(n,:))
184
185     plot(elev_deg,SNR_BW(n,:),'-','LineWidth',1.5,'
           DisplayName',['BW = ',num2str(BW_DL(n)*10^-3,
           formatSpec),' KHz'])
186
187 end
188
189 for n=1:1:length(Mod_index)
190
191 %     yline(SNRmin(n),'-',[Mod_list(n,:),' SNR min'])
192     plot(elev_deg,SNRmin_DL(n)*ones(1,length(elev_deg)),'-'
           ,'LineWidth',1,'DisplayName',[Mod_list(n,:),' $SNR_{
           min}$'])
193
```

```
end

fname = 'UHFdownlink2';

picturewidth = 20; % set this parameter and keep it forever
hw_ratio = 0.65; % feel free to play with this ratio
set(findall(hfig,'-property','FontSize'),'FontSize',15) % adjust fontsize to your document

legend
set(findall(hfig,'-property','Box'),'Box','off') % optional
set(findall(hfig,'-property','Interpreter'),'Interpreter','latex')
set(findall(hfig,'-property','TickLabelInterpreter'),'TickLabelInterpreter','latex')
set(hfig,'Units','centimeters','Position',[3 3 picturewidth hw_ratio*picturewidth])
pos = get(hfig,'Position');
set(hfig,'PaperPositionMode','Auto','PaperUnits','centimeters','PaperSize',[pos(3), pos(4)])
print(hfig,fname,'-dpdf','-painters','-fillpage')
print(hfig,fname,'-dpng','-painters')
hold off;




%% Uplink

% Modulation parameters
BER_UL  = 1e-7; % Minimum bit error rate
Gc_BPSK_UL = 3.2;
Gc_GMSK_UL = 3.6;
a = 0.9;

EbN0_BPSK_UL =     (erfcinv(BER_UL*2))^2; EbN0_BPSK_UL = 10*log10(EbN0_BPSK_UL)-Gc_BPSK_UL; EbN0_BPSK_UL = 10^((EbN0_BPSK_UL)/10);
EbN0_GMSK_UL = 1/a*(erfcinv(BER_UL*2))^2; EbN0_GMSK_UL = 10*log10(EbN0_GMSK_UL)-Gc_GMSK_UL; EbN0_GMSK_UL = 10^((EbN0_GMSK_UL)/10);
EbN0_QPSK_UL =     (erfcinv(BER_UL*2))^2; EbN0_QPSK_UL = 10*log10(EbN0_QPSK_UL)-Gc_BPSK_UL; EbN0_QPSK_UL = 10^((EbN0_QPSK_UL)/10);

EbN0_DL       = [EbN0_GMSK_DL,EbN0_BPSK_DL,EbN0_QPSK_DL];

```

```
231 for c=1:length(EbN0_DL)
232     SNRmin_UL(:,c) = 10*log10( EbN0_DL(c)*log2(Mod_index(c)
        ) );
233 end
234
235 % Calling Uplink
236 % ********** UPLINK **********
237
238
239 % Link budget for different Bandwidths
240 formatSpec ='%04.1f';
241
242 Ptx = max(Pt_UL); % W
243
244 hfig=figure;
245 % title('UHF LinkBudget Uplink')
246 % subtitle(['SNR vs elevation for different Bandwidths','(
    Ptx = ',num2str(Ptx),' W, BER = ',num2str(BER_UL),')']);
247 hold on;grid minor
248 xlabel('Elevation angle (deg)');xticks(0:20:180);xlim
    ([0,180]);
249 ylabel('SNR (dB)');yticks(0:5:40);ylim([0,40]);
250 Ptx = 10*log10(Ptx);
251 for n=1:length(BW_UL)
252
253     SNR_BW(n,:) = Ptx + G_GS + GT_sat - Lpol - Lfs_UL -
        Latm - 10*log10(k*BW_UL(n));
254
255 %     leg4(n,:) = ['BW = ',num2str(BW_DL(n)*10^-3,
    formatSpec),' KHz'];
256
257 %     plot(elev_deg,SNR_BW(n,:))
258
259     plot(elev_deg,SNR_BW(n,:),'-','LineWidth',1.5,'
        DisplayName',['BW = ',num2str(BW_DL(n)*10^-3,
        formatSpec),' KHz'])
260
261 end
262
263 for n=1:1:length(Mod_index)
264
265 %     yline(SNRmin(n),'-',[Mod_list(n,:),' SNR min'])
266       plot(elev_deg,SNRmin_UL(n)*ones(1,length(elev_deg)),'
          -','LineWidth',1,'DisplayName',[Mod_list(n,:),' $
          SNR_{min}$'])
267
268 end
269
```

```
% legend(leg4);legend('boxoff');legend('Location','
    northeast')
legend

fname = 'UHFuplink1';

picturewidth = 20; % set this parameter and keep it forever
hw_ratio = 0.65; % feel free to play with this ratio
set(findall(hfig,'-property','FontSize'),'FontSize',15) %
    adjust fontsize to your document

set(findall(hfig,'-property','Box'),'Box','off') % optional
set(findall(hfig,'-property','Interpreter'),'Interpreter','
    latex')
set(findall(hfig,'-property','TickLabelInterpreter'),'
    TickLabelInterpreter','latex')
set(hfig,'Units','centimeters','Position',[3 3 picturewidth
     hw_ratio*picturewidth])
pos = get(hfig,'Position');
set(hfig,'PaperPositionMode','Auto','PaperUnits','
    centimeters','PaperSize',[pos(3), pos(4)])
print(hfig,fname,'-dpdf','-painters','-fillpage')
print(hfig,fname,'-dpng','-painters')
hold off;
```

C.2. S-Band

```
clear;clc;close all;tit = 'S-Band link budget';

%%%%%%%%%%%%%%%%%%%%%%%%
% S -Band Link Budget %
%%%%%%%%%%%%%%%%%%%%%%%%

%% CONSTANTS

% Propagation constants
c   = 3e8;                % Light speed (m/s)
f_UL = 2110e6;        % Max frequency (Worst Lfs case) (Hz)
f_DL = 2290e6;        % Max frequency (Worst Lfs case) (Hz)
lambda_UL = c/f_UL;     % Wave length
lambda_DL = c/f_DL;     % Wave length
k   = 1.38064852E-23;    % Boltzman's constant
T0 = 290;                % Temperatura (K)


% Orbit parameters
```

```
Re   = 6371E3;        % Earth radius (m)
h    = 600E3;         % Orbit height (m)
w    =  10e3;         % Atmosphere width (m)

elev_deg = 5:5:175;          % Elevation angles (deg)
elev_rad = deg2rad(elev_deg);% Elevation angles (rad)

SR    = sqrt( (Re+h)^2 -(Re*cos(elev_rad)).^2 ) -Re*sin(elev_rad); % Satellite slant range
w_atm = sqrt( (Re+w)^2 -(Re*cos(elev_rad)).^2 ) -Re*sin(elev_rad); % Atmospheric width vs elevation angle

%% Link Budget initial constrains

% Transmission params
Pt    = [0.25,0.5,1];  % Transmission power from cubesat (W)
Pt_DL = 10*log10(1);  % Transmitted power (W)

BW   = [0.5,1,2]*1e6;  % Bandwidth

Mod_list  = ['GMSK';'BPSK';'QPSK'];
Mod_index = [2,2,4];

%% GAIN

% Ground station antenna gain
Ae_GS  = 0.5;                        % Ground station antenna efficiency
D_GS   = 3;                         % Ground station antenna diameter (m)
A_GS   = pi*(D_GS/2)^2;              % Ground station antenna effective area (m^2)
G_GS = 10*log10( (4*pi)/(lambda_DL^2) * Ae_GS * A_GS );
disp(['Ground Station antenna: Diameter = ',num2str(D_GS),' m. Gain = ',num2str(G_GS),' dBi.'])

% Satellite antenna gain
G_sat = 7; % dBi

% Code gain
Gc = 3.2;  % Reed Solomon code gain (dB)

%% LOSSES

% Free space losses
Lfs_DL  = 20*log10(4*pi*SR/lambda_DL);  % Free space losses (dB)
```

```
60 Lfs_UL  = 20*log10(4*pi*SR/lambda_UL);  % Free space losses
       (dB)
61
62 % Polarization loses
63 Lpol = 3; % (dB)
64
65 % Pointing losses
66 ErrorAngle = 3; % Pointing error angle (deg)
67 HPBW_GS = 70*(lambda_DL/D_GS);           % Half power
       beamwidth in degrees
68 Lpointing = 12*(ErrorAngle/HPBW_GS)^2; % Pointing losses (
       dB)
69
70 disp(' ')
71 % disp(['The free space losses for 90 deg of elevation are
       ',num2str(min(Lfs)),' dB.'])
72 disp(['The pointing losses are ',num2str(Lpointing),' dB
       for an error angle of ',num2str(ErrorAngle),' deg.'])
73
74 %% Noise
75
76 % Factor de merito de la ground station
77 GT_GS_DL = 9;
78
79 % Satellite antenna temperature
80 Ta_sat      = 300;
81 NF_sat      = 10;    % Satellite noise factor
82 Tsys_sat    = Ta_sat + T0*( 10^(NF_sat/10) - 1); % System
       temperature (Ts = Ta + Teq)
83 GT_sat      = G_sat - 10*log10(Tsys_sat); % Satelite Gain-
       to-noise-temperature
84
85
86 %% DOWNLINK
87
88 % Modulation parameters
89 BER_DL  = 1e-5; % Minimum bit error rate
90 Gc_BPSK_DL = 4.31;
91 Gc_GMSK_DL = 4.77;
92 a = 0.9;
93
94 EbN0_BPSK_DL =     (erfcinv(BER_DL*2))^2; EbN0_BPSK_DL =
       10*log10(EbN0_BPSK_DL)-Gc_BPSK_DL; EbN0_BPSK_DL = 10^((
       EbN0_BPSK_DL)/10);
95 EbN0_GMSK_DL = 1/a*(erfcinv(BER_DL*2))^2; EbN0_GMSK_DL =
       10*log10(EbN0_GMSK_DL)-Gc_GMSK_DL; EbN0_GMSK_DL = 10^((
       EbN0_GMSK_DL)/10);
```

```
96  EbN0_QPSK_DL =     (erfcinv(BER_DL*2))^2; EbN0_QPSK_DL =
       10*log10(EbN0_QPSK_DL)-Gc_BPSK_DL; EbN0_QPSK_DL = 10^((
       EbN0_QPSK_DL)/10);
97
98  EbN0_DL       = [EbN0_GMSK_DL,EbN0_BPSK_DL,EbN0_QPSK_DL];
99
100 for c=1:length(EbN0_DL)
101     SNRmin_DL(:,c) = 10*log10( EbN0_DL(c)*log2(Mod_index(c)
          ) );
102 end
103
104 % % Modulation params
105 % EbN0_GMSK_DL = 1/a*(erfcinv(BER_DL*2))^2; % for GMSK BT =
       0.3
106 % EbN0_BPSK_DL  = (erfcinv(BER_DL*2))^2;
107 % EbN0_QPSK_DL  = (erfcinv(BER_DL*2))^2;
108 % EbN0_DL = [EbN0_GMSK_DL,EbN0_BPSK_DL,EbN0_QPSK_DL];
109 % for c=1:length(EbN0_DL)
110 %     SNRmin_DL(:,c) = 10*log10(EbN0_DL(c)*log2(Mod_index(c
       )));
111 % end
112
113 % Calling Downlink
114 % ********** DOWNLINK **********
115
116 B = min(BW); % Hz
117 Ptx = max(Pt); % W
118
119
120 % Link budget for different transmitted powers
121 formatSpec =['%0',num2str(length(num2str(max(Pt)))+3),'.2f'
       ];
122
123 PIRE = 10*log10(Pt) + G_sat;
124
125 hfig = figure;
126 % title('S-Band LinkBudget Downlink')
127 % subtitle(['SNR vs elevation for different Transmitted
       Powers ','(BW = ',num2str(B*1e-6),' MHz, BER = ',num2str
       (BER_DL),')']);
128 hold on;grid minor;
129 xlabel('Elevation angle (deg)');xticks(0:20:180);xlim
       ([0,180]);
130 ylabel('SNR (dB)');
131
132 for n=1:length(Pt)
133
```

```
134     SNR_Pt(n,:) = 10*log10(Pt(n)) + G_sat + GT_GS_DL -
           Lfs_DL - Lpol - Lpointing - 10*log10(k*B) ;
135
136 %     plot(elev_deg,SNR_Pt(n,:),'-','LineWidth',1.5,'
        DisplayName',['Ptx = ',num2str(Pt(n),formatSpec),' W']);
137
138     if Pt(n) == Ptx
139         plot(elev_deg,SNR_Pt(n,:),'k-','LineWidth',1.5,'
               DisplayName',['Ptx = ',num2str(Pt(n),formatSpec)
               ,' W']);
140     else
141         plot(elev_deg,SNR_Pt(n,:),'-','LineWidth',1.5,'
               DisplayName',['Ptx = ',num2str(Pt(n),formatSpec)
               ,' W']);
142     end
143
144 end
145
146 plot(elev_deg,SNRmin_DL(1)*ones(1,length(elev_deg)),'-','
        Color',"#7E2F8E",'LineWidth',1.5,'DisplayName',[Mod_list
        (1,:),' $SNR_{min}$']); % GMSK
147 plot(elev_deg,SNRmin_DL(2)*ones(1,length(elev_deg)),'-','
        Color',"#77AC30",'LineWidth',1.5,'DisplayName',[Mod_list
        (2,:),' $SNR_{min}$']); % BPSK
148 plot(elev_deg,SNRmin_DL(3)*ones(1,length(elev_deg)),'-','
        Color',"#4DBEEE",'LineWidth',1.5,'DisplayName',[Mod_list
        (3,:),' $SNR_{min}$']); % QPSK
149
150 legend
151 fname = 'SBandDownlink1';
152 picturewidth = 20; % set this parameter and keep it forever
153 hw_ratio = 0.65; % feel free to play with this ratio
154 set(findall(hfig,'-property','FontSize'),'FontSize',15) %
        adjust fontsize to your document
155 set(findall(hfig,'-property','Box'),'Box','off') % optional
156 set(findall(hfig,'-property','Interpreter'),'Interpreter','
        latex')
157 set(findall(hfig,'-property','TickLabelInterpreter'),'
        TickLabelInterpreter','latex')
158 set(hfig,'Units','centimeters','Position',[3 3 picturewidth
         hw_ratio*picturewidth])
159 pos = get(hfig,'Position');
160 set(hfig,'PaperPositionMode','Auto','PaperUnits','
        centimeters','PaperSize',[pos(3), pos(4)])
161 print(hfig,fname,'-dpdf','-painters','-fillpage')
162 print(hfig,fname,'-dpng','-painters')
163 hold off;
164
```

```
165
166
167 % Link budget for different Bandwidths
168 formatSpec =['%0',num2str(length(num2str(max(BW*1e-3)))-1),
       '.1f'];
169
170
171
172 hfig = figure;
173 % title('S-Band LinkBudget Downlink')
174 % subtitle(['SNR vs elevation for different Bandwidths',' (
       Ptx = ',num2str(Ptx),' W, BER = ',num2str(BER_DL),')']);
175 hold on;grid minor;
176 xlabel('Elevation angle (deg)');xticks(0:20:180);xlim
       ([0,180]);
177 ylabel('SNR (dB)');
178
179 for n=1:length(BW)
180
181     SNR_BW(n,:) = 10*log10(Ptx) + G_sat + GT_GS_DL - Lfs_DL
            - Lpol -Lpointing - 10*log10(k*BW(n));
182
183 %     plot(elev_deg,SNR_BW(n,:),'-','LineWidth',1.5,'
       DisplayName',['BW = ',num2str(BW(n)*10^-3,formatSpec),'
       KHz']);
184
185     if BW(n) == B
186         plot(elev_deg,SNR_BW(n,:),'k-','LineWidth',1.5,'
               DisplayName',['BW = ',num2str(BW(n)*10^-6,
               formatSpec),' MHz']);
187     else
188         plot(elev_deg,SNR_BW(n,:),'-','LineWidth',1.5,'
               DisplayName',['BW = ',num2str(BW(n)*10^-6,
               formatSpec),' MHz']);
189     end
190
191 end
192
193 plot(elev_deg,SNRmin_DL(1)*ones(1,length(elev_deg)),'-','
       Color',"#7E2F8E",'LineWidth',1.5,'DisplayName',[Mod_list
       (1,:),' $SNR_{min}$']); % GMSK
194 plot(elev_deg,SNRmin_DL(2)*ones(1,length(elev_deg)),'-','
       Color',"#77AC30",'LineWidth',1.5,'DisplayName',[Mod_list
       (2,:),' $SNR_{min}$']); % BPSK
195 plot(elev_deg,SNRmin_DL(3)*ones(1,length(elev_deg)),'-','
       Color',"#4DBEEE",'LineWidth',1.5,'DisplayName',[Mod_list
       (3,:),' $SNR_{min}$']); % QPSK
196
```

```
fname = 'SBandDownlink2';
legend
picturewidth = 20; % set this parameter and keep it forever
hw_ratio = 0.65; % feel free to play with this ratio
set(findall(hfig,'-property','FontSize'),'FontSize',15) % adjust fontsize to your document
set(findall(hfig,'-property','Box'),'Box','off') % optional
set(findall(hfig,'-property','Interpreter'),'Interpreter','latex')
set(findall(hfig,'-property','TickLabelInterpreter'),'TickLabelInterpreter','latex')
set(hfig,'Units','centimeters','Position',[3 3 picturewidth hw_ratio*picturewidth])
pos = get(hfig,'Position');
set(hfig,'PaperPositionMode','Auto','PaperUnits','centimeters','PaperSize',[pos(3), pos(4)])
print(hfig,fname,'-dpdf','-painters','-fillpage')
print(hfig,fname,'-dpng','-painters')
hold off;


%% UPLINK

% % Modulation parameters
% BER_UL      = 1e-7;
% EbN0_BPSK_UL            = (erfcinv(BER_UL*2))^2;
                % Minimum EbN0 for a BPSK modulation
% a = 0.9; EbN0_GMSK_UL   = 1/a*(erfcinv(BER_UL*2))^2;
% EbN0_QPSK_UL            = (erfcinv(BER_UL*2))^2;
% EbN0_UL       = [EbN0_GMSK_UL,EbN0_BPSK_UL,EbN0_QPSK_UL];
% for c=1:length(EbN0_UL)
%     SNRmin_UL(:,c) = 10*log10(EbN0_UL(c)*log2(Mod_index(c)));
% end

% Modulation parameters
BER_UL  = 1e-7; % Minimum bit error rate
Gc_BPSK_UL = 3.2;
Gc_GMSK_UL = 3.6;
a = 0.9;

EbN0_BPSK_UL =     (erfcinv(BER_UL*2))^2; EbN0_BPSK_UL = 10*log10(EbN0_BPSK_UL)-Gc_BPSK_UL; EbN0_BPSK_UL = 10^((EbN0_BPSK_UL)/10);
EbN0_GMSK_UL = 1/a*(erfcinv(BER_UL*2))^2; EbN0_GMSK_UL = 10*log10(EbN0_GMSK_UL)-Gc_GMSK_UL; EbN0_GMSK_UL = 10^((EbN0_GMSK_UL)/10);
```

```
EbN0_QPSK_UL =     (erfcinv(BER_UL*2))^2; EbN0_QPSK_UL =
   10*log10(EbN0_QPSK_UL)-Gc_BPSK_UL; EbN0_QPSK_UL = 10^((
   EbN0_QPSK_UL)/10);

EbN0_DL       = [EbN0_GMSK_DL,EbN0_BPSK_DL,EbN0_QPSK_DL];

for c=1:length(EbN0_DL)
    SNRmin_UL(:,c) = 10*log10( EbN0_DL(c)*log2(Mod_index(c)
       ) );
end

% Calling Uplink
% ********** UPLINK **********


% Link budget for different Bandwidths
formatSpec =['%0',num2str(length(num2str(max(BW*10^-3)))-1)
   ,'.1f'];

Ptx = 4; % W

hfig = figure;
% title('S-Band LinkBudget Uplink')
% subtitle(['SNR vs elevation for different Bandwidths','(
   Ptx = ',num2str(Ptx),' W, BER = ',num2str(BER_UL),')']);
hold on;grid minor;
xlabel('Elevation angle (deg)');xticks(0:20:180);xlim
   ([0,180]);
ylabel('SNR (dB)');yticks(0:5:30);ylim([0,30]);

for n=1:length(BW)

    SNR_BW_UL(n,:) = 10*log10(Ptx) + G_GS + GT_sat - Lfs_UL
       - Lpol - 10*log10(k*BW(n));

%     plot(elev_deg,SNR_BW(n,:),'-','LineWidth',1.5,'
   DisplayName',['BW = ',num2str(BW(n)*10^-3,formatSpec),'
   KHz']);

    plot(elev_deg,SNR_BW_UL(n,:),'-','LineWidth',1.5,'
       DisplayName',['BW = ',num2str(BW(n)*10^-6,formatSpec
       ),' MHz']);

end

plot(elev_deg,SNRmin_UL(1)*ones(1,length(elev_deg)),'-','
   Color',"#7E2F8E",'LineWidth',1.5,'DisplayName',[Mod_list
   (1,:),' $SNR_{min}$']); % GMSK
```

```
plot(elev_deg,SNRmin_UL(2)*ones(1,length(elev_deg)),'-','Color',"#77AC30",'LineWidth',1.5,'DisplayName',[Mod_list(2,:),' $SNR_{min}$']); % BPSK
plot(elev_deg,SNRmin_UL(3)*ones(1,length(elev_deg)),'-','Color',"#4DBEEE",'LineWidth',1.5,'DisplayName',[Mod_list(3,:),' $SNR_{min}$']); % QPSK

fname = 'SBandUplink1';
legend
picturewidth = 20; % set this parameter and keep it forever
hw_ratio = 0.65; % feel free to play with this ratio
set(findall(hfig,'-property','FontSize'),'FontSize',15) % adjust fontsize to your document
set(findall(hfig,'-property','Box'),'Box','off') % optional
set(findall(hfig,'-property','Interpreter'),'Interpreter','latex')
set(findall(hfig,'-property','TickLabelInterpreter'),'TickLabelInterpreter','latex')
set(hfig,'Units','centimeters','Position',[3 3 picturewidth hw_ratio*picturewidth])
pos = get(hfig,'Position');
set(hfig,'PaperPositionMode','Auto','PaperUnits','centimeters','PaperSize',[pos(3), pos(4)])
print(hfig,fname,'-dpdf','-painters','-fillpage')
print(hfig,fname,'-dpng','-painters')
hold off;
```

C.3. X-Band

```
clear;clc;close all;
%%%%%%%%%%%%%%%%%%%%%%%%
% X -Band Link Budget %
%%%%%%%%%%%%%%%%%%%%%%%%

%{

The main aim of this script is to simulte the link budget of the X-Band
Communications system for the three different pointing modes, which are:

    - No pointing
    - Partial pointing
    - Complete pointing

```

```
15 The objective is to find the optimal antenna type for the
      comms system.
16
17 %}
18
19 %% Antenna Constrains
20
21 AntennaType = 0;
22
23 if      AntennaType == 0    % Single Patch Antenna
24     G_sat    = 6;           % Average Gain for a X-Band
         single patch antenna
25     disp(['Satelite antenna: Single Patch Antenna: Gain = '
         ,num2str(G_sat),' (dBi).'])
26 else                        % 2x2 Patch Antenna
27     G_sat    = 10;          % Average Gain for a X-Band 2x2
         patch antenna array
28     disp(['Satelite antenna: 2x2 Patch Antenna array: Gain
         = ',num2str(G_sat),' (dBi).'])
29 end
30
31
32 %% CONSTANTS
33
34 f = 8400e6;      % Worst frequency case for X-Band (Worst
      free space losses)
35
36 % Propagation constants
37 c=3e8;               % Light speed (m/s)
38 lambda = c/f;        % Wave length (m)
39 k = 1.38064852E-23; % Boltzman's constant
40 T0 = 290;           % Temperatura (K)
41
42 % Orbit parameters
43 Re   = 6371E3;       % Earth radius (m)
44 h    = 600E3;        % Orbit height (m)
45 w    =  10e3;        % Atmosphere width (m)
46
47 elev_deg = 5:5:175;          % Elevation angles (deg)
48 elev_rad = deg2rad(elev_deg);% Elevation angles (rad)
49
50 SR    = sqrt( (Re+h)^2 -(Re*cos(elev_rad)).^2 ) -Re*sin(
      elev_rad); % Satellite slant range
51 w_atm = sqrt( (Re+w)^2 -(Re*cos(elev_rad)).^2 ) -Re*sin(
      elev_rad); % Atmospheric width vs elevation angle
52
53 %% Link Budget initial constrains
54
```

```
Pt      = [0.25,0.5,1];           % Possible transmission
   powers from cubesat (W)
BW      = [1,2.5,5]*1e6; % Possible bandwidths

%% Gain

% Ground station antenna gain
e_GS    = 0.5;                          % Ground station
   antenna efficiency
D_GS    = 2.4;                          % Ground station
   antenna diameter (m)
A_GS    = pi*(D_GS/2)^2;                % Ground station
   antenna effective area (m^2)
G_GS    = 10*log10( (4*pi)/(lambda^2) * e_GS * A_GS );
disp(['Ground Station antenna: Diameter = ',num2str(D_GS),'
    m. Gain = ',num2str(G_GS),' dBi. HPBW = ',num2str(70*(
   lambda/D_GS)),' deg.'])

% Code gain
Gc = 3.2;           % Reed-Solomon(255,233) code gain (dB)

%% Losses

% Free space losses
Lfs  = 20*log10(4*pi*SR/lambda);  % Free space losses (dB)

% Atmospheric losses
T = 3;                                          %
   Temperature (C)
Patm = 83.43e3;                                 %
   Atmospheric pressure at Montsec (Pa)
rho_wv = 15;                                    % Waper
   vapour and oxigen density (g/m^3)
Latm = gaspl(w_atm,f,T,Patm,rho_wv)';

% Polarization loses
Lpol = 3; % (dB)

% Pointing losses
ErrorAngle = 0.75; % Pointing error angle (deg)
HPBW_GS = 70*(lambda/D_GS);           % Half power
   beamwidth in degrees
Lpointing = 12*(ErrorAngle/HPBW_GS)^2; % Pointing losses (
   dB)

disp(' ')
disp(['The free space losses for 90 deg of elevation are ',
   num2str(min(Lfs)),' dB.'])
```

```
91  disp(['The atmospheric for 90 deg of elevation are ',
       num2str(min(Latm)),' dB.'])
92  disp(['The pointing losses are ',num2str(Lpointing),' dB
       for an error angle of ',num2str(ErrorAngle),' deg.'])
93
94  % disp(['El factor de ganancia (G_{A} - L_{Pointing})',
       num2str(G_GS-Lpointing),'dB'])
95
96  %% Noise
97
98  % https://wiki.nanosatlab.space/books/montsec-ground-
       station/page/test-report-20230223-uhf-indoor-equipment-
       measurements
99
100 % Antenna temperature
101 Ta_GS  = 38;  % Ground Station Antenna Temperature (K)
102
103 % Receiver noise temperature
104 NF_GS  = 7;                          % Ground Station Noise
       Factor (dB)
105 Teq_GS = T0*( 10^(NF_GS/10) -1 );  % Ground Station Noise
       equivalent temperature (dB)
106
107 % System temperture
108 Tsys_GS = Ta_GS + Teq_GS; % Temperatura absoluta del
       sistema
109
110
111 %% Link Budget modulation parameters
112
113 % Modulation parameters
114 BER     = 1E-5; % Minimum bit error rate
115 Gc_BPSK = 3.2;
116
117 % Minimum Eb/N0 for a BPSK
118 EbN0_BPSK = (erfcinv(BER*2))^2; EbN0_BPSK = 10*log10(
       EbN0_BPSK) - Gc_BPSK; EbN0_BPSK = 10^((EbN0_BPSK)/10);
119
120 % Minimum SNR for a BPSK
121 SNRmin = 10*log10(EbN0_BPSK * log2(2));
122
123 %% Single Patch Antenna
124
125 G_sat = 6;
126 Antenna='Single patch antenna';
127
128 % Link budget for different transmitted powers
129 fname = 'XBand_SinglePatch1';
```

```
formatSpec = '%04.2f';
B = BW(1);
SNR_Pt = [];
hfig  = figure;
hold on;grid minor;
% title(['X-Band Link Budget (',Antenna,')'] )
% tit=['SNR for a BPSK system (BW = 1 MHZ, BER = 1e-5,
   SNRmin = ',num2str(SNRmin),' dB)'];
% subtitle(tit);
xlabel('Elevation angle (deg)');xticks(0:20:180);xlim
   ([0,180]);
ylabel('SNR (dB)');
for n=1:length(Pt)
    PIRE = 10*log10(Pt(n)) + G_sat;
    SNR_Pt(n,:) = 10*log10(Pt(n)) + G_sat + G_GS - Lfs -
       Latm - Lpol - Lpointing - 10*log10(k*Tsys_GS*B);
    plot(elev_deg,SNR_Pt(n,:),'-','LineWidth',1.5,'
       DisplayName',['Ptx = ',num2str(Pt(n),formatSpec),' W
       '])
end
plot(elev_deg,SNRmin*ones(1,length(elev_deg)),'k-','
   LineWidth',1.25,'DisplayName',['BPSK $SNR_{min}$'])
legend
picturewidth = 20; % set this parameter and keep it forever
hw_ratio = 0.65; % feel free to play with this ratio
set(findall(hfig,'-property','FontSize'),'FontSize',15) %
   adjust fontsize to your document
set(findall(hfig,'-property','Box'),'Box','off') % optional
set(findall(hfig,'-property','Interpreter'),'Interpreter','
   latex')
set(findall(hfig,'-property','TickLabelInterpreter'),'
   TickLabelInterpreter','latex')
set(hfig,'Units','centimeters','Position',[3 3 picturewidth
    hw_ratio*picturewidth])
pos = get(hfig,'Position');
set(hfig,'PaperPositionMode','Auto','PaperUnits','
   centimeters','PaperSize',[pos(3), pos(4)])
print(hfig,fname,'-dpdf','-painters','-fillpage')
print(hfig,fname,'-dpng','-painters')
hold off;


% Link budget for different Bandwidths
fname = 'XBand_SinglePatch2';
formatSpec = '%04.1f';
Ptx = max(Pt); % W
SNR_BW = [];
PIRE= 10*log10(Ptx) + G_sat;
```

```
hfig = figure;
hold on;grid minor;
% title(['X-Band Link Budget (',Antenna,')'])
% tit=['SNR for a BPSK system (Ptx = 1 W, BER = 1e-5,
   SNRmin = ',num2str(SNRmin),' dB)' ];
% subtitle(tit);
xlabel('Elevation angle (deg)');xticks(0:20:180);xlim
   ([0,180]);
ylabel('SNR (dB)');
for n=1:length(BW)
    SNR_BW(n,:) = 10*log10(Ptx) + G_sat + G_GS - Lfs - Latm
        - Lpol - Lpointing - 10*log10(k*Tsys_GS*BW(n));
    plot(elev_deg,SNR_BW(n,:),'-','LineWidth',1.5,'
       DisplayName',['BW = ',num2str(BW(n)*1e-6,formatSpec)
       ,' MHz'])
end
plot(elev_deg,SNRmin*ones(1,length(elev_deg)),'k-','
   LineWidth',1.25,'DisplayName',['BPSK $SNR_{min}$'])
legend
picturewidth = 20; % set this parameter and keep it forever
hw_ratio = 0.65; % feel free to play with this ratio
set(findall(hfig,'-property','FontSize'),'FontSize',15) %
   adjust fontsize to your document
set(findall(hfig,'-property','Box'),'Box','off') % optional
set(findall(hfig,'-property','Interpreter'),'Interpreter','
   latex')
set(findall(hfig,'-property','TickLabelInterpreter'),'
   TickLabelInterpreter','latex')
set(hfig,'Units','centimeters','Position',[3 3 picturewidth
    hw_ratio*picturewidth])
pos = get(hfig,'Position');
set(hfig,'PaperPositionMode','Auto','PaperUnits','
   centimeters','PaperSize',[pos(3), pos(4)])
print(hfig,fname,'-dpdf','-painters','-fillpage')
print(hfig,fname,'-dpng','-painters')

%% 2x2 Patch Antenna

G_sat = 10;
Antenna='2x2 patch array antenna';

% Link budget for different transmitted powers
fname = 'XBand_PatchArray1';
formatSpec = '%04.2f';
B = BW(1);
SNR_Pt = [];
hfig  = figure;
hold on;grid minor;
```

```
% title(['X-Band Link Budget (',Antenna,')'])
% tit=['SNR for a BPSK system (BW = 1 MHZ, BER = 1e-5,
   SNRmin = ',num2str(SNRmin),' dB)'];
% subtitle(tit);
xlabel('Elevation angle (deg)');xticks(0:20:180);xlim
   ([0,180]);
ylabel('SNR (dB)');
for n=1:length(Pt)
    PIRE = 10*log10(Pt(n)) + G_sat;
    SNR_Pt(n,:) = 10*log10(Pt(n)) + G_sat + G_GS - Lfs -
       Latm - Lpol - Lpointing - 10*log10(k*Tsys_GS*B);
    plot(elev_deg,SNR_Pt(n,:),'-','LineWidth',1.5,'
       DisplayName',['Ptx = ',num2str(Pt(n),formatSpec),' W
       '])
end
plot(elev_deg,SNRmin*ones(1,length(elev_deg)),'k-','
   LineWidth',1.25,'DisplayName',['BPSK $SNR_{min}$'])
legend
picturewidth = 20; % set this parameter and keep it forever
hw_ratio = 0.65; % feel free to play with this ratio
set(findall(hfig,'-property','FontSize'),'FontSize',15) %
   adjust fontsize to your document
set(findall(hfig,'-property','Box'),'Box','off') % optional
set(findall(hfig,'-property','Interpreter'),'Interpreter','
   latex')
set(findall(hfig,'-property','TickLabelInterpreter'),'
   TickLabelInterpreter','latex')
set(hfig,'Units','centimeters','Position',[3 3 picturewidth
    hw_ratio*picturewidth])
pos = get(hfig,'Position');
set(hfig,'PaperPositionMode','Auto','PaperUnits','
   centimeters','PaperSize',[pos(3), pos(4)])
print(hfig,fname,'-dpdf','-painters','-fillpage')
print(hfig,fname,'-dpng','-painters')
hold off;


% Link budget for different Bandwidths
fname = 'XBand_PatchArray2';
formatSpec = '%04.1f';
Ptx = max(Pt); % W
SNR_BW = [];
PIRE= 10*log10(Ptx) + G_sat;
hfig = figure;
hold on;grid minor;
% title(['X-Band Link Budget (',Antenna,')'])
% tit=['SNR for a BPSK system (Ptx = 1 W, BER = 1e-5,
   SNRmin = ',num2str(SNRmin),' dB)' ];
```

```
% subtitle(tit);
xlabel('Elevation angle (deg)');xticks(0:20:180);xlim
    ([0,180]);
ylabel('SNR (dB)');
for n=1:length(BW)
    SNR_BW(n,:) = 10*log10(Ptx) + G_sat + G_GS - Lfs - Latm
        - Lpol - Lpointing - 10*log10(k*Tsys_GS*BW(n));
    plot(elev_deg,SNR_BW(n,:),'-','LineWidth',1.5,'
       DisplayName',['BW = ',num2str(BW(n)*1e-6,formatSpec)
       ,' MHz'])
end
plot(elev_deg,SNRmin*ones(1,length(elev_deg)),'k-','
   LineWidth',1.25,'DisplayName',['BPSK $SNR_{min}$'])
legend
picturewidth = 20; % set this parameter and keep it forever
hw_ratio = 0.65; % feel free to play with this ratio
set(findall(hfig,'-property','FontSize'),'FontSize',15) %
   adjust fontsize to your document
set(findall(hfig,'-property','Box'),'Box','off') % optional
set(findall(hfig,'-property','Interpreter'),'Interpreter','
   latex')
set(findall(hfig,'-property','TickLabelInterpreter'),'
   TickLabelInterpreter','latex')
set(hfig,'Units','centimeters','Position',[3 3 picturewidth
    hw_ratio*picturewidth])
pos = get(hfig,'Position');
set(hfig,'PaperPositionMode','Auto','PaperUnits','
   centimeters','PaperSize',[pos(3), pos(4)])
print(hfig,fname,'-dpdf','-painters','-fillpage')
print(hfig,fname,'-dpng','-painters')
```

APPENDIX D. MAGNETORQUER DESIGN MATLAB CODE

This appendix includes the code used to simulate the magnetorquers, along with an explanation of its organization and functioning.

The code is organized into different folders, each serving the purpose of housing specific types of files. The folders are:

- **General folder**: This folder is where the main scripts are stored to initiate the simulation. These files are configurable to obtain the desired type of simulation.
- **Configuration files**: This folder stores the files that contain the initial variables to simulate a magnetorquer.
- **Data**: In this folder, any simulation data files that need to be stored are saved.
- **Functions**: All files containing functions are stored in this folder.
- **Results**: The results of simulations that need to be stored are saved in this folder.

Below are the files used for the design of the magnetorquers of the 3Cat-8:

D.1. Main scripts

D.1.1. MainSaturationAnalisys

This is the main script to simulate the Z axis magnetorquer manufactured on the 4^{th} chapter of this Bachelor's thesis. This file calls all the functions to execute the simulation.

```
% Title:          Saturation analisys 4th version
% Description:    The main objective of this script is to
   plot the saturation
%                 vs the number of turns of the three
   magnetorquers that will
%                 be installed in the 3Cat-8 Satellite.
% Author:         Alberto Cruz Martinez

%% INITIATE THE SIMULATION

clear; clc; close all
format longg;
    % Add to path the folder
    addpath('Config files')
    addpath('Data')
    addpath('Functions')
    addpath('Results')
    run("Config files\config_Magnetorquers.m")
```

```
17      % LOAD MQT DATA
18      load('../Magnetorquers/Data/Data_Magnetorquers.mat')
19
20  %%  INITIAL PARAMETERS
21
22      formatSpec = '%.4f';    % Plot legend format
23      NumTurns=1e6;
24      Turns = (1:1:NumTurns); % Vector with the number of
            turns
25
26      Z_Turns = [];
27      Z_Saturations = [];
28      Z_Powers = [];
29
30  %% Z AXIS
31  disp(' ')
32  disp('
        ------------------------------------------------------
        ');
33  disp('MAGNETORQUER Z');
34  disp(' ')
35
36  %t4=figure(4);
37
38  Zfig1=figure(1);
39  hold on;
40  % title('Magnetorquer Z Magnetic moment ($I_{max} = 1 A$)')
        ;
41  xlabel('Number of turns');
42  ylabel('Magnetic momentum [$A \cdot m^2$]');
43  fname1 = 'MTQz1';
44
45  Zfig2=figure(2);
46  hold on;
47  % title('Magnetorquer Z power consumption');
48  xlabel('Number of turns');
49  ylabel('Power Consumption [W]');
50  fname2 = 'MTQz2';
51
52
53  for n=1:1:length(Cable_sections)
54
55      Diameter = Cable_sections(n);
56
57      NumTurnsPerLayer = floor(MQT_Z.MaxW/Diameter);
58
59      maxHeight = MQT_Z.MaxH;
60
```

```
61      c1 = MQT_Z.C1 - Diameter;
62      c2 = MQT_Z.C2 - Diameter;
63
64      AR1 = MQT_Z.AR1;
65
66      b = c1*AR1;
67
68      a1 = c1-2*b;
69      a2 = c2-2*b;
70
71      [Z_SAT,Z_POWER,Z_Params,Z_Layers] =
           fun_Compute_SaturationPower(Diameter,NumTurns,
           NumTurnsPerLayer,I,a1,a2,b,c1,c2,AR1,maxHeight);
72      Z_Turns         = (1:1:length(Z_SAT));
73      figure(1);hold on;legend;legend('Location','southeast')
           ;xlim([0 250]);
74      plot(Z_Turns,Z_SAT,'-','LineWidth',1.5,'DisplayName',['
           d = ',num2str(1e3*Cable_sections(n),formatSpec),' mm
           ']);
75      figure(2);hold on;legend;legend('Location','southeast')
           ;ylim([0 6])
76      plot(Z_Turns,Z_POWER,'-','LineWidth',1.5,'DisplayName'
           ,['d = ',num2str(1e3*Cable_sections(n),formatSpec),'
            mm']);
77
78  end
79  picturewidth = 20; % set this parameter and keep it forever
80  hw_ratio = 0.6; % feel free to play with this ratio
81  set(findall(Zfig1,'-property','FontSize'),'FontSize',15) %
       adjust fontsize to your document
82  set(findall(Zfig2,'-property','FontSize'),'FontSize',15) %
       adjust fontsize to your document
83  set(findall(Zfig1,'-property','Box'),'Box','off') %
       optional
84  set(findall(Zfig1,'-property','Interpreter'),'Interpreter',
       'latex')
85  set(findall(Zfig1,'-property','TickLabelInterpreter'),'
       TickLabelInterpreter','latex')
86  set(Zfig1,'Units','centimeters','Position',[3 3
       picturewidth hw_ratio*picturewidth])
87  pos = get(Zfig1,'Position');
88  set(Zfig1,'PaperPositionMode','Auto','PaperUnits','
       centimeters','PaperSize',[pos(3), pos(4)])
89  print(Zfig1,fname1,'-dpdf','-painters','-fillpage')
90  set(findall(Zfig2,'-property','Box'),'Box','off') %
       optional
91  set(findall(Zfig2,'-property','Interpreter'),'Interpreter',
       'latex')
```

```
set(findall(Zfig2,'-property','TickLabelInterpreter'),'
   TickLabelInterpreter','latex')
set(Zfig2,'Units','centimeters','Position',[3 3
   picturewidth hw_ratio*picturewidth])
pos = get(Zfig2,'Position');
set(Zfig2,'PaperPositionMode','Auto','PaperUnits','
   centimeters','PaperSize',[pos(3), pos(4)])
print(Zfig2,fname2,'-dpdf','-painters','-fillpage')
hold off;
```

D.2. Configuration files

This is the configuration file used for simulating the Z axis magnetorquer manufactured on the 4^{th} chapter of this Bachelor's thesis. In this file, the design variables are initialized and saved in the *Data* folder. Then, the main file will call these data to use them.

```
clc; clear;
delete('../Data/Data_Magnetorquers.mat')

%%  SIMULATION PARAMETERS

%   NUMBER OF TURNS TO SIMULATE
    NumTurns    = 5000;

%   Diameter of the section of cable [m]

    Cable_sections = (1e-3)
       *[0.2546,0.2859,0.3211,0.3606,0.4049,0.4547];

%   Power supply parameters

    I = 1;     % Maximum current [A]

    f = 250e3;    % Triskel PWM frequency;

%%  MAGNETORQUER PARAMETERS


%   Magnetorquer Z Dimensions

    MQT_Z.C1    = 104.4*10^-3;                  % [m]
    MQT_Z.C2    = 95.6*10^-3;                  % [m]

    MQT_Z.B     = (9.54+8.31)/2 * 1e-3;         % [m]

    MQT_Z.MaxW  = 8*1e-3;                       % [m]

```

```
    MQT_Z.A1     = MQT_Z.C1 - 2*MQT_Z.B;      % [m]
    MQT_Z.A2     = MQT_Z.C2 - 2*MQT_Z.B;      % [m]

    MQT_Z.AR1    = MQT_Z.B/MQT_Z.C1;
%   MQT_Z.AR2    = MQT_Z.B/MQT_Z.C2;        % NO SE USA PARA LOS CALCULOS

    MQT_Z.MaxH   = 4e-3;                    % [m]



%% SAVE AND CLEAR VARIABLES


save('../Data/Data_Magnetorquers','MQT_X','MQT_Y','MQT_Z','Cable_sections', 'I','NumTurns',"f")
clear('MQT_X','MQT_Y','MQT_Z','Cable_sections', 'I','NumTurns')
```

D.3. Functions

D.3.1. Area of the magnetorquer computation function

This function estimates the area of a turn of a magnetorquer.

```
function [Area] = fun_Area_Magnetorquer(c1,c2, b)
%{
    Function that calculates the Area of an octogon (The magnetorquer's shape)
%}
%{
    Inputs:
        - c :
        - b :
%}
%{
    Outputs:
        - Area: The area described by the turn
%}


    Area = c1*c2 - 2 * b^2;


end
```

D.3.2. Height of the magnetorquer computation function

This function estimates the height occupied by a magnetorquer with the number of layers and the diameter of the cable.

```
function [Width_Average] = fun_Compute_AverageHeight(
   numLayers, Diameter)

%{
    Function that calculates the Width of the magnetorquer
       in an
    optimistic approach (More compact as possible)
%}
%{
    Inputs:
        - Diameter : diameter of the section of the wire [
           mm]
        - numTurns : Number of accumulation of spires
%}
%{
    Outputs:
        - width_optimistic: The width of the whole
           magnetorquer
%}

    Width_Optimistic = (numLayers - 1) * (sqrt(3)/2) *
       Diameter + Diameter;

    Width_Pesimistic = numLayers * Diameter;

    Width_Average = (Width_Pesimistic+Width_Optimistic)/2;

end
```

D.3.3. Magnetorquer simulation function

This function simulates a magnetorquer for a given cable diameter.

```
function [SAT,POWER,MTQ_params,MQT_Layers] =
   fun_Compute_SaturationPower(Diameter,NumTurns,
   NumTurnsPerLayer,I,a1,a2,b,c1,c2,AR1,maxHeight)

    h = Diameter * sqrt(3)/2;

    L               = 0;
    Long            = [];

    A               = 0;
```

```
    v_Area          = [];

    Resistance      = [];
    Inductance      = [];

    SAT             = [];

    POWER           = [];

    MQT_Layers      = [];

    c1_o     = c1;
    c2_o     = c2;

    NumLayers = 1;
    i=0;
    while i < NumTurns

        j=0;
        if ( (-1)^NumLayers ) == -1

            while j < NumTurnsPerLayer % Odd Layers

                [l]          = fun_Length(a1,a2,b);
                L            = L + l;
                Long         = [Long L];

                [R]          = fun_Resistance(Diameter,L);
                Resistance   = [Resistance R];

                [Area]       = fun_Area_Magnetorquer(c1,c2,
                   b);
                A            = A + Area;
                v_Area       = [v_Area Area];

                SAT          = [SAT A*I];

                POWER        = [POWER I^2*(R/2)]; % Req = R
                   //R = R^2/2*R = R/2

                j = j + 1;
                i = i + 1;

                MQT_Layers = [MQT_Layers,NumLayers];

                if i == NumTurns
                    break
                end
```

```
55              end
56          else
57
58              while j < (NumTurnsPerLayer - 1) % Even Layer
59
60                  [l]          = fun_Length(a1,a2,b);
61                  L            = L + l;
62                  Long         = [Long L];
63
64                  [R]          = fun_Resistance(Diameter,L);
65                  Resistance   = [Resistance R];
66
67                  [Area]       = fun_Area_Magnetorquer(c1,c2,
                        b);
68                  A            = A + Area;
69                  v_Area       = [v_Area Area];
70
71                  SAT          = [SAT A*I];
72
73                  POWER        = [POWER I^2*(R/2)]; % Req = R
                        //R = R^2/2*R = R/2
74
75                  j = j + 1;
76                  i = i + 1;
77
78                  MQT_Layers = [MQT_Layers,NumLayers];
79
80                  if i == NumTurns
81                      break
82                  end
83              end
84          end
85
86          c1 = c1 - 2*h;
87          c2 = c2 - 2*h;
88
89          b  = c1 * AR1;
90
91          a1 = c1 - 2*b;
92          a2 = c2 - 2*b;
93
94          [avHeight] = fun_Compute_AverageHeight(NumLayers,
                Diameter);
95
96          if avHeight > maxHeight
97              break
98          end
99
```

```
        if c1 <= 0 || c2 <= 0 || a1 <= 0 || a2 <= 0
            break
        end
        NumLayers = NumLayers+1;

    end

    MTQ_params.Long = Long;
    MTQ_params.Resistance = Resistance;
    MTQ_params.Inductance = Inductance;
    MTQ_params.v_Area = v_Area;
    disp(['Max number of turns for d = ',num2str(Diameter*1
       e3),' mm: ',num2str(length(SAT))])

end
```

D.3.4. Length of the magnetorquer computation function

This function computes the length of a magnetorquer.

```
function [l] = fun_Length(a1,a2,b)

%{
    Function that calculates the Length of a turn in the
       magnetorquer for
    an octogonal shape.
%}
%{
    Inputs:
        - a : diameter of the section of the wire [m]

%}
%{
    Outputs:
        - l: The length of the turn [m]
%}

    l = 2*a1 + 2*a2 + 4 * sqrt(2*b^2);

end
```

D.3.5. Resistance of the magnetorquer computation function

This function computes the resistance of a magnetorquer.

```
function resistance = fun_Resistance(d,l)
```

```
%{
    Function that calculates the resitance of a copper wire
%}
%{
    Inputs:
        - d: diameter of the section of the wire [m]
        - l: longitud of the wire [m]
%}
%{
    Outputs:
        - resistance: resistance of the wire [ohms]
%}
    resistivity = 1.72e-8;                              % resistivity of copper [ohms*m]
    resistance = resistivity * l / (pi * (d/2)^2);
end
```